LIÈGE université
Sciences Appliquées

Estimating human joint torques and muscle activations: A new approach to inverse dynamics without ground reaction data

A thesis submitted in partial fulfillment of the requirements
for the degree of Doctor of Philosophy (Phd) in Engineering Science

by

Romain VAN HULLE

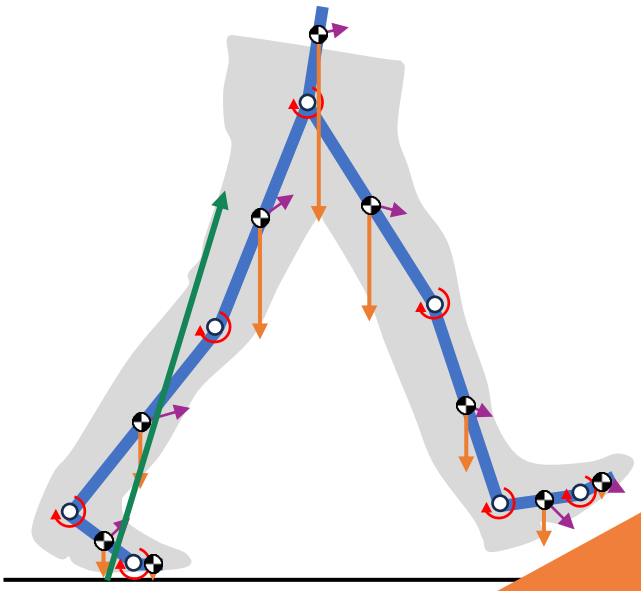

Supervisor: Prof. Olivier BRÜLS

DOCTORAL COLLEGE IN AEROSPACE AND MECHANICS

MARCH 10TH, 2026

Abstract

The primary aim of this thesis is to develop a novel inverse dynamics method to evaluate joint torques and muscle forces for analysing human gait. Classical inverse dynamics methods rely on the direct measurement of ground reaction forces (GRFs), which still faces major challenges in various environments, particularly outside controlled laboratory settings. While advancements in kinematic measurements have facilitated the acquisition of motion data in diverse contexts, the reliance on expensive force platforms restricts the scope of biomechanical studies.

The objective of this thesis is to overcome these limitations and eliminate the need for force platform data in the context of inverse dynamics analysis. To achieve this, a comprehensive review of existing kinematic and dynamic analysis methods, as well as foot-ground contact models, was conducted. The research led to the creation of a two-dimensional model based on fundamental assumptions about foot-ground interaction, which was later extended to a three-dimensional model. The first fundamental assumption is the non-penetrability of the feet into the ground, which enables the replacement of experimentally measured ground reaction forces by kinematic constraints between the feet and the ground within the contact model. These constraints are enforced by reaction forces that represent the resulting ground contact forces. The second assumption concerns the distribution of these reaction forces among the two feet in the double support phase. A least-squares approach is adopted within the equation of motion solver of the musculoskeletal model to allocate the components of the reaction loads among the contacting feet. The third assumption is that the position of the centre of pressure (COP) along the foot can be estimated as a function of the foot orientation in its sagittal plane. This methodology ensures a redistribution of the ground reactions, without relying on direct force plate measurements. The 3D model was used in conjunction with the OpenSim software to evaluate joint torques, muscle activations, and muscle forces during human gait. The results showed good agreement with a standard OpenSim workflow for most joint torques, particularly in the sagittal plane. Muscle activation and some torque estimations exhibited a higher sensitivity to input uncertainties: several major muscle groups displayed consistent activation patterns, while others, especially those associated with knee motion, showed larger discrepancies. Despite these limitations, the model was able to reproduce physiologically meaningful trends, indicating its potential to provide useful internal biomechanical information without relying on force plate measurements.

In addition to the theoretical developments and numerical implementation, this thesis includes a critical analysis of the results obtained. The proposed framework has been systematically compared both to alternative modelling approaches from the literature and to more conventional methods that rely on experimental force platforms measurements. This comparative evaluation highlights the strengths and limitations of the method, and provides

valuable insights into its applicability and accuracy for estimating internal biomechanical quantities such as joint torques and muscle activations.

Acknowledgements

First and foremost, I would like to express my sincere gratitude to my supervisor, Olivier, for his trust and patience throughout this long journey. Thank you for giving me the opportunity to be a researcher in the Laboratory of Motion Analysis and for your continuous guidance and support.

My warm thanks go to the members of the jury for accepting to evaluate my work. I appreciate the time and effort you dedicated to reviewing my thesis and for your insightful feedback.

I am also grateful to the Department of Aerospace and Mechanical Engineering for the confidence placed in me during these years as a teaching assistant. It was through this experience that I discovered an unexpected passion for teaching and knowledge sharing.

A heartfelt thank you to my former colleagues at ULiège and current collegues at A&R for the many discussions, lunch and coffee breaks, and unforgettable evenings. In particular, I would like to thank Julien and Marco for their camaraderie and support.

Enfin, merci à ma famille, pour son amour et son soutien indéfectible durant toutes ces années.

Je ne peux conclure ces remerciements sans m'adresser à toi, Brunella. Lorsque nous nous sommes mariés, nous nous sommes promis d'être là l'un pour l'autre "dans la joie comme dans la douleur" : merci d'avoir tenu cette promesse avec une tendresse infinie, et d'avoir été présente à mes côtés à chaque instant, dans les jours lumineux comme dans les plus sombres. Je t'aime. Je n'aurais pas pu accomplir grand-chose sans toi, et si cette thèse est aujourd'hui achevée, c'est entièrement grâce à toi.

Charlotte, je pense à toi chaque jour. Cette thèse t'est dédiée, ainsi qu'à tes petits frères, Georges et Jacques.

Contents

List of Figures

List of Tables

★

Pour Charlotte

Chapter 1

Introduction

1.1 Context of the thesis

Biomechanics is a multidisciplinary field that investigates the mechanical aspects of living organisms, delving into the analysis of their movements, structures, and physiological functions. By integrating principles from physics, biomechanics seeks to unravel the intricacies of how biological systems, in humans, animals, or other organisms, interact with their surroundings. This includes the examination of internal forces, external influences, and the mechanical properties of tissues, aiming to gain a comprehensive understanding of the biomechanical principles governing the behaviours and capabilities of living organisms.

It aims at distinguishing patterns of motion in different activities, including how muscles, bones, joints and central nervous system produce the movement. Biomechanics relies upon knowledge in anatomy, physics, mechanics, and chemistry.

Biomechanical analyses are carried out in several domains. For example, in medicine, certain pathologies affect movement and coordination: their early detection can improve a patient's situation. In physiotherapy, these analyses will directly influence the rehabilitation strategy, or the shape of a prosthesis. We can also mention sport, where the search for performance is generally essential to achieve success. Recent video games use motion recognition as the main gameplay mechanic (i.e., the set of rules, systems, and interactions that define how the game is played): teaching players certain dance choreographies, learning gymnastic, yoga movements, etc. Biomechanical studies can also be predictive. For example, they can investigate how the choice of a specific treatment will affect the movement of a patient. In robotics, collaboration between humans and robots is becoming a key component of the fourth industrial revolution, and therefore, robots need to learn and predict the motion of the humans to avoid injuries and help the best way they can.

Historically, the first analytical tools to describe the motion were the naked eye and basic measuring instruments to scale the subject. Studies were more rudimentary and only revealed the most obvious things. The diagnosis of pathologies was based entirely on the expert's opinion, and the exchanges of observations were difficult or even impossible. Pioneering works by Muybridge and Marey in the late 19th century marked an important turning

point, introducing early motion capture techniques through sequential photography and chronophotography. However, it was not until the second half of the 20th century that technological advances made it possible to develop better measuring instruments, and, combined with recording cameras, to better define certain objective parameters. Clinical studies have therefore been carried out in order to establish standards and the emergence of new fields of study.

After having carried out studies of descriptions of movements, scientists have sought to study what caused the motion: joint torques, muscular forces and activation, as well as the role of the central nervous system. Inverse dynamics analyses were performed to study and understand human motion. By solving the equations of motion, linking the internal and external forces of a body to its movement, speed and acceleration, it is possible to estimate the joint torques and muscles forces based on experimental motion data and information about the external forces acting on the human body, in particular, gravity and ground reaction forces. If gravity forces can be evaluated using a simple model, ground reaction forces have to be measured or estimated using a numerical foot/ground model.

Over the past decades, the quality of kinematic measurements has significantly advanced, enabling the easy acquisition of such data in various settings. As a result, kinematic studies are no longer confined to laboratory environments.

Direct measurement of reaction forces can be achieved using force platforms. However, due to their cost and limited portability, measuring contact forces is typically restricted to laboratory experiments. This limitation confines comprehensive studies to simple activities conducted within the laboratory setting. By utilizing contact models rather than direct force measurements, researchers can overcome logistical challenges associated with force platform use. Additionally, these models offer the flexibility to conduct analyses in diverse environments beyond traditional laboratory settings, facilitating in-situ data collection wherever relevant. This approach not only expands the scope of biomechanical research but also enhances its applicability in real-world scenarios, ranging from clinical assessments to sports performance evaluations and beyond.

In the literature, one generally distinguishes compliant and rigid foot models. Compliant models use the deformation of the foot sole and the ground to estimate the ground reaction forces with simple equations. However, measuring this deformation is often beyond the capabilities of the current motion capture technologies, and the use of compliant model is mostly restricted to predictive analysis. Rigid models do not require the local compliance since they rely on a non-penetration condition. With rigid models available in the literature, the ground reaction forces are usually estimated from the global acceleration of the body and empirical laws are necessary to define the repartition of the forces between both feet. The presented work provides a general numerical approach to solve the inverse dynamics problem when no ground reaction force measurement is available using a novel foot/ground contact model.

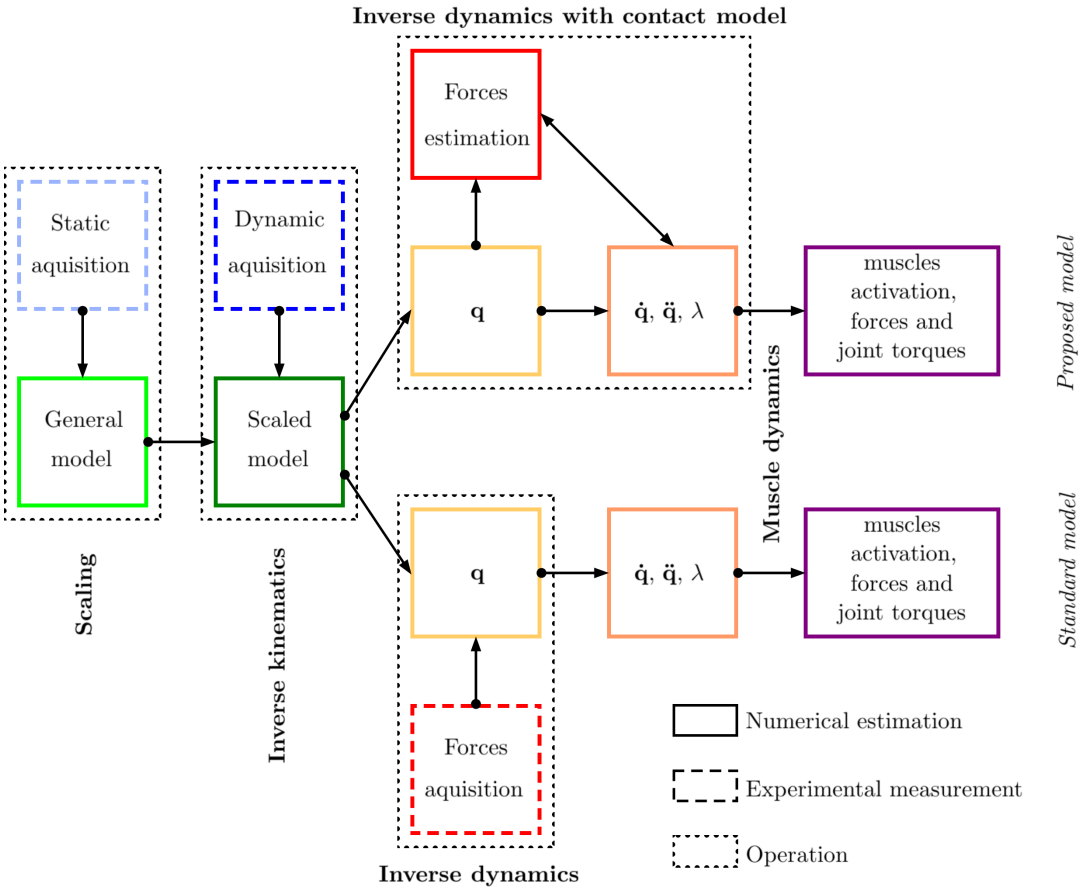

FIGURE 1.1: Proposed and standard inverse dynamics schemes

1.2 Objective of the thesis

Figure 1.1 represents the typical workflow of the inverse dynamics analysis of a biomechanical system. For this type of analysis, the movement is known (generally measured experimentally) and the objective is to estimate the forces at the origin of this movement. For a biomechanical study, these forces can be the joint torques generated by muscle contraction, or more directly the force of contraction of these muscles. It is possible to go further by estimating the activity of the central nervous system which drives the activity of the muscles.

In Figure 1.1, the first step is the definition of a general musculoskeletal model. This comprises segments, rigid or not, assembled by joints, and which may contain muscle models. This model is scaled to the subject via a static experimental measurement. This scaled model can be set in motion on the basis of the motion measured during a kinematic study in order to know the position and relative rotation of each of the segments.

With a standard resolution model, the external ground reaction forces are measured and it is possible to directly define the joint torques without a contact model. However, measuring these forces can be difficult or expensive. The information may also not be complete. In this case, the recourse to a numerical model of contact can be considered. We propose in this thesis to

introduce such a contact model in the musculoskeletal model to find the joint torques and the reaction forces on the ground.

Finally, from the joint torques, it is possible to evaluate muscle forces and activation thanks to the muscle model.

The goal of this thesis research is to develop such a new approach in the inverse dynamics analysis of the human gait in three dimensions. The main purpose is to develop a numerical foot/ground model to estimate properly the ground reaction forces, as well as the muscle activation when an experimental measurement of the ground reaction forces is not available.

Beyond fundamental biomechanical insights, the development of musculoskeletal models and inverse dynamics approaches is strongly motivated by their potential clinical and applied relevance. In particular, such models provide quantitative tools for the assessment of joint and muscle loading in a wide range of contexts. They can support the evaluation of rehabilitation procedures following musculoskeletal injuries, help characterize gait deficiencies associated with neurological disorders such as stroke or Parkinson's disease. They contribute to the analysis and optimization of knee or hip joint prosthesis implantation, and transfemoral and transtibial prostheses, where an accurate estimation of internal efforts is essential for improving comfort, efficiency, and long-term outcomes. Finally, such models can be extended to sport biomechanics, where they offer a framework to investigate performance, injury mechanisms, and loading patterns under realistic movement conditions.

More broadly, reducing the experimental constraints required for force estimation opens perspectives for the analysis of daily-life activities outside laboratory environments, for instance in home-based or ambulatory settings. Such an approach could facilitate the integration of biomechanical analysis into routine clinical practice, enabling the monitoring of patients undergoing rehabilitation, the assessment of gait impairments related to neurological or musculoskeletal disorders, and the evaluation of treatment strategies such as orthopaedic interventions or prosthetic fittings. Beyond clinical applications, the method could also be extended to field-based sport analysis, where laboratory instrumentation is impractical. This would allow the investigation of performance-related movement strategies, fatigue effects, or injury mechanisms, thereby broadening the applicability of musculoskeletal modelling to real-world scenarios.

1.3 Organisation of the thesis

Chapter 2 reviews the fundamental concepts of multibody systems modelling, and the current methods of gait analysis with some background on the terminology of human modelling. A history of the methods of gait analysis is also described, as well as the modern measurement instruments present in the Laboratory of Motion Analysis of the University of Liège.

Chapter 3 describes the experiments carried out in the laboratory in order to establish a set of data useful for the development of our digital model.

These experiences were the opportunity to supervise a student in physiotherapy during his master thesis (Gautier et al., 2016). Typical experimental results are presented for a test of a subject. As this thesis is not a study of walking behaviour, no statistical results are presented.

Chapter 4 refers to the development of our first model for analysing gait in two dimensions. The method and results were published in the Journal of Biomechanics (Van Hulle et al., 2020). The contact is modelled as a set of unilateral constraints and the ground reaction forces is therefore represented by the Lagrange multipliers associated to these constraints. The proposed model relies on the hypothesis that the human body tends to minimize the global set of reactions forces: the least-square evaluation of the Lagrange multipliers provides an estimation of the contact forces between the feet and the ground. The criterion of activation of the contact constraints is inspired by the work of Alart and Curnier, 1991, and relies on the gap measured between the foot and the ground and the estimated value of the local contact force. The position of the centre of pressure (COP) is implicitly defined in terms of the kinematic measurement and the estimated reaction forces.

In Chapter 5, the previously developed model from two dimensions (2D) is extended to a three-dimensional (3D) framework, with the aim of utilizing this model in a comprehensive study of muscle effort estimation. The various assumptions of the 2D model are reviewed, along with their limitations.

In Chapter 6, the 3D contact model is employed within the OpenSim software, a tool commonly used for comprehensive biomechanical studies, to estimate joint torques, muscle activation, and efforts. This comprehensive study highlights the limitations of our model and naturally provides suggestions for future improvement.

Chapter 7 concludes this thesis and proposes some future perspectives.

Chapter 2

Fundamentals and state of the art

In this chapter, fundamental concepts in multibody system dynamics and in biomechanics are first developed.

The human body, from an engineer's point of view, can be considered as a complex multibody system composed of different segments, the limbs, connected together with kinematic joints. The terminology of human motion in general, and various activities, such as gait and run, are described in the second and third sections. A more important focus is put on the human gait, given that it is an activity of capital importance in everyday life, and that many studies already focus on this subject, making it easier to develop and compare models.

A fourth section describes the tools to analyse experimentally the gait and other human motion.

Finally, a fifth section develops different numerical models present in the literature and the basic mathematical and physical knowledge needed to model numerically the human motion.

2.1 Fundamental concepts of multibody systems

A multibody system is an assembly of rigid and/or flexible elements connected by joints and force elements (spring, damper, ...). In this section, we will limit our focus to the concepts of two-dimensional multibody systems. In Figure 2.1, an example of a 2D multibody system is shown. This system is composed of three rigid bodies numbered in Roman numerals. These bodies I and II are interconnected by the joint CD and a spring element FG connects the bodies II and III. The centre of gravity and the orientation of each body is also shown.

Following the finite element terminology (Géradin and Cardona, 2001), the different bodies can be defined in terms of nodes (letters in Figure 2.1). For example, the body I is composed of three nodes A (centre of gravity), B (linked to the ground) and C (linked to the body II). The coordinates of each node of this first body can be expressed either in the fixed inertial frame $\{O, \overrightarrow{E_1}, \overrightarrow{E_2}\}$ or in the body-attached frame $\{O, \overrightarrow{e_{I,1}}, \overrightarrow{e_{I,2}}\}$.

If this system is subjected to a set of external forces, its equation of motion is expressed in the generic form of differential algebraic equations (Angeles

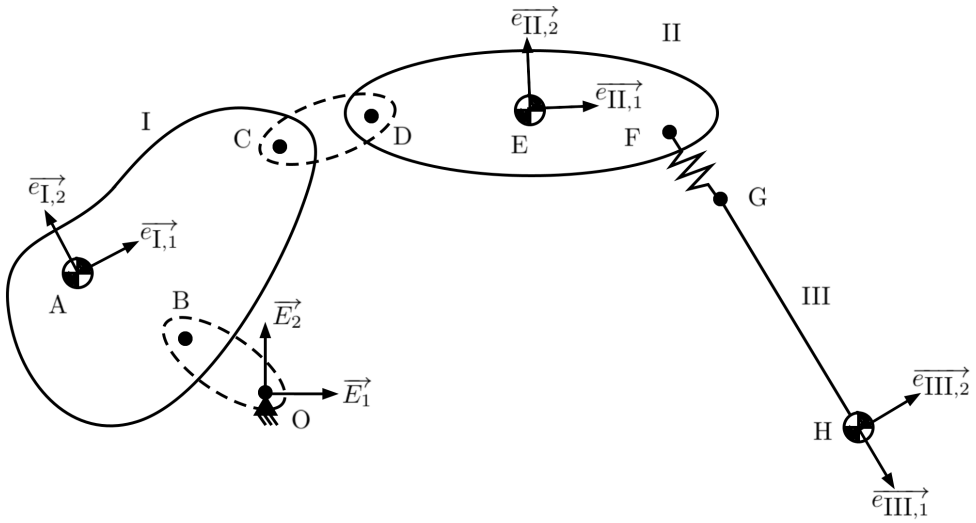

FIGURE 2.1: 2D multibody system

and Kecskeméthy, 1995), (Géradin and Cardona, 2001):

$$\mathbf{M}(\mathbf{q})\ddot{\mathbf{q}}+\mathbf{f}^{gyr}(\mathbf{q},\dot{\mathbf{q}})+\mathbf{f}^{damp}(\mathbf{q},\dot{\mathbf{q}})+\mathbf{f}^{int}(\mathbf{q})+\mathbf{g}_{\mathbf{q}}^{\mathrm{T}}\boldsymbol{\lambda} = \mathbf{f}^{ext}(t)+\mathbf{A}(\mathbf{q})\mathbf{f}^{act}(t) \quad (2.1)$$

$$\mathbf{g}(\mathbf{q}) = \mathbf{0} \quad (2.2)$$

where $\mathbf{q}$ is the vector of generalized coordinates, $\mathbf{M}$ is the mass matrix, $\mathbf{f}^{gyr}$ is the vector of gyroscopic forces (centripetal and Coriolis), $\mathbf{f}^{damp}$ is the vector of damping forces, $\mathbf{f}^{int}$ is the vector of internal forces, $\mathbf{g}$ and $\mathbf{g_q}$ the vector of kinematic constraints and its gradient matrix, $\boldsymbol{\lambda}$ is the vector of Lagrange multipliers representing the reaction forces associated with the constraints, $\mathbf{f}^{ext}$ is the vector of external forces, $\mathbf{f}^{act}(t)$ is a vector of applied actuator forces and torques and $\mathbf{A}$ is the incidence matrix of the actuators.

Equation (2.1) represents the dynamic equilibrium of the multibody system. It represents the balance between all the forces acting on the system (internal and external) and the dynamic effect of the acceleration. Equation (2.2) represents the constraints acting on the system, here at the position level. These constraints are based on the body conditions (rigid, flexible,...), the type of joints,... Mathematically speaking, the equations of motion are usually highly non linear and have a large number of degrees of freedom.

It is possible to solve the equations of motion of a mechanism, and based on the unknown parameters (position/velocity/acceleration or the forces), the problem will be qualified as a direct dynamic problem or an inverse dynamic analysis, as depicted in Figure 2.2.

2.1.1 Direct dynamic problem

For a direct dynamic problem, excepted for the reaction forces, the forces acting on the system are known, either over time, or as a function of the position/velocity of some given component. The objective of this kind of simulation is therefore to find the configuration (position/velocity/ acceleration) of

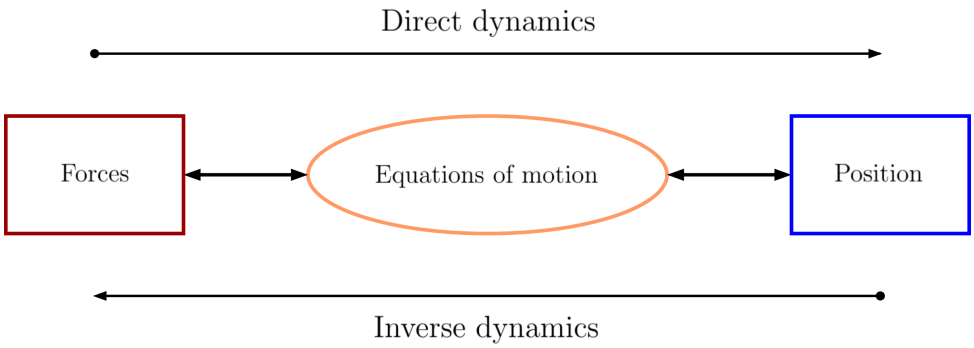

FIGURE 2.2: Direct and inverse dynamics

the system over time as a function of an initial configuration and the known forces.

To solve this kind of problem, one uses time integrators with the initial configuration as a starting point in order to establish the solution, time step by time step. There are two main time integrator families: explicit and implicit schemes, that we shall briefly introduce for systems without constraints.

The explicit schemes compute the configuration of the system at a given time step only according to previous time steps. For example, the explicit Euler method is written as:

$$\mathbf{y}_{i+1} = \mathbf{y}_i + h\mathbf{f}(\mathbf{y}_i, t_i) \tag{2.3}$$

where $\mathbf{f}$ represents the non linear differential equations linked to the dynamic equilibrium, and h is the numerical time step. The resolution method is generally quite straightforward, easy to implement and not demanding in terms of numerical resources. However, these methods are subject to exponential numerical instabilities, which therefore do not allow long simulations with many degrees of freedom to be carried out.

The implicit schemes solve the problem iteratively. To compute the configuration of a given time step, it is necessary not only to use the configuration of the system in the previous time step but also the current value of the configuration of the calculated time step:

$$\mathbf{y}_{i+1} = \mathbf{y}_i + h\mathbf{f}(\mathbf{y}_i, \mathbf{y}_{i+1}, t_i) \tag{2.4}$$

Given their iterative nature, these methods are slower and more expensive in terms of numerical resources. However, they have the advantage of greatly reduce the instabilities in the computed solutions. These schemes are thus more adequate for long simulations with numerous degrees of freedom. Depending on the degree of accuracy sought and the numerical damping requested, several schemes exist, such as the generalized-α method, for example, or more particular cases of this method, such as Newmark, Hilbert-Hugues-Taylor or even Chung-Hulbert.

Relevant software on the market to solve direct dynamic problems are RecurDyn, MSC Adams, NX Simcenter and the Samcef Mecano (now included

in Siemens/Simcenter).

2.1.2 Inverse dynamic analysis

Conversely to the direct dynamic problems, inverse dynamic analysis aims to find the forces at the origin of a known motion (position, velocity and acceleration). Motion is usually measured experimentally to obtain the vector of generalized coordinates. This vector can later be derived to obtain the velocity and acceleration vectors.

In Equation (2.1), the gyroscopic forces $\mathbf{f}^{gyr}$, the damping forces $\mathbf{f}^{damp}$, the internal forces $\mathbf{f}^{int}$ and the external forces $\mathbf{f}^{ext}$ are expressed as function of the positions and/or velocities, which leads to a straightforward evaluation of those forces. The remaining unknowns are the actuator forces $\mathbf{f}^{act}$ depending on time and the Lagrange multipliers $\boldsymbol{\lambda}$.

The formulation of the constraints can change between the direct and inverse dynamic analyses. If an actuator motion is imposed, for example a constant rotation around an axis, translation along a rail on a machine or a rotation of a limb around a joint in a biomechanical body, a driving bilateral constraint is added to the system. If the movement is measured but is not controlled by an actuator (as in the case of a pendulum for example), then the movement is considered as free and no additional bilateral constraint should be taken into account in the model. When an actuator is modelled as a driving constraint, the associated Lagrange multiplier represents the force or the torque necessary for the actuator to impose this movement on the system. This means that the applied actuator forces $\mathbf{A}(\mathbf{q})\mathbf{f}^{act}(t)$ present in the direct dynamic model are substituted by a contribution of Lagrange multipliers of the driving constraints in the inverse dynamic model. Equations (2.1) can be adapted:

$$\mathbf{M}(\mathbf{q})\ddot{\mathbf{q}}+\mathbf{f}^{gyr}(\mathbf{q},\dot{\mathbf{q}})+\mathbf{f}^{damp}(\mathbf{q},\dot{\mathbf{q}})+\mathbf{f}^{int}(\mathbf{q})+(\mathbf{g_q}^{bilat})^{\mathrm{T}}\boldsymbol{\lambda}^{bilat}+(\mathbf{g_q}^{driving})^{\mathrm{T}}\boldsymbol{\lambda}^{driving} = \mathbf{f}^{ext}(t) \quad (2.5)$$

$$\mathbf{g}(\mathbf{q},t) = \mathbf{0} \quad (2.6)$$

With the set of constraints $\mathbf{g}$ including bilateral constraints dependent on the generalized coordinates, and driving constraints explicitly dependent on time:

$$\mathbf{g} = \begin{bmatrix} \mathbf{g}^{bilat}(\mathbf{q}) \\ \mathbf{g}^{driving}(\mathbf{q},t) \end{bmatrix} \quad (2.7)$$

And the associated Lagrange multipliers:

$$\boldsymbol{\lambda} = \begin{bmatrix} \boldsymbol{\lambda}^{bilat} \\ \boldsymbol{\lambda}^{driving} \end{bmatrix} \quad (2.8)$$

To solve the equations of motion for the extended set of Lagrange multipliers, Equation (2.5) has to be inverted. However, depending on the number of degrees of freedom, constraints, and actuators, the problem can be under- or overdetermined, so that a unique solution is not always achievable. A

unique solution can still be found by introducing hypotheses to remove the indetermination, such as minimizing the forces or the energy of the system.

2.1.3 Contacts

The study of contacts between bodies or with the ground is frequent in multibody dynamics analysis.

In direct dynamics, contact models make it possible to define the change of momentum, and to define the trajectory of the various bodies after the impact. In inverse dynamics, it is the contact forces which are generally sought after.

To represent mathematically a contact condition using a rigid body assumption, there are two main families of methods: compliant and rigid contact models, depicted in Figure 2.3.

Compliant contact model

Compliant contact models allow a penetration of the different bodies which may represent some unmodelled deformations. On Figure 2.3, in blue, the ball bounces on the ground and a penetration is computed. An equivalent stiffness and damping coefficient are associated to the contact model to represent the contact force as a function of the penetration amplitude and the penetration velocity during the impact process. Mathematically, for example, the contact force is:

$$\text{if} \quad y_A > r \quad \text{then} \quad f_A^{cont} = 0 \tag{2.9}$$

$$\text{if} \quad y_A \leq r \quad \text{then} \quad f_A^{cont} = -k(y_A - r) \tag{2.10}$$

where f_A^{cont} is the contact force, k is the contact stiffness, y_A the vertical position of the ball and r its radius. If necessary, damping effects can be taken into account (Lankarani and Nikravesh, 1994).

In the equations of motion (2.1) and (2.5), the contact forces can be included as an additional force $\mathbf{f}^{cont}$.

Compliant contact models are often used for direct dynamic problems and the time integrator algorithm will iterate at each time step to compute the dynamic equilibrium of the system. The contact stiffness has to be determined if compliance exists, but is generally chosen very high to approach the assumption of rigid bodies and prevent unphysical penetrations. This can have numerical consequences, like the creation of a ill-conditioned stiffness matrix, or the need to use of a very small time step. Choosing a stiffness coefficient based on physical properties can therefore lead to numerical issues, while alternative choices result in non-physical behaviour.

If used in inverse dynamics analyses, the penetration/deformation should be measured, which is generally beyond what cameras can capture today. This is why a rigid contact model was preferred in this work.

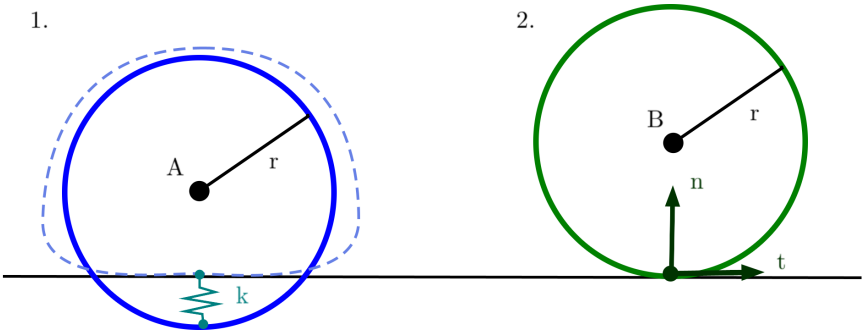

FIGURE 2.3: Bouncning balls: compliant contact model (1. blue), rigid contact model (2. green)

Rigid contact model

Unlike compliant contact models, rigid contact models do not allow penetration. The contact is this time represented by a unilateral constraint of non-penetrability between the bodies (Chen et al., 2013). In Figure 2.3, on the right, the bouncing ball is not allowed to penetrate the ground and one can distinguish two axes: normal and tangent to the contact surface (we still limit ourselves to 2D models for the moment). The coordinates in the horizontal (tangential) and vertical (normal) directions are x_B and y_B.

The contact on the normal axis is represented by a unilateral constraint, and is mathematically transcribed by:

$$\mathrm{g}^n(\mathbf{q}) = y_B \geq 0, \quad \lambda^n \geq 0, \quad \mathrm{g}^n(\mathbf{q})\lambda^n = 0 \tag{2.11}$$

where g^n is the normal unilateral contact constraint and λ^n is its associated Lagrange multiplier representing the normal contact force. Equation (2.11) is a complementarity equation representing the fact that either the contact is inactive ($g > 0$, a gap is present) and therefore there can not be any contact force ($\lambda = 0$), either the contact is active ($g = 0$, no gap is present) and the contact force can be positive (assuming that a normal contact force can only be repulsive). Equation (2.11) can also be written as:

$$0 \leq \mathrm{g}^n \quad \perp \quad \lambda^n \geq 0 \tag{2.12}$$

On the tangential axis, when contact occurs, either the two bodies slide on each other and the contact is said to be slipping, or the relative tangent velocities is null and the contact is sticking. Depending on the type of contact, different sets of equations will have to be applied. For example, in the Coulomb's friction law, the sticking conditions are expressed as:

$$\dot{\mathrm{g}}^t(\mathbf{q}) = \dot{x}_B = 0 \quad \text{and} \quad \lambda^t \leq \mu\lambda^n \tag{2.13}$$

where λ^t is the tangential contact force and μ is the static friction coefficient.

A rigid contact model does not provide a direct evaluation of the contact forces in contrast to compliant contact models. To obtain these values, the

equation of motion must be solved. In Equations (2.1) and (2.5), the contact terms will appear in the constraints and in their associated Lagrange multipliers. Depending on the problem, direct or inverse dynamics, the solution method will be different and some other new parameters might be necessary.

In direct dynamics, the expression of the unilateral constraints are sufficient to prevent the penetration of the bodies. However, nothing allows us to predict the behaviour of the bodies after the impact, and an impact law has to be taken into account. For example, a Newton impact law can be used to define the post-impact velocities of the bodies based on the pre-impact velocities and a coefficient of restitution. Mathematically:

$$\dot{g}^n(t^+) = e\dot{g}^n(t^-) \tag{2.14}$$

where $\dot{g}^n$ is the normal gap velocity vector (time-derivative of the normal gap), t^- and t^+ the instants of pre- and post-impact respectively and e the coefficient of restitution. In this case, the coefficient of restitution must be in the interval $[0; 1]$, where 0 represents a completely inelastic shock (all the energy is dissipated) and 1 a completely elastic one (all the energy is transferred). With this new information, a time integrator can compute the positions and velocities of every body, time step by time step.

In inverse dynamics, an impact law is not required because the motion is measured thus known before and after the impact. The size of the constraints vector will change from time step to time step and redundant constraints may appear. This can lead to an absence or an infinity of solutions. Some hypotheses will have to be made to be able to solve the equations of motions or to pick a preferred solution. Depending on the system or activity, the hypotheses can vary largely, and we will describe the most commonly used ones in biomechanics in the next section.

2.2 The human body as a multibody mechanism

To be able to study the equations of motion of the human body, it is essential to first model the human body and therefore establish the terminology commonly used in biomechanics. Also, in this section, the extension to 3D models is considered, in particular, the representation of finite rotation in 3D is addressed.

2.2.1 Anatomical reference position, planes and axes of the human body

The human body is defined with respect to three reference planes and six axes passing by the global centre of mass. These planes and axes are defined using anatomical points corresponding to a reference anatomical position of the human body: standing up, feet and knees facing front, arms along the trunk and forearm in supination, as can be seen in Figure 2.4. The transverse plane divides the body into upper and lower parts of equal mass, is parallel to the ground plane and perpendicular to the superior/inferior axis.

The frontal plane divides the body into front and back parts of equal mass, and is perpendicular to the anterior/posterior axis. Finally, the sagittal plane divides the body into right and left parts of equal mass, and is therefore perpendicular to the right/left axis.

When describing a single limb, these same planes and axes are used around the centre of gravity of this particular limb with a similar approach. The extremities of a limb are named according to their position from the global centre of mass. The proximal extremity is the closest to the global centre of mass of the body, while the distal extremity is the furthest.

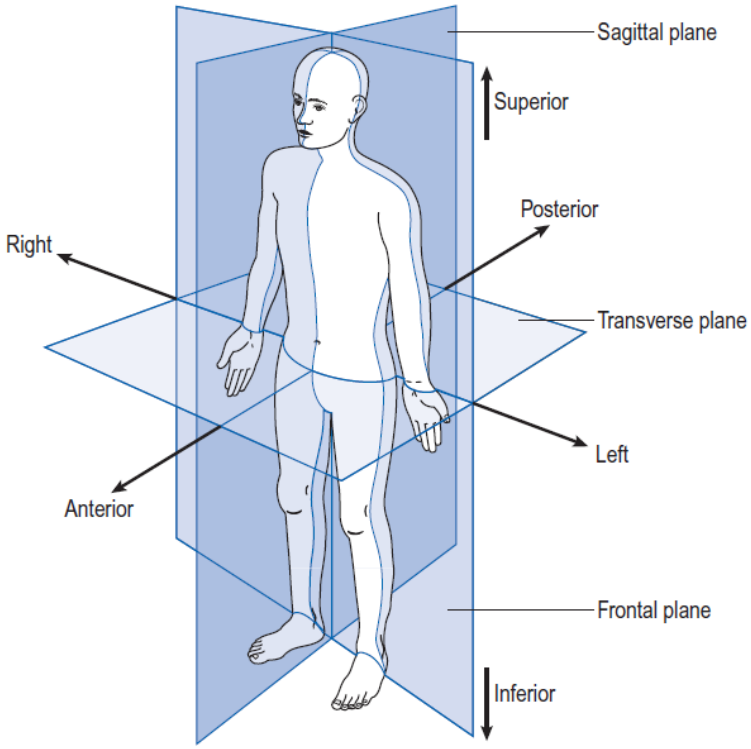

FIGURE 2.4: The anatomical position, with three reference planes and six fundamental directions (Whittle, 2007)

2.2.2 Defining the angles

To define the angular position of a multibody system, such as the human body, it is possible to use absolute angles, with respect to a fixed frame of reference, or relative angles between the bodies. For the human body, these relative angles are called joint angles. These two types of angles are related to each other, as we will show.

Orientation angles

In three dimensions, the absolute angles are defined as a combination of three successive rotations around the centre of gravity of the segment, with respect to an inertial reference frame (usually taken parallel/perpendicular to the

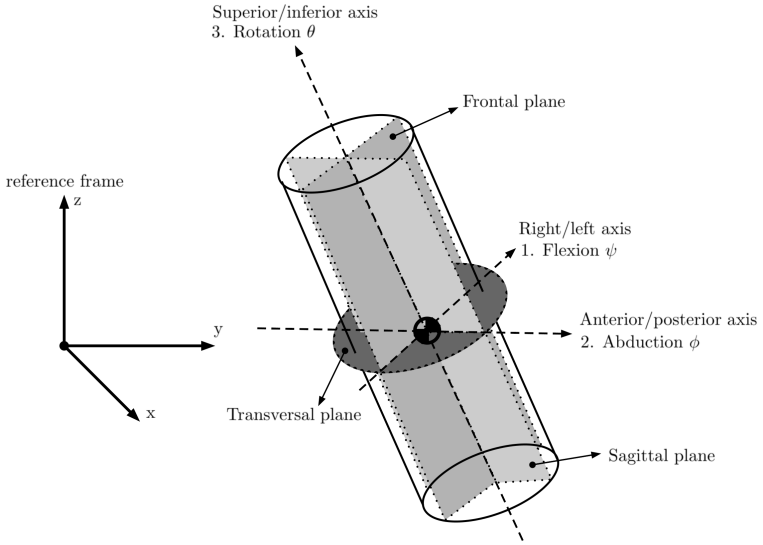

FIGURE 2.5: Absolute angles of a single limb

ground). Considering the reference planes of the studied limb, the combination of rotations is composed of the flexion/extension ψ in the sagittal plane first, then the abduction/adduction ϕ in the frontal plane and finally the external/internal rotation θ in the transverse plane, as seen in Figure 2.5. This sequence of rotations is a variation of the Bryant angles, a parametrization widely used in aeronautical, mechanical or nautical applications.

It should be noted that the choice of orientation parametrization is an important subject. The proposed approach based on a sequence of three rotations about predefined axes leads to singularities when $\phi = \frac{\pi}{2} + k\pi$. However, in the specific case of human walking, which is predominantly a sagittal-plane motion with moderate adduction/abduction amplitudes, the selected parametrization does not encounter singular configurations and remains well suited for the intended analyses. As such, this representation provides a good compromise between interpretability, numerical stability, and adequacy for the studied movement. More general representations, such as quaternions, may be preferable in other contexts, particularly to avoid singularities in motions involving large 3D rotations.

The absolute angles thus give the relation of a free vector attached to the limb expressed in the reference configuration by the variable $\mathbf{\Delta X}$ and in the current configuration by the variable $\mathbf{\Delta x}$. Mathematically, this relation is given by:

$$\Delta \mathbf{x} = \underbrace{\begin{bmatrix} \cos\psi\cos\phi + \sin\psi\sin\phi\sin\theta & \sin\psi\sin\phi\cos\theta - \cos\psi\sin\theta & \sin\psi\cos\phi \\ \cos\phi\sin\theta & \cos\phi\cos\theta & -\sin\phi \\ \cos\psi\sin\phi\sin\theta - \sin\psi\cos\theta & \cos\psi\sin\phi\cos\theta + \sin\psi\sin\theta & \cos\psi\cos\phi \end{bmatrix}}_{=\mathbf{R_{abs}}} \Delta \mathbf{X} \tag{2.15}$$

where $\mathbf{R}_{abs}$ is the rotation matrix corresponding to the sequence.

Relative angles

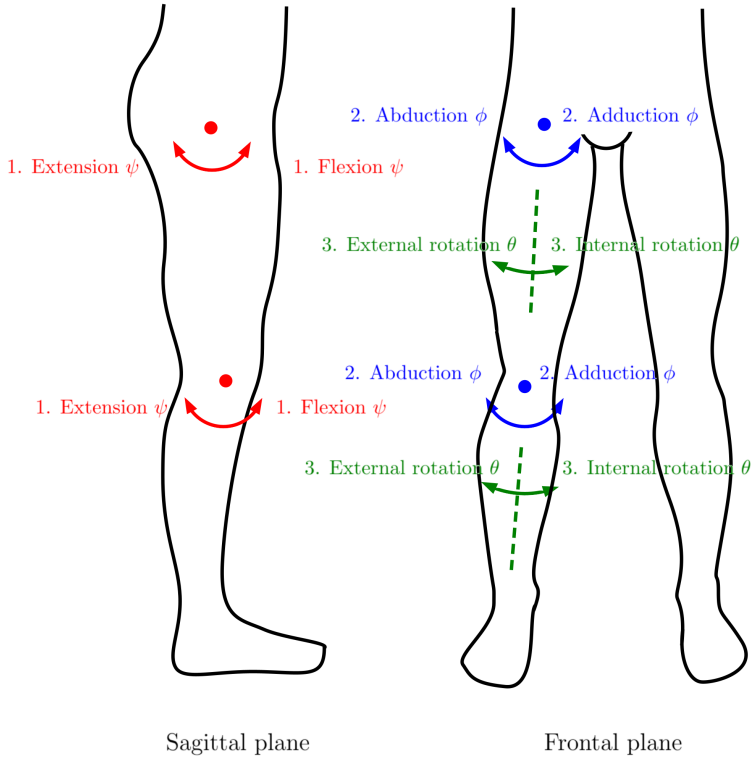

FIGURE 2.6: Motion and rotation around the hip and knee joints

More than the absolute orientation of a limb, it is often useful to have an expression of the relative joint angles between two consecutive limb, as shown in Figure 2.6. The parametrization of this relative rotation relies on the flexion/extension ψ, then the abduction/adduction ϕ and finally the external/ internal rotation θ of the distal segment with respect to the proximal limb.

The relation between the absolute orientation of the proximal and distal limbs, and the relative rotation matrix is based on Equation (2.15) and the fact that the relative rotation is the orientation of the distal limb with respect to the local proximal limb frame:

$$\mathbf{R}_{abs,proximal}^{\mathrm{T}}\mathbf{R}_{abs,distal} = \mathbf{R}_{rel} \tag{2.16}$$

Having the absolute orientation of each limb, the relative rotation $\mathbf{R}_{rel}$ can be evaluated using Equation (2.16), and the relative joint angles corresponding to this matrix can then be extracted.

2.2.3 Representing the human body in terms of nodes and coordinates

To describe the motion of a multibody system, relative or absolute coordinates can be chosen (Géradin and Cardona, 2001). For biomechanical problems, relative independent coordinates $\mathbf{q}(t)$ (e.g. joints relative angles and

pelvis position and orientation) are usually used (Uchida and Delp, 2021; Nasr and McPhee, 2025), and no bilateral constraint needs to be considered in the equations of motion (Equation (2.1) and (2.2)).

Absolute coordinates can also be chosen: compared to relative coordinate formulations, this approach leads to simpler equations of motion and a straightforward evaluation of the reaction forces in the bodies and joints, which are represented by the Lagrange multipliers. For applications in biomechanics, absolute generalized coordinates $\mathbf{q}(t)$ can include the spatial coordinates of the extremities and of the centre of mass of each segment, the absolute orientation angles of each segment, and the relative joint angles between two consecutive segments.

2.3 Description of the motion

2.3.1 Generalities

Human movements are varied and complex. Each joint behaves differently and the number of degrees of freedom is large. Depending on the activity, some simplifications will be possible. For example, walking or running are essentially two-dimensional activities, the spine can generally be simplified as a single body (the trunk), etc.

Before dealing in more detail with certain activities such as the gait, the degrees of freedom of each joint of the lower limb will be presented as well as their usual modelling.

Description of the lower limb

Usually, the centre of gravity is linked to the pelvis. This part of the body is often used as the main reference to localize and define the position of the human body and motion under study. A reference is always needed to position a multibody system in space, using either fundamental, relative or absolute coordinates.

Most of the numerical models used to analyse motion represent the pelvis and the bones as rigid bodies (Winter, 2009). Notice that some other studies used finite element methods to fully model the bone deformation due to the tendons and muscles (Phillips et al., 2007). In this thesis, the rigid body assumption is made for the bones and more details will be provided in Chapters 4 and 5.

A shown in Figure 2.7, the lower limb of the human body is subdivided in three main parts: the thighs, the legs and the feet (Spägele et al., 1999). The foot can be subdivised again into two parts: the midfoot and the toes. Each segment comprises one or several bones and can usually be represented as a rigid body. Between each segment, a joint constrains the relative motion.

The hip joint (or acetabulofemoral joint) is a ball-and-socket, so that the spherical head of the femur is able to rotate in the acetabulum of the pelvis. This joint has three degrees of freedom in rotation: flexion/extension, abduction/adduction, and internal/external rotation. Twenty-two groups of

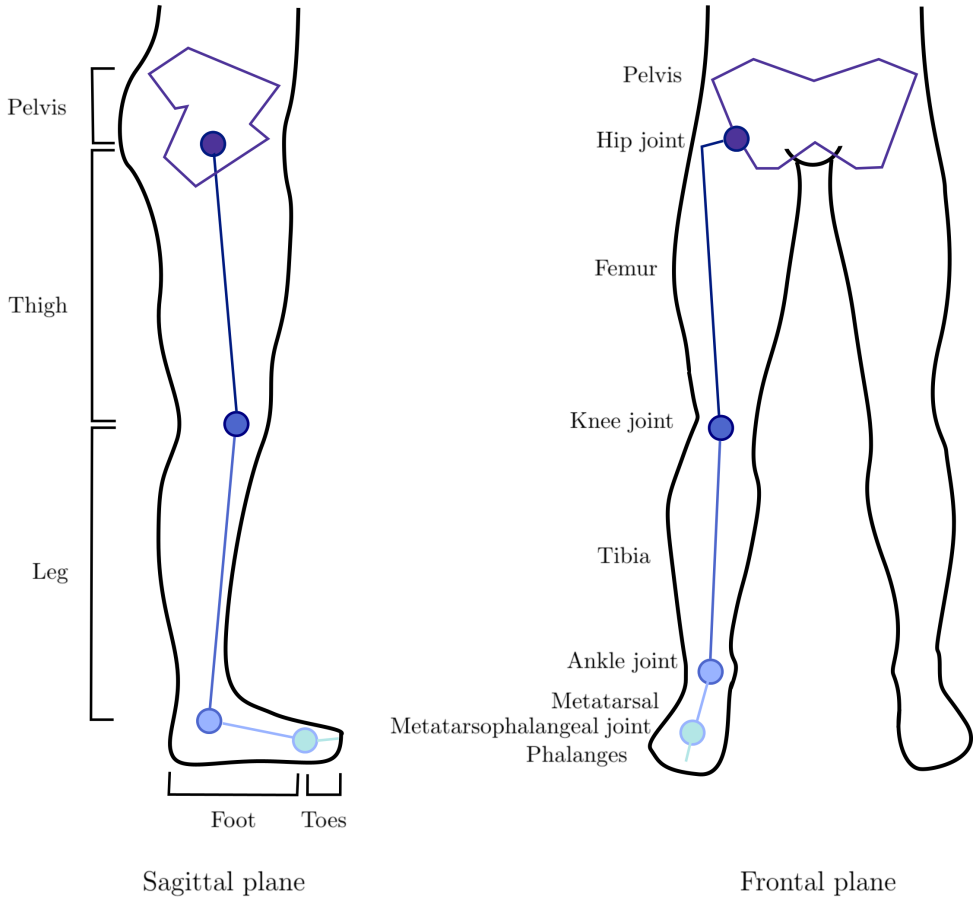

FIGURE 2.7: Bodies, bones and joints of the lower limbs

muscles control the hip joint (Byrne et al., 2010). In the literature, spherical joints are the most common model used to represent the hip (Anderson and Pandy, 2001; Taylor et al., 2004). More complex models have also been proposed, as in (Anderson, 2007).

The knee joint is a modified hinge joint, composed of two parts: the tibiofemoral joint (between the femur and the tibia) and the patellofemoral joint (between the femur and the patella). This combination of closely spaced joints allows mainly the flexion/extension of the knee, while controlling a slight internal/external rotation. In the literature, the knee joint is often represented as a hinge joint in 2D (Xiang et al., 2011), or a constrained spherical joint in 3D (Arnold et al., 2010). More advanced models do exist, as in (Wismans et al., 1980; Richard et al., 2016).

The ankle joint is a complex mechanism that includes three separate joints: the talocrural joint (hinge joint between the tibia and the talus), the subtalar joint (plane joint between the talus and the calcaneus), and the inferior tibiofibular joint (surface joint between the tibia and the fibula). This assembly allows a three degrees of freedom rotation (flexion/extension, adduction/abduction, internal/external rotation). The ankle joint, as a whole, can be modelled in two dimensions as a simple hinge (Pàmies-Vilà et al., 2018), or as four-bar linkage (Leardini et al., 1999). In three dimensions, the ankle joint can be represented by a spherical joint (Koopman et al., 1995), or by a more accurate representation as in (Delp et al., 1990; Mok et al., 2011; Carbone et al., 2015).

Finally, the metarsophalangial joints are condyloid joints that allow three constrained rotation between the midfoot to the toes. When all the toes are modelled as one, the metarsophalangial joint is either represented as a hinge joint (Delp et al., 1990), or as a constrained spherical joint (Koopman et al., 1995). An interphalangeal joint connects each bone of the toes. The interphalangeal joint acts as a hinge joint. The toes and the interphalangeal joints are usually not modelled for global motion studies (as gait, etc).

2.3.2 Normal healthy gait

Walking is the most common activity of everyday life. It involves the lower limbs and, to a lesser extent, the upper limbs which will keep the body in balance by acting as a (inverted) pendulum.

In the literature, many studies describe it and interpret all the parameters affecting it. It seemed interesting to us to start with a study of healthy human gait in order to be able to base ourselves on other research and to establish a first numerical skeletal model.

Describing healthy gait patterns and parameters is important as they will represent the standard behaviours and properties needed in gait analysis, and deviation will be estimated based on that.

Terminology of the gait cycle

The gait is usually presented as a cycle consisting in two consecutive steps, starting with the heel strike of one foot and ending with the heel strike of the same foot, as depicted in Figure 2.8. For a given leg, the gait cycle is divided into two phases: the stance phase (the foot is in contact with the ground) and the swing phase (the foot is not in contact).

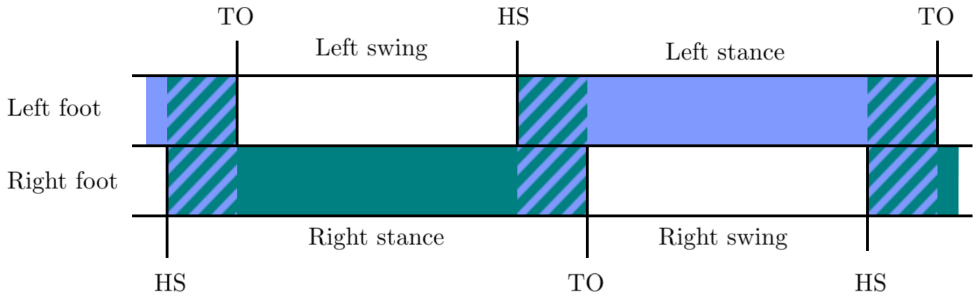

FIGURE 2.8: Timing of single and double support during one gait cycle, starting with right initial contact. HS: heel strike, TO: toe off, green: right support; blue, left support.

The gait cycle begins with the right foot initial contact, and the double support reception phase (10% of the duration). The following phase is the single support stance phase (40%). The other foot takes off and the centre of gravity of the human body moves forward. The next phase is the double support propulsion phase (10%). The other foot touches the ground and begins its reception phase. During this phase the reference foot pushes the centre of gravity forward to keep moving. Finally, the reference leg enters the swing phase (40%) where it oscillates and prepares for the landing and reception phase, beginning a new cycle.

Based on this sequence, several contact events are commonly identified: the heel-strike, the toe-strike, the heel-off and the toe-off. To these events one may add the metatarsal-strike (resp. off), when the metarsophalangial joint between the foot and the toes lands on (resp. takes off) the ground.

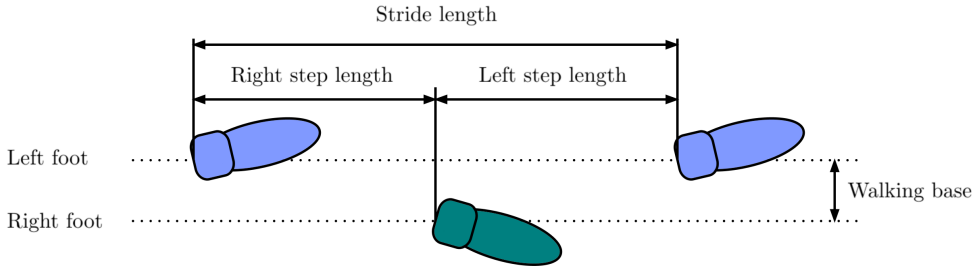

FIGURE 2.9: Geometrical parameter of the stride

Finally, the stride length is defined as the distance covered in one gait cycle, and a step as the distance between two consecutive heel-strike contact points, as in Figure 2.9. The walking cadence is the number of gait cycle per second and the walking speed is the product between the cadence and the stride length.

The stride length and the stance phase duration are correlated to the walking speed as shown in Figure 2.10 (Stoquart et al., 2008).

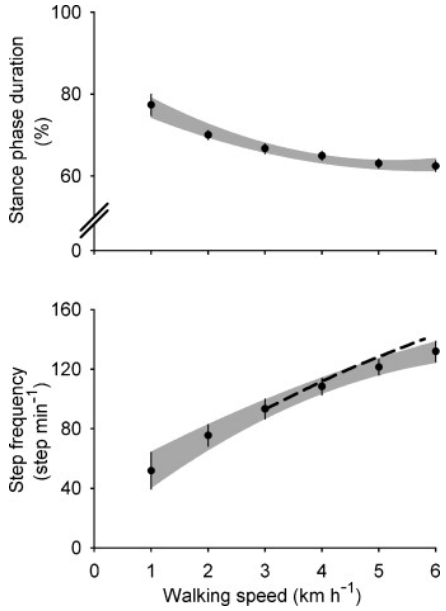

FIGURE 2.10: Stance phase duration (% of gait cycle time, upper graph) and the step frequency as a function of walking speed. Data from (Oberg et al., 1993) (obtained on the ground) are shown by the dash line.(Stoquart et al., 2008)

Kinematics of the gait cycle

The angles in the sagittal plane of the hip, the knee and the ankle are shown in Figure 2.11. The gait is a mainly two dimensional motion, in the sagittal plane.

Dynamics of the gait cycle

As mentioned previously, several types of forces act on the human body during a gait cycle: external forces, internal forces, inertial forces and reaction forces.

External forces The external forces are the weight acting on the whole human body (constant) and the ground reaction forces (GRF) acting on the feet when contact occurs, and only depends on the repartition of masses among the different limbs of the body.

The centre of pressure is the point where the moment of all the contact forces acting on the foot is null, and its path is shown in Figure 2.12. The centre of pressure moves forward along the foot during the gait: its initial position corresponds to the heel at the initial contact with the ground and the final position corresponds to the hallux when it leaves the ground. The trajectory of the centre of pressure goes to the external side of the foot to maintain balance during the gait.

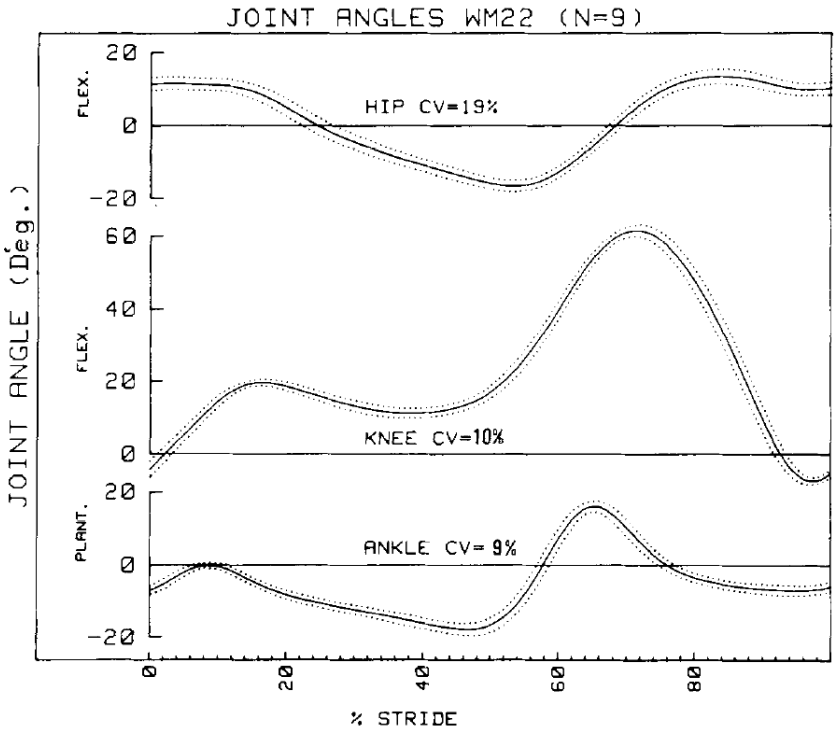

FIGURE 2.11: Sagittal plane joint angles (degrees) during a single gait cycle of right hip, knee and ankle. (Winter, 1984)

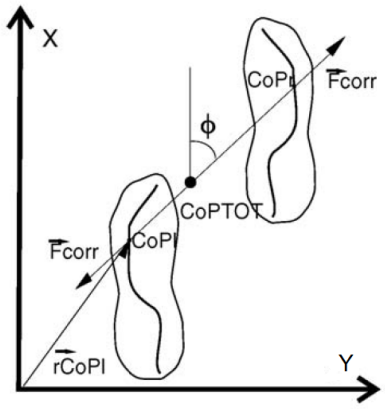

FIGURE 2.12: View of the walking surface from above, showing the centre of pressure, adapted from (Forner-Cordero et al., 2006)

The ground reaction force resultant (Figure 2.13) acts on the centre of pressure (Figure 2.12). They can be measured experimentally, estimated or numerically computed, as will be shown in Sections 2.4 and 2.5.

As can be seen on Figure 2.13, the main component of the ground reaction forces is on the vertical axis (Marasovič et al., 2009). The component is always positive: this force is repulsive and the foot can not penetrate the ground. At the heel-strike, the force starts from zero, and increases rapidly after that. The full-body weight is reached at the toe-off of the other foot (the beginning of the single-support phase). The force continues to increase due to inertia effects and reaches its maximum at approximatively 107% of the body weight - depending on the walking speed. The vertical ground reaction forces decreases slowly to reaches 85% of the body weight. As the human body moves forward, its centre of gravity experiences an acceleration downward: the human body is "falling". Before being in complete imbalance, the body pushes forward and upward, and a second peak similar to the first one is visible. The second foot heel-strike occurs and the value of the contact force falls to zero at the toe-off.

The fore-aft component comes second in terms of amplitude. At the heel-strike, the contact force is equal to zero. It increases to reaches 20% of the body-weight as the single-contact phase begins. The force is positive: the body is decelerating and the foot is prevented to slip forward, it is the reception phase. As the body is moving forward and "falls" forward, the fore-aft component decreases and goes back to zero when the heel rises. The force becomes negative (propulsion phase) and the human body is pushed forward. It reaches its minimum at the end of the single support phase, and decreases back to zero at the toe off.

The lateral component has the smallest amplitude : between 5 and 10% maximum, depending on the subject and the walking speed. This component tends to vary more from one subject to another, due to the variation in the gait patterns. It is usually oriented towards the internal side of the human body, the feet being generally placed slightly outside to maintain lateral balance during gait.

Actuator forces In biomechanics, the actuator forces are the forces exerted by the muscles to generate joint torques. A group of muscles works mainly in contraction, therefore there will be at least two different groups of muscles per degree of freedom at each joint (e.g., one for the flexion, and one for the extension). However, in reality, there are many more muscle groups per axis of rotation. According to the literature (Calais-Germain, 2004), the hip has seventeen groups of muscles, the knee has fourteen groups and the ankle has twenty groups that work and contract together in order to achieve the desired motion.

In order to contract and develop a force, a group of muscles has to be activated by the central nervous system. The brain will generate an electrical nerve impulse and a calcium-dependant mechanism in order to generate and control the contraction of the different groups of muscles (Ebashi et al., 1969).

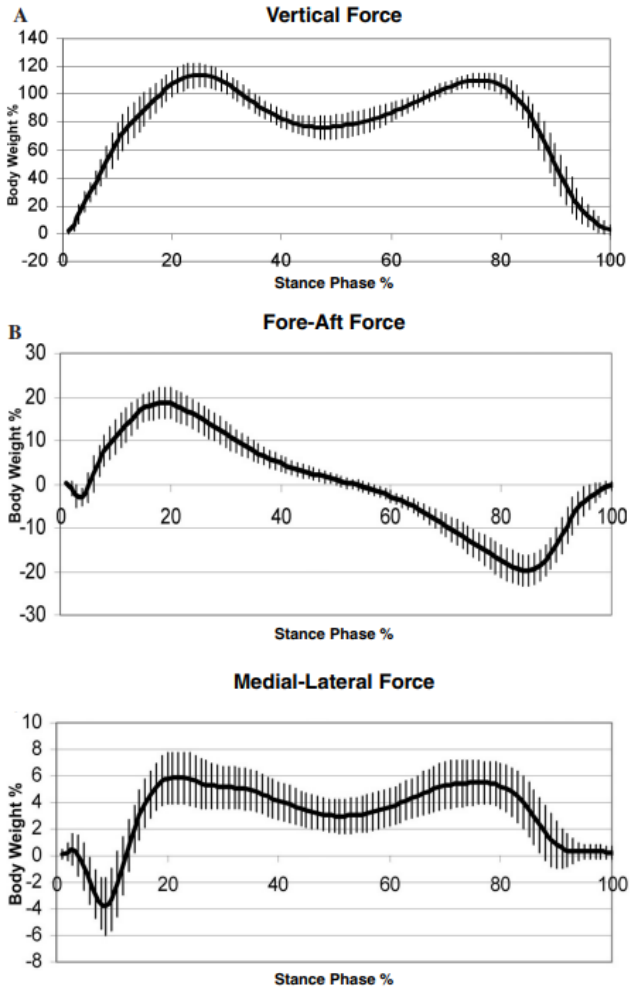

FIGURE 2.13: Vertical, fore–aft and lateral components of the ground reaction force, in % of body weight (Kitaoka et al., 2006)

The joint torques depend on the resultant muscle forces and on the position of the attachment points of tendons and muscle groups around the joint. The application of this torque on the joint then produces the desired motion.

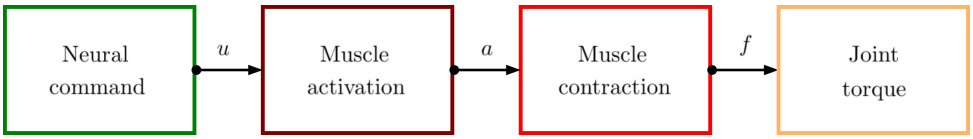

FIGURE 2.14: Schematic view of the muscle contraction principle

Figure 2.14 represents a schematic view of the neural command affecting the motion of the human body. An electromyographic signal is sent by central nervous system to the muscle. Based on this signal, and the type of muscle, the group will activate and contract. This contraction will develop a force, and alongside the external forces acting on the human body, will generate a joint torque, hence a motion. The vast majority of muscle activation models are based on the work of (Hill, 1938), linking the muscle force to the level of activation a and the activation rate $\dot{a}$.

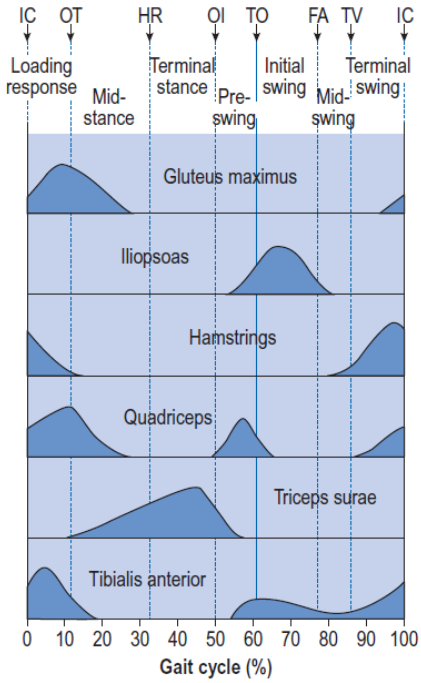

FIGURE 2.15: Typical activity of major muscle groups during the gait cycle (Whittle, 2007)

Usual patterns of muscles activation of the main muscle groups used for gait can be seen in Figure 2.15.

Modelling each muscle group and making the appropriate assumptions to address potential redundancy can be complex or undesirable, depending on the study. In certain cases, although actuator forces are generated by muscle groups, it is possible to simplify the model and assume that the actuator generates the joint torques, as illustrated in Figure 2.14.

Segment	**Segment weight/Total body weight**	**Proximal Centre of mass/Segment length**	**Density**
Foot	0.0145 M	0.5	1.1
Leg	0.0465 M	0.433	1.09
Thigh	0.1 M	0.433	1.05
Head, arms and trunk (HAT)	0.678 M	0.626	-

TABLE 2.1: Anthropometric data based on (Winter, 2009)

Inertial forces The inertial forces appear when a mass is subjected to an acceleration. The magnitude of this force is therefore related to the mass of each limb and to the amplitude of the linear and angular acceleration.

The mass matrix is developed by experimental measurements or with anthropometric tables.

A direct experimental measurement provides a number of subject specific data. However, obtaining the mass, inertia, and centre of mass location of each limb of an alive subject can be time consuming and eventually expensive. Methods have been published to speed up the process of experimental measurements (Hatze, 1975).

However, it is not always possible or necessary to obtain an extremely precise measurement of the anthropometric data of the subject. In this case, one can refer to anthropometric tables, which represent statistical values of mass, inertia and position of the centre of gravity based on macroscopic data of the subject, such as the size, the weight, the diameter of certain limbs, etc. Although the data is not subject specific, these tables have the advantage of giving realistic estimates based on few experimental measurements. An example of an anthropometric table can be consulted at Table 2.1.

Reaction forces The reaction forces represented by some Lagrange multipliers $\boldsymbol{\lambda}$ in Equation (2.1) are related with the constraints imposed on the system. There are several types of constraints acting on the human body.

For example, the length of each body segment (and bone) has to be constant through time, as a consequence of the rigid body hypothesis. The reaction forces related with these "rigid body" constraints are the internal efforts keeping the distance constant. The relative motion of the proximal and distal segments is restricted by the type of joint between them. The reaction forces at the joints will keep the segments attached and ensure an equilibrium with the other forces acting on the body segment, such as the muscle forces.

If a unilateral constraint is used to represent the contact between the foot and the ground, the reaction force enforcing the constraint represents the ground reaction forces.

Summary of forces classification

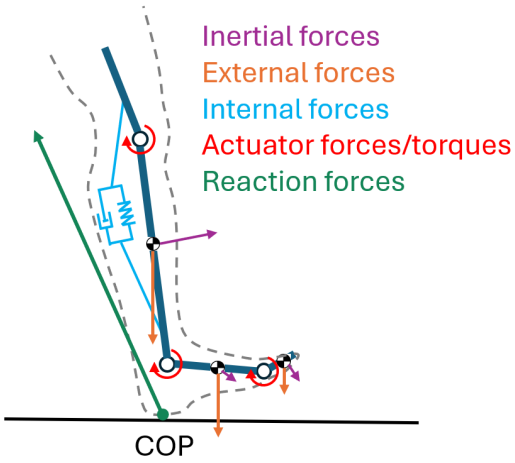

FIGURE 2.16: Free-body diagram of a leg in contact with the ground, showing inertia forces (magenta), external forces (orange), internal forces (cyan), actuator (red), and reaction forces (green)

In summary, the forces discussed in this thesis can be classified into five categories, and are depicted in Figure 2.16.

The first category comprises inertial forces, arising from the acceleration and masses of the various moving segments.

The second category includes external forces, where gravity alone acts on the different segments.

The third category encompasses internal forces, which represent elastic and/or dissipative elements, such as muscles modelled by the Hill model (Hill, 1938), utilized in Chapter 6.

The fourth category consists of actuator forces, which are represented by joint torques in Chapters 4 and 5, or by muscle forces in Chapter 6.

Finally, the fifth category includes reaction forces: the ground reaction forces and torques, as well as the reaction forces and torques at the joints.

When contact is active, the segment in contact is fully constrained. Thus, in 2D, two ground reaction forces and one moment are required to constrain two translations and one rotation, while in 3D, three forces and three moments are necessary to constrain three translations and three rotations.

Joint reactions are essential for constraining relative movements that are restricted by a joint. In 2D, revolute joints generate two reaction forces to constrain translations. In 3D, revolute joints generate three reaction forces and two moments to constrain three translations and two rotations. Spherical joints generate only three forces to constrain the three translations.

In direct dynamics, the actuator forces $\mathbf{f}^{act}$ are given, and one can compute the motion and the reaction forces by solving the equation of motion.

In inverse dynamics, we introduce driving constraints for the relative joints motion. The joint torques are represented by the Lagrange multipliers of the driving constraints of the relative joint motion, but we do not introduce driving constraints and Lagrange multipliers for the pelvis, because there is no related actuator.

2.3.3 Normal healthy running

Running is considered today as one of the most recreational activities performed by people. Studies about running patterns are continuously increasing in importance. This is why it seems judicious to us to define the terminology, the kinematics and the forces at play during a running cycle.

Terminology of the running cycle

According to (Novacheck, 1998) and in Figure 2.17, the evolution from the stand-still to the maximum speed goes as follow. At point *A*, the human body is not moving and both feet are on the ground. There is only one stance phase with double support, and we can not describe this as a cycle strictly speaking. As the walking speed increases, the double support phase tends to become smaller, until point *B*. At this point, there is no more double support phase and this activity is called running. Again, as the velocity increases, periods of double floating (no contact on the ground) increase. At point *C*, the initial contact of the foot on the ground changes from a hindfoot contact to a forefoot contact. In other words, running differs from walking by the absence of a double support phase, and by a generally higher speed of movement.

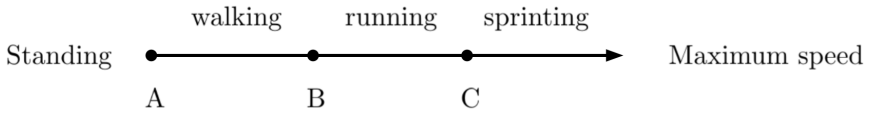

FIGURE 2.17: Difference between walking, running and sprinting

As can be seen in Figure 2.18, as in the gait cycle, we consider the starting moment by the initial contact of a reference foot. The first support phase, proportionally shorter than during a gait cycle, is composed of the reception (the initial contact and the recovery of the equilibrium). This initial contact is usually with the heel for running at lower speed, and with the forefoot for higher speed (sprinting). The second part of this phase is propulsion, when the body pushes forward to continue moving. The next stage is a phase of double floating where both feet are in the air without any contact with the ground. The cycle ends with the support phase of the opposite foot and a new double floating phase.

Kinematics of the running cycle

The angles in the sagittal plane of the hip, the knee and the ankle are shown in Figure 2.19 for different conditions of running (inclined, and level). Running is a mainly two dimensional motion, in the sagittal plane. Generally

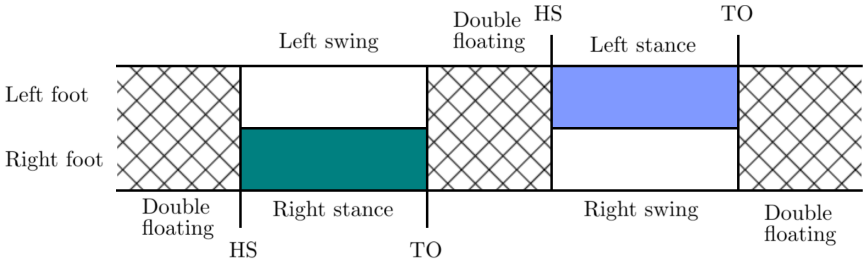

FIGURE 2.18: Running cycle

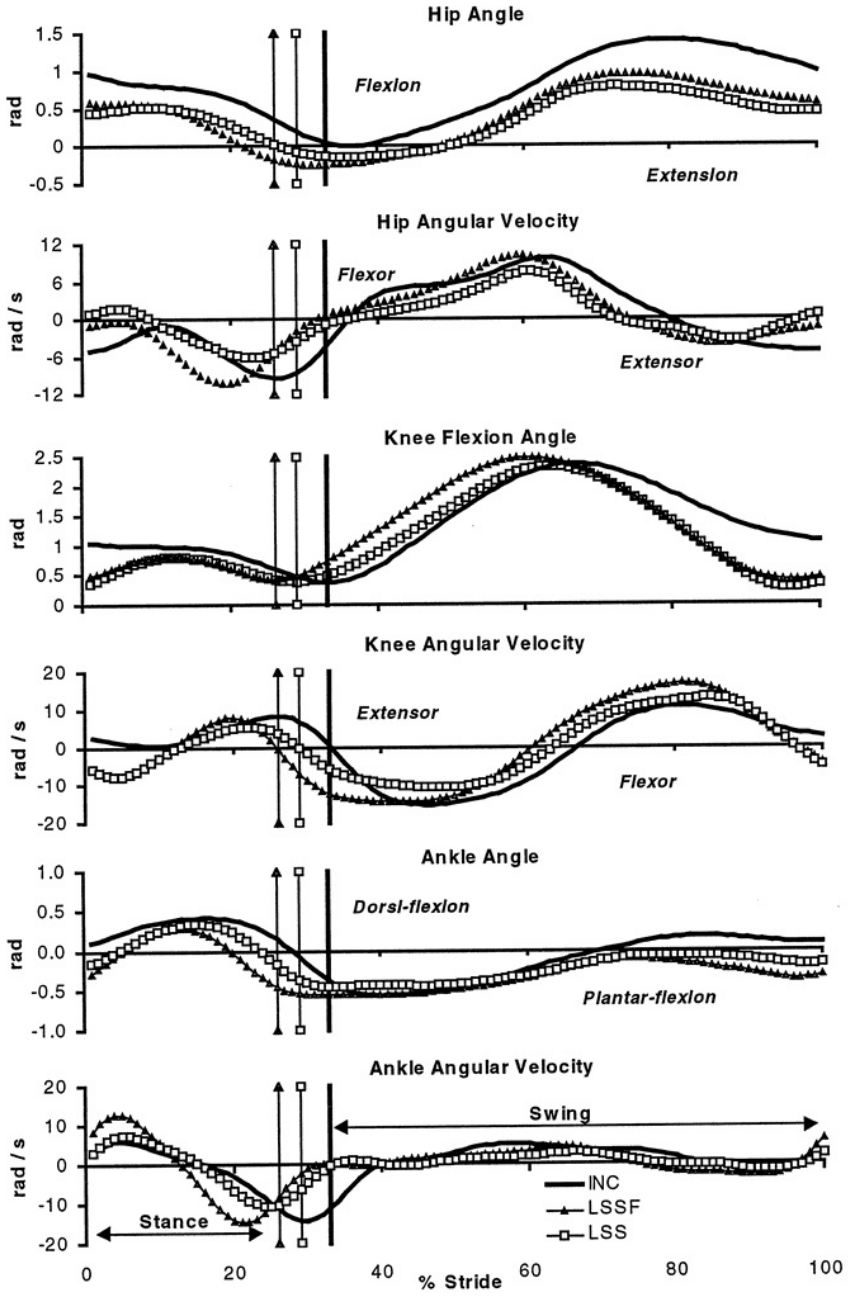

FIGURE 2.19: Kinematics of the running gait, (Swanson and Caldwell, 2000). INC: Inclined running; LSS: Level running; LSSF: Level running with the same stride frequency as INC

speaking, the maximum values of the relative angles are greater than the ones measured during gait tests.

Dynamics of the running cycle

As for any other activities, four types of forces are acting on the human body during running: external, internal, inertial and reaction forces.

As the inertial and reaction forces are obtained as in the case of gait, these forces will not be described here. The anthropometric tables remain the same, therefore, for the inertial forces, only the acceleration will affect the amplitude of these forces. The external forces are composed of the constant gravity forces acting on the whole human body. As the joint reaction forces depend on the amplitude of all the others in order to obtain a balance, it is not necessary to describe them either.

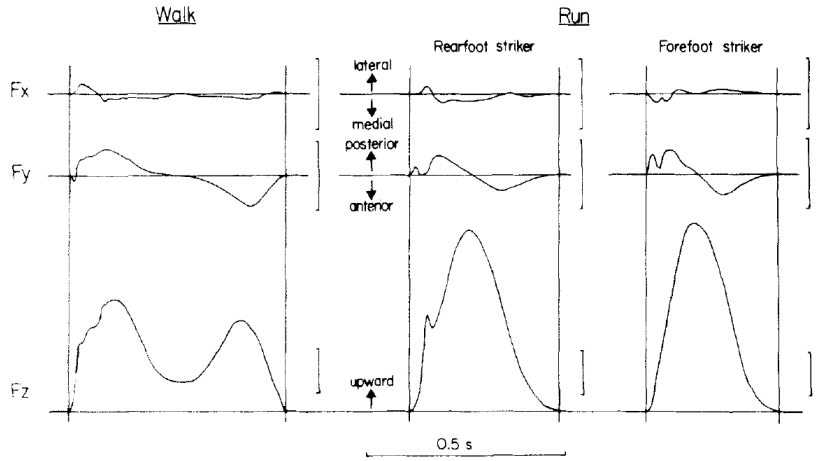

FIGURE 2.20: Shapes of the vertical, fore–aft and lateral components of the ground reaction forces for gait, running with rearfoot initial contact and midfoot initial contact (Nilsson and Thorstensson, 1989)

Ground reaction forces Figure 2.20 compares the shapes of the ground reaction forces on the three axis for gait and running. The lateral and fore-aft components show a lot of similarities. Lateral forces are used primarily to maintain movement in the sagittal plane. As the lateral disturbances are equivalent, so are the ground reaction forces on this axis. The front-to-rear components are also equivalent: as the body tries to keep a constant speed, the landing and propulsion forces are similar.

The main difference is in the vertical component. A more precise visualization of different configuration of running can be seen in Figure 2.21.

The shape of the curve is made up of two peaks. The first peak, of lower intensity and shorter duration, is the shock of reception. The second peak is the active force peak. The presence of the shoe cushioned the impact and the loading rate. Conversely, barefoot, we notice the presence of several small impact peaks, and a higher loading rate. The presence or absence of shoes does not affect the intensity of active force peak. The position of the foot

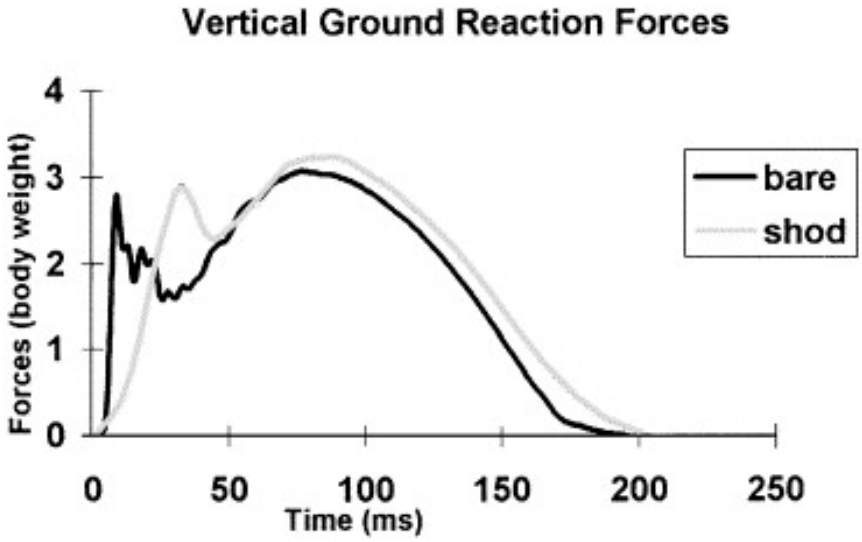

(a) Barefoot and shod running

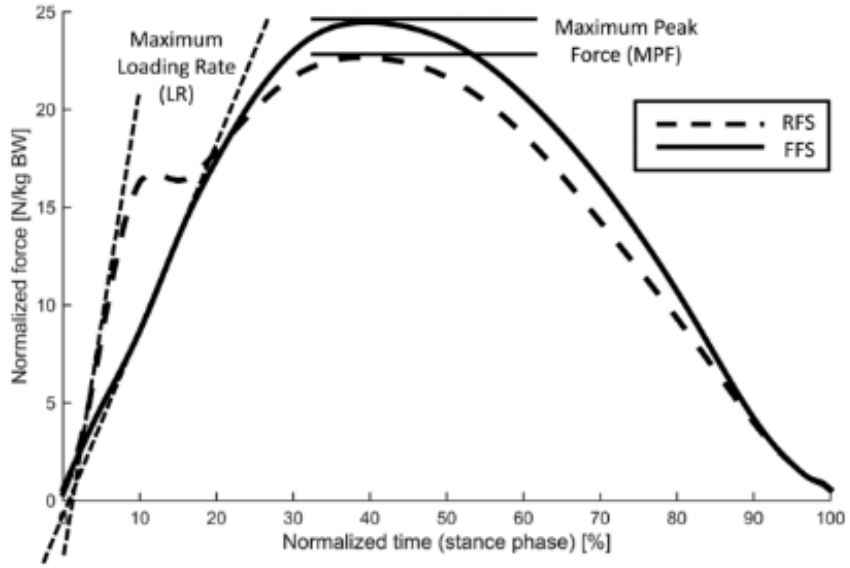

(b) Rearfoot and forefoot running

FIGURE 2.21: Vertical ground reaction forces for barefoot VS shod running (De Wit et al., 2000) and rearfoot VS forefoot running (Knorz et al., 2017)

during impact also has an effect. We can notice that in the case of a rearfoot running, the impact of the heel increases the loading rate, unlike a forefoot running, which dampens it. On the other hand, the tendency is reversed concerning the active force peak , more important for a forefoot running than a rearfoot running.

2.4 Experimental gait analysis

2.4.1 With the naked eye

Analysing the gait of a subject with the naked eye is the more common and simplest way to become aware of its possible faults. By looking at the joints, a keen eye, as a physician or a physiotherapist, can perceive a pathology or a compensation due to an injury.

To quantify the gait variation from the norm, indexes have been developed: e.g. the Visual Gait Assessment Scale (VGAS) or the Edinburgh Visual Gait Score (EVGS). The VGAS relies on six parameters and assigns a score to define the pathological gait of children with cerebral palsy. It was first described by Koman et al. (Koman et al., 1994) then improved by Dickens et al. (Dickens and Smith, 2006). This index shows good intra-observer but a low inter-observer reliability due to difficulties in standardizing tests (Maathuis et al., 2005). The EVGS is used for a more general description of the gait but its reliability is again highly correlated with the experience of the examiner (Ong et al., 2008).

Overall, even with standardized criterion, the visual analysis of the gait remains highly subjective and varies according to the expertise of the examiners (Krebs et al., 1985). The human eye can not detect precise details of the kinematics, and forces can not be quantified. Therefore, acquisition tools have been invented.

2.4.2 Acquisition of kinematic data

Throughout history, direct measurement devices of kinematics parameters of the gait have considerably evolved, from the goniometers used to measure the relative angle between two segments to the optoelectronic systems or the sensorless motion capture devices.

The Laboratory of Motion Analysis (LAM) of the University of Liège is equipped with four optoelectronic cameras (Codamotion system; Charnwood Dynamics; Rothley, UK). This system uses active markers which emit an infrared light flash captured by the cameras. Using triangulation of the light signals, the markers are located in the laboratory coordinates system in three dimensions, with a margin of error of less than a millimetre.

The motion during the gait of a subject can be reconstituted by measuring the positions of the markers placed on anatomical points of the human body (Schwartz et al., 2010). By filtering and time-deriving the position of

the markers, it is possible to obtain the velocity and acceleration of the segments, and the relative angle at the joints can also be computed easily by post-processing.

Faulty results may have several sources. At best, a wrong calibration of the system will shift in space the markers positions, or at worse make it impossible to obtain these position by triangulation. The relative motion between the rigid underlying bones and the surrounding soft tissues, commonly referred to as soft tissue artifacts (STA), are known to be one of the main sources of error in optical motion capture and can significantly affect the accuracy of estimated segment kinematics. The amplitude of the STA varies with the anatomical location; marker placement therefore aims to target regions where these amplitudes are minimal. Also, improper lighting in the laboratory can alter the visibility of markers (Cappozzo et al., 2005).

2.4.3 Acquisition of the ground reaction forces

Force platforms can accurately measure the contact reaction along three axes, and provide a good estimation for every type of motion (healthy or pathological gait, run, jump, etc) or for static position, in posturology for example. A force platform is usually able to measure in three dimensions the applied forces, the location of the centre of pressure, and the ground reaction moments (Sutherland, 2005).

Their cost and implementation in the laboratory tend to complicate some studies. A large number of force platforms is necessary to estimate a pathological gait on a long distance, or the race of a sprinter on a specific track.

The LAM is equipped with two force platforms (Kistler force-plate; Kistler Instrumente AG, Switzerland).

2.4.4 Acquisition of the muscles activity and force

Electromyograph devices (EMG) measure the electric activity of a muscle that varies during its contraction. These electrodes can be placed under (intramuscular electrode) or above (surface electrode) the skin. To avoid unnecessary pain during in-vivo tests, surface electrode are most frequently used. The electric activity is measured below the electrode with a depth of 20 to 25 millimetres, limiting the collected data to surface muscles.

Depending on its position and the depth of the muscle, the electric potential measured can vary. To facilitate the interpretation of the activity of the muscle, a test of maximum contraction can be performed to calibrate the measurement. The envelope of the EMG signal is used during the test to represent the activity in terms of a percentage.

The EMGs do not directly measure the force developed by the muscle. To estimate its value, maximal voluntary contraction force tests or isokinetic tests can be performed to obtain the maximum force developed by muscle groups. If this information is combined with the muscle electrical activity, it is possible to estimate the muscle force (Aratow et al., 1993; Doorenbosch and Harlaar, 2004; Raison, 2009).

2.4.5 Quantified Gait Analysis

A Quantified Gait Analysis (QGA) measures simultaneously the kinematics, the ground reaction forces and the muscles activity, described in the previous section, as in Figure 2.22. QGA were performed for this thesis and the methods and results will be detailed in Chapter 3.

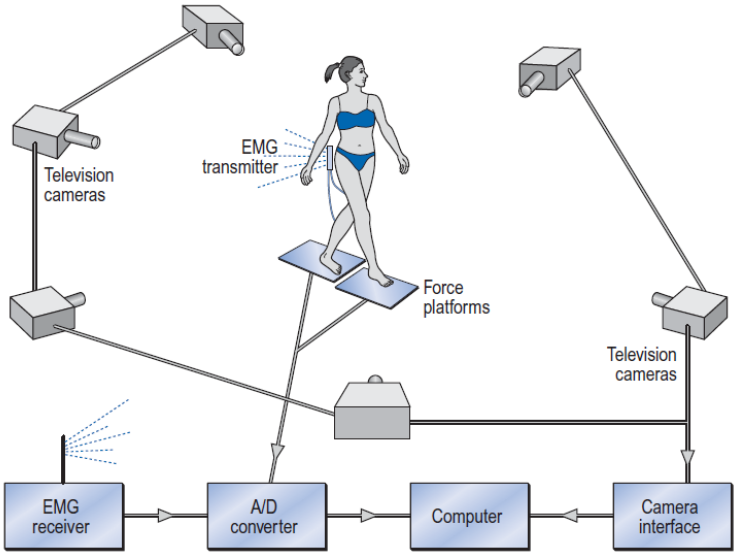

FIGURE 2.22: The gait analysis equipment, with a six camera kinematic system, two force platforms and an EMG telemetry system (Whittle, 2007)

2.5 Numerical gait modelling

As described in Section 2.4, the gait analysis can be fully performed experimentally. However, each experimental devices has its limitations: e.g. difficulties for the subject to land their feet on specific force platforms, difficulties to estimate deep muscle forces, etc.

When a part of the information is lacking, one can use numerical analyses to compute and estimate the behaviour of the human body.

2.5.1 Direct dynamics analysis

Direct dynamics, or more commonly "dynamics", is the study of the forces acting on a mechanical system and their effects on the motion.

For these simulations, as in Figure 2.23 the motion is unknown and the global set of forces should be given (ground reaction forces and joint torques deriving from the muscle forces). These analysis are very frequent in robotics (where the motor torques are controlled) but are more difficult in biomechanics because of the difficulty to know all the forces acting on the human body.

To be able to predict the position of each limb in a direct dynamics analysis, all the forces should be known precisely, which can be very difficult to obtain experimentally. Moreover, the human body is under-actuated (Gupta

and Kumar, 2017): there are a lower number of actuators than degrees-of-freedom, since the human body is not fixed to the ground. Added to the large number of degrees of freedom, this property leads to inaccurate models of the human motion. Numerical predictions of the gait exist nonetheless, as in (Anderson and Pandy, 2001), (Ackermann and van den Bogert, 2010) or (Martin and Schmiedeler, 2014).

To cope with these instabilities and approximation, some hypotheses have to be made to solve the equation of motion, such as an optimization of the motion, or modelling a feedback law.

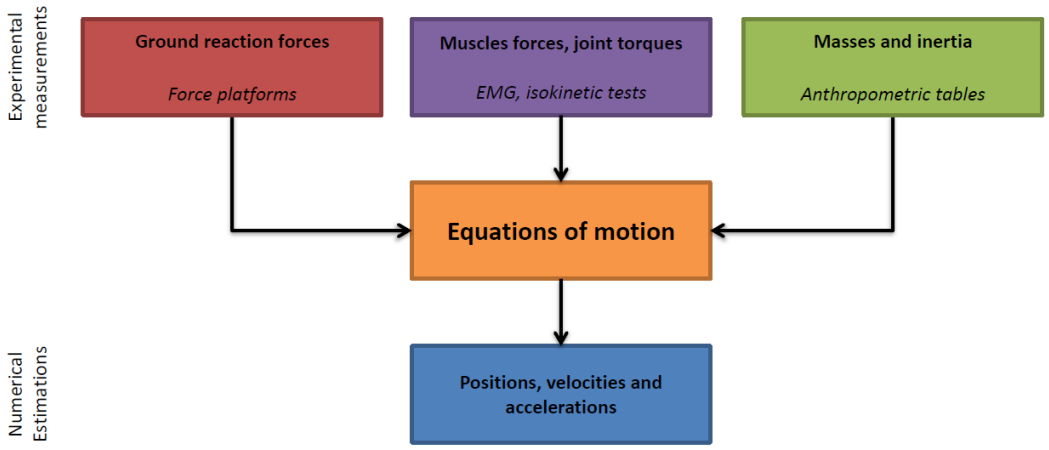

FIGURE 2.23: Schematic view of a direct dynamics simulation

In the model of (Anderson and Pandy, 2001), an optimization technique is developed based on an observation implying that humans tend to walk in a way that minimize the metabolic energy (Ralston, 1976). Their musculoskeletal model comprises 10 rigid segments, 23 degrees-of-freedom and 54 musculotendons units. The joints were simplified using ball-and-socket joints (3 dof) for the lumbar joint (between the rigid trunk and the pelvis) and for the hips, using hinge joints (1 dof) for the knees and the metatarsal joints and using universal joints (2 dof) to model the ankle.

The cost function to minimize was the sum of different aspects of the metabolic energy, such as the metabolic heat rate of the whole body, the activation heat rate, the maintenance heat rate, the shortening heat rate and the mechanical work rate of each muscles per unit of displacement (Anderson, 1999). Finally, some constraints were added to impose a cycle pattern for the gait (initial and final joint angular displacements should be the same).

Minimizing the cost function for the constrained optimization problem leads to an optimized realistic gait pattern for each subject of the study. However, this model revealed discrepancies between numerical and experimental data, due to the simplification and hypotheses in the development of the model.

The method developed by (Ackermann and van den Bogert, 2010) is also an optimization technique. However, instead of minimizing the metabolic energy, the cost function was this time the sum of the weighted muscle activations, while varying the power of this activation. This also lead to realistic

gait patterns and showed also the possibility to consider other cost functions, and not only the energy.

The model proposed by (Martin and Schmiedeler, 2014) is a mixed optimization/feedback model. To determine some parameters of the gait, a feedback model is developed to match the numerical predictive gait patterns to a set of experimental measurements. Based on these results, the model can accurately predict a gait pattern by minimizing the square of the joint torques.

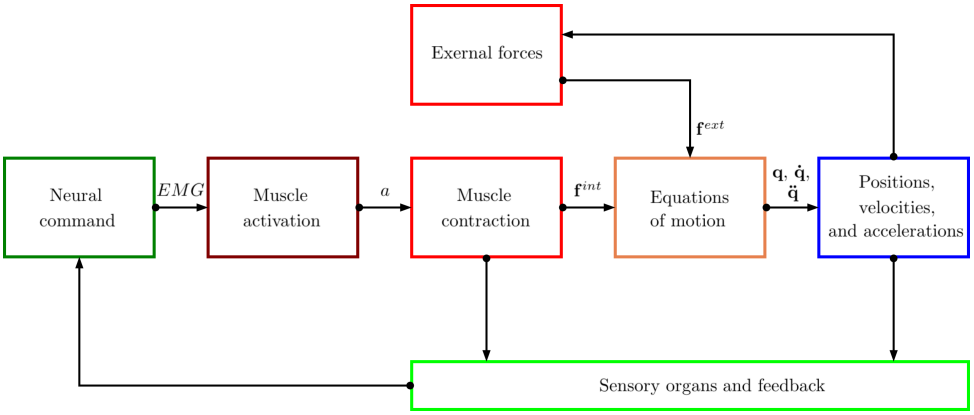

FIGURE 2.24: Schematic view of a direct dynamics simulation of a human motion, using feedback control, based on (Buchanan et al., 2004)

Finally, some models rely only on a feedback system and estimate the neural command needed to activate the muscle, as depicted in Figure 2.24. A feedback is given by the muscles (level of activation, contraction forces,...) or by the position of each limb. Usually, feedback models try to match a motion pattern (motion-driven feedback) or the achievement of a goal (task-driven feedback). (Todorov and Jordan, 2002) proposed a method to find an optimal feedback control law based on stochastic analysis. Their model used feedback to correct the motion when the deviations interfere with the task goals, allowing some variability in the motion patterns. This mixed formulation combines both feedback methods.

2.5.2 Inverse dynamics analysis

Inverse dynamics is a method used to compute the forces and torques at the origin of a given motion. In this case, the motion of the different segments is known and the goal is to find the muscle forces, joint torques and/or the ground reaction forces.

When the ground reaction forces are measured and only the joint torques and muscle forces are sought, we speak of inverse dynamics analysis without contact model, and conversely, when the ground reaction forces are also unknown, of inverse dynamics analysis with contact model.

As shown in Figure 2.25, the inverse dynamics analyses without contact model are the most common method to analyse the human gait. The ground reaction forces are measured with force platforms, and the positions of the

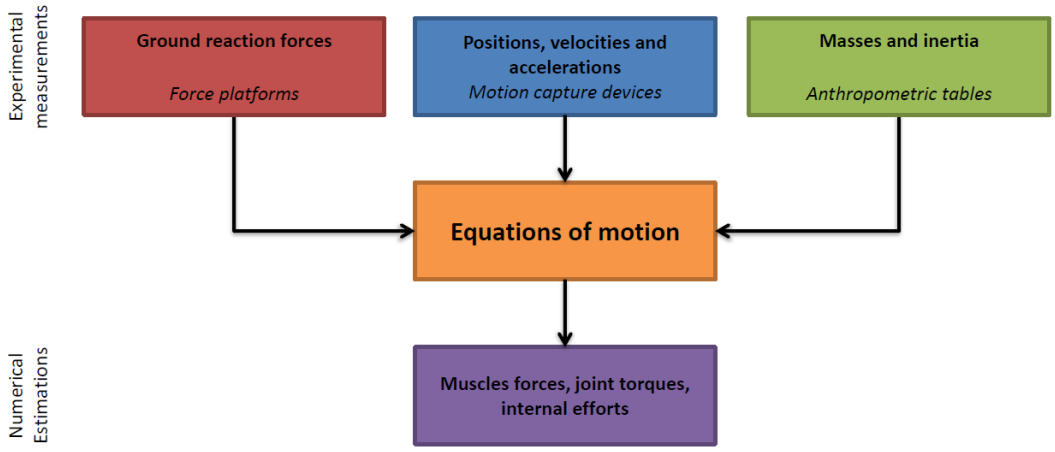

FIGURE 2.25: Schematic view of an inverse dynamics simulation without contact model

limbs are captured with cameras. The mass matrix is developed with anthropometric tables or by experimental measurements, and as in Section 2.5.1, the equations of motion of the system must be solved. Equations (2.1) and (2.2) remain the same but the new unknowns are the internal forces. The motion (position, velocities and accelerations) are known and measured experimentally.

There are several software used to perform inverse dynamics analyses, like OpenSim, AnyBody, etc.

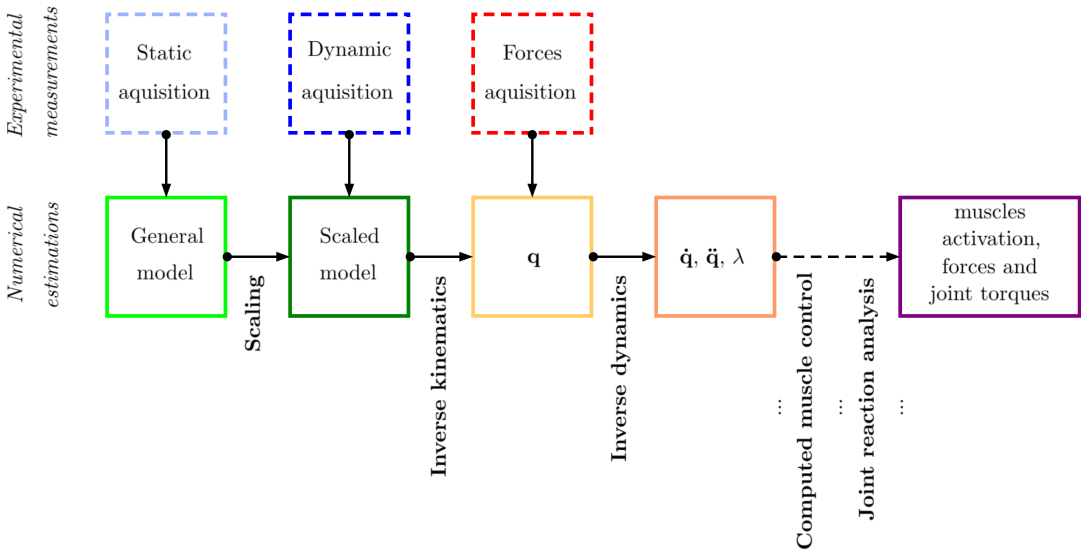

FIGURE 2.26: Flowchart of OpenSim software

In Figure 2.26, a simplified flowchart of OpenSim is presented: it represents the majority of inverse dynamics schemes used in biomechanics.

First, a general musculoskeletal model is used for the ongoing study. This model is either provided by the software or can be directly developed by the user. This model is an assembly of segments connected by joints, allowing

certain degrees of freedom. Muscles elements and the attachment points are also defined between each segments. Numerical markers are linked to the segments and are used to locate the numerical model in space. An anthropometric table is defined alongside the model so that, based on the dimension of each segments, a mass, inertia and centre of gravity location can be numerically estimated.

A static test has to be provided in order to scale the general musculoskeletal model. The location of experimental markers matching the position of the numerical markers in the model are measured. The total mass of the subject and these measurements are exploited with anthropometric tables to estimate the length, masses and inertia of each segments. The general musculoskeletal model is scaled using all this information. To scale each segment, the software minimizes the distance between each experimental and numerical markers, in a least square sense.

Once the model is scaled, it is possible to perform dynamic studies. The first step is to correlate the experimental markers with the numerical markers. Once again, to find the position of each segment at each time step, a minimization of the error on the position of the numerical markers is carried out in a least squares sense. This stage is called inverse kinematics and makes it possible to define the vector of the generalized coordinates and the controlled degrees of freedom.

The next stage is the inverse dynamics, properly speaking. In order to obtain the vector of speeds and accelerations, the vector of generalized coordinates is derived temporally. Being an experimental signal, it is generally affected by noise and filtering is necessary to obtain consistent results. The filter used can be for example a Butterworth zero shift low-pass filter with a cut-off frequency depending on the activity studied. For gait, the cut-off frequency is generally chosen at 6 Hz. External forces are added to the study during this stage. The gravity is chosen constant and depends on the position of the centres of gravity and the mass of each segment, calculated during the scaling and in the previous stage. The inverse dynamics stage makes it possible to define the articular joint torques necessary for the realization of the motion.

Finally, it is possible to evaluate the activation and the muscular efforts as well as the joint efforts, the torques at the joints being known, and the parameters of the muscles being defined by the scaled model (point of attachment around the joints, maximum forces, etc.). These stages use optimization and control techniques in order to deal with the redundancy of the muscles groups.

This method provides complete results and allows to obtain a description of the behaviour of all muscles, joints and segments of the human body during the activity studied. However, the reliability of the obtained results strongly depends on the quality of the experimental measurements and on the modelling assumptions (optimization and control techniques to estimate muscle activation). In particular, accurate kinematic data and precise measurements of ground reaction forces are required, making the approach sensitive to measurement noise and OpenSim's modelling assumptions.

2.5.3 Foot/ground contact models

If force platforms can accurately measure the contact reaction along three axes, and provide a good estimation for every type of motion (healthy or pathological gait, run, jump, etc), their cost and implementation in the laboratory tend to complicate some studies. A large number of force platforms is necessary to estimate a pathological gait on a long distance, or the race of a sprinter on a specific track. It is often difficult to obtain a complete information. These limitations motivates the development of contact models between the feet and the ground as a substitute of direct measurements.

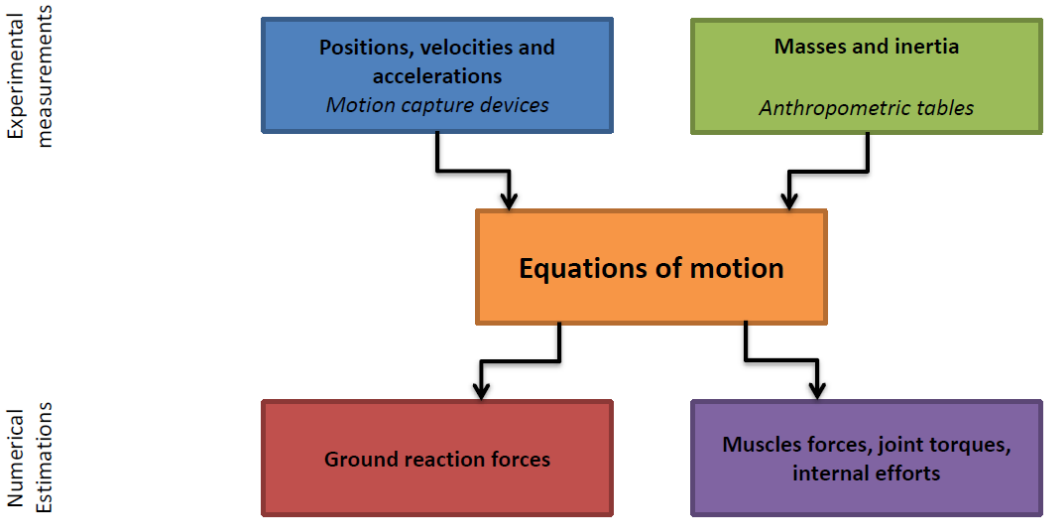

FIGURE 2.27: Schematic view of an inverse dynamics simulation without contact model

Different methods are available in the literature and can be classified in three major categories: empirical, compliant or rigid models. We present here a selection of models that are representative of the state of the art. For a more comprehensive review, the reader is referred to the work of (Saraiva et al., 2022).

Empirical models

Empirical models lead to rather simple equations. The GRF can be computed from the measurement of the global centre of gravity displacement, as in (Farley and González, 1996) or (McMahon and Cheng, 1990). This model, used for running tests, assimilates the leg in stance phase to a spring. The displacement of the center of gravity of the human body deforms this equivalent spring and a reaction force is thus calculated, as in Figure 2.28. The vertical ground reaction force is given, in this model, by:

$$F = k_{leg}(\Delta y + L_0(1 - \cos\theta))) \tag{2.17}$$

where k_{leg} is the equivalent stiffness of the leg, Δy the vertical variation of the centre of gravity of the body, L_0 the initial length of the leg, and θ the angle

between the contact point and the centre of gravity. This model shows some limitations: there is no clear definition of the contact point, and therefore of the angle θ, and the relative stiffness varies with the subject (depending on the mass, height, running speed,...).

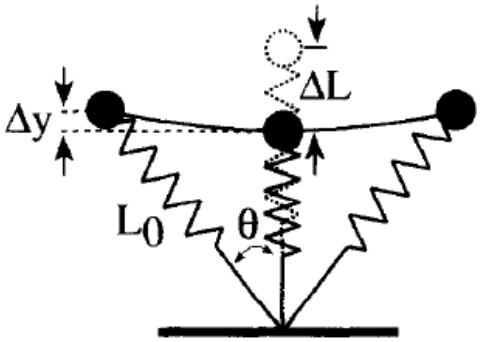

FIGURE 2.28: Running is modeled as simple spring-mass system bouncing along the ground (McMahon and Cheng, 1990)

Some other models were directly based on statistical data as in (Keller et al., 1996). In this study, data linking the scaled vertical ground reaction force and the walking/running speed are collected, as in Figure 2.29.

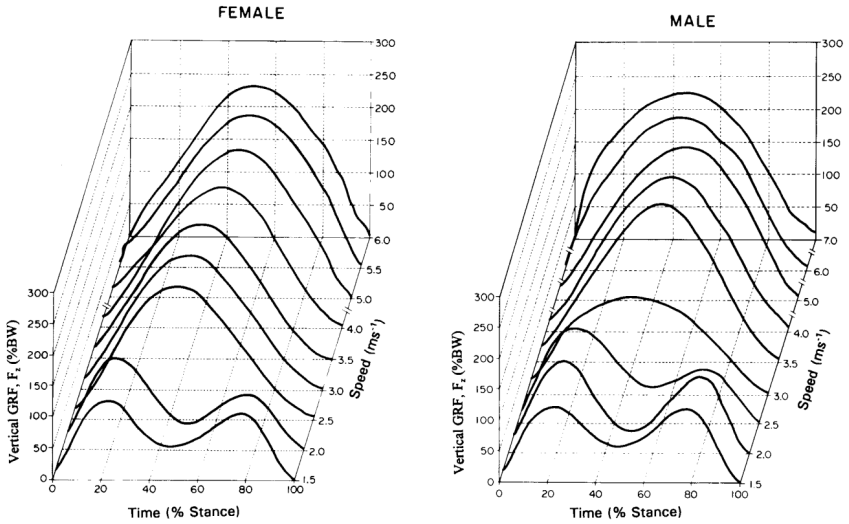

FIGURE 2.29: Vertical GRF, time histories patterns as a function of running speed (Keller et al., 1996)

Empirical model can eventually give a good first guess, but they hardly give a subject specific estimation of the ground reaction forces.

Compliant models

Compliant models represent the local deformation of the foot sole and the ground during the contact. This approach is similar to a finite element method, where the computed deformation of the contact elements on the foot soles are directly linked to the ground reaction forces.

The model of (Gilchrist and Winter, 1996) was one of the first developed for direct dynamics simulation purposes: nine ideal viscoelastic elements (or spring-dampers) are vertically fixed between the foot and the ground when contact is considered active. The musculoskeletal model of the foot was composed of two segments linked by one revolute joint representing the metatarsophalangeal joint. The stiffness of these elements is chosen linear, while the coefficient of damping is non-linear and follows a third order polynomial law in terms of the vertical position of the contact element. The deformation of these elements gives the vertical ground reaction force. The horizontal friction force is modelled as a function of the velocities of the contact point. The centre of pressure is not directly computed. Each contact element develops a force, and the balance of all these forces provides the centre of pressure. However, the multiple contact constraints (several constraints lock the same rigid body) require caution in the obtained response. Moreover, the presence of stiffness elements implies the penetration of the foot into the ground. To limit this non physical defect, a large value of the stiffness must be chosen, which can also be a source of numerical problems. To address these issues, the model was modified and is still widely used to compute the ground reaction forces: e.g. (Anderson and Pandy, 2001), (Ackermann and van den Bogert, 2010),... These methods vary by the number of selected contact elements, the value of the stiffness or the damping, or the contact activation criterion, but all keep the same fundamental idea.

In (Baker and Robb, 2006), (Scott and Winter, 1993), (Moreira et al., 2009) (Figure 2.30), or (Lin et al., 2018) the sole is modelled by deformable spheres in 2D or 3D of different radii, stiffness and damping coefficients are used to better represent the behaviour of the foot sole during gait or run, giving an estimation of the ground reaction forces. This is an extension of the method of (Gilchrist and Winter, 1996), since the element deforms along several axes and not just one. There is also more penetration since the sole of the foot is no longer defined as a rigid body and becomes deformed. However, there remains the redundancy of constraints which must be treated with great care to obtain a coherent estimation of the centre of pressure. On the horizontal axis, to take into account the friction between the foot and the ground, (Lin et al., 2018) uses a model of Coulomb friction law:

$$F_t \leq \mu F_n \tag{2.18}$$

where F_t (resp. F_n) is the tangent (resp. normal) ground reaction force, and μ is the coefficient of friction.

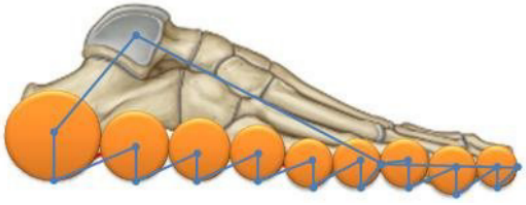

FIGURE 2.30: Schematic view of the foot with deformable spheres (Moreira et al., 2009)

All these compliant models require an experimental measurement of the compliance between the foot and the ground, whose value might change from one subject to another. The use of compliant models for direct dynamics simulation is quite successful but their use in inverse dynamics is hardly achievable because it would require an accurate measurement of the foot sole deformation, which is beyond the capabilities of usual motion capture technologies; they are mostly used for predictive models in numerical simulation.

Rigid models

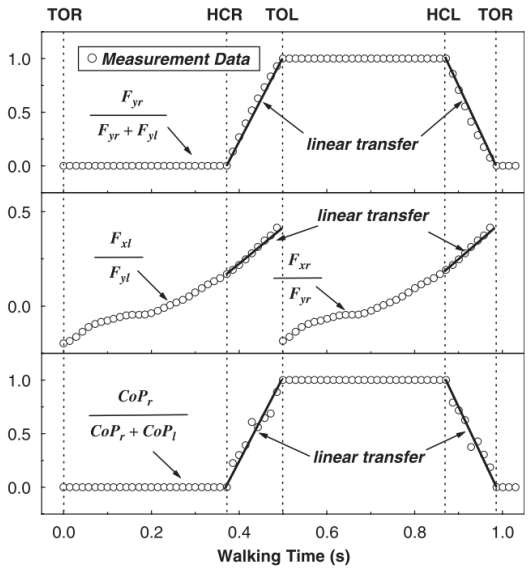

FIGURE 2.31: Calculated transfer ratios (solid lines), based on linear assumptions, compared with measurement data from (Winter, 2009). F_{xr}, F_{yr}, F_{xl} and F_{yl} are the horizontal and vertical ground forces at the right and left foot. CoP_r and CoP_l are centres of pressure for right and left foot. CoP is defined as $(M_{an} - F_x y_{an})/F_y$. In the double support phase from right heel contact (HCR) to left toe off (TOL), the vertical force transfer ratio r_{t_fy} increases from 0 to 1, the horizontal force transfer ratio r_{t_fx} increases from $r_{t\_fx}^{(HC)}$ to $r_{t\_fx}^{(TO)}$, while the CoP transfer ratio rt_cop increases from 0 to 1. (Ren et al., 2007)

Rigid models neglect the deformation of the foot and the ground and simply rely on a non-penetration condition. Hence, they do not involve any local stiffness and damping parameters, and they do not require any precise evaluation of the foot sole deformation. In (Koopman et al., 1995), (Allard et al., 1998) or (Ren et al., 2005; Ren et al., 2007), the ground reaction forces are equivalent to the global acceleration of the body, splitted between both feet, according to an empirical linear law during the double support, as in Figure 2.31. Mathematically, in (Koopman et al., 1995), the ground reaction forces are given by:

$$\begin{aligned} \mathbf{F_R} &= f \sum_{i=1}^{N} m_i(\ddot{\mathbf{x}}_i - \mathbf{g}) \\ \mathbf{F_L} &= (1-f) \sum_{i=1}^{N} m_i(\ddot{\mathbf{x}}_i - \mathbf{g}) \end{aligned} \tag{2.19}$$

where $\mathbf{F}$ are the force vectors in 3 dimensions, i is the segment, N the number of segments, $\ddot{\mathbf{x}}_i$ is the acceleration vector of the centre of gravity of the i^{th} segment in 3 dimensions, and $\mathbf{g}$ the gravity vector. The shift function f represents the transition from one foot to the other during the gait. This function, as depicted by Figure 2.31, is linear by parts. It is equal to zero during the swing phase and one during the single support phase, with a linear transition during the double support phase.

In the 2D model of (Koopman et al., 1995), developed for direct dynamics analysis with constrained motion (to avoid inverse dynamics derivations and smoothing), the centre of pressure is defined using a geometric constraint. The foot sole is define by a curve and is directly linked to the orientation of the foot segment when it is in contact with the ground.

Although this formulation of the contact forces has a clear biomechanical interpretation and a simple numerical implementation, it is directly related to the activity under study via the shift function f. The hypothesis of a healthy gait with a linear transition from one foot to the other sometimes quickly reaches its limits. For example, for the healthy gait, we can see in Figure 2.31 that the transition of the experimental vertical reaction force is slightly higher than the linear estimation in the reception phase, and slightly lower in the propulsion phase. These limitations have motivated the development of more accurate contact models between the foot and the ground.

The method developed by (Oh et al., 2013) to estimate the ground reaction forces and moments uses an artificial neural network (ANN) method for the double support phase and a standard method for the single support phase, as in (Koopman et al., 1995). The artificial neural network was based on the experimental results of 43 subjects and verified by testing the results obtained for 5 other subjects. The inputs given to this ANN were the positions and accelerations of different anatomical points and centre of mass of the human body and the output were the ground reactions forces and moments in 3 dimensions. This method provided a representation of the ground reaction forces and moments than standard methods. The centre of pressure can be deduced from the forces and moments, but is therefore linked to the estimation errors of both parameters. However, this method was again based on experimental data (used to train the artificial neural network), and shows its limits when the studied activity deviates strongly from the healthy gait, which has motivated the development of more general models.

The method of (Fluit et al., 2014) uses several contact points per rigid foot and muscle-like actuators to evaluate the ground reaction forces through the muscle recruitment optimisation problem. On Figure 2.32, the position of the contact points are shown alongside the profile of the contact reaction forces.

The method developed by (Skals et al., 2017) is similar, with 18 contact points per foot. First, a criterion is used in order to determine the active contact points, that is to say, the different locations where the feet are in contact with the ground. This criterion is based on measurements of the vertical position of the point of contact and of its global velocity, which, if they are below a critical threshold, will make the contact active or not. Once all the contact points have been determined, three muscle-like actuators are defined between each active contact point and the ground, with a predefined maximum force. These fictitious actuators are therefore treated as muscles when solving the equations of motion, which makes it possible to define an activation of the actuator and therefore the force necessary to maintain the contact points at the ground level. The level of activation is estimated by an optimization technique which minimizes the cube of the activation of all the muscles at each time step. This assumption weighs the redundancy of constraints (during the phase of double support, or between the points of contact being on the same rigid segment) and makes it possible to select a preferred solution during the resolution of the equations of motion. Like most of the compliant models presented above, the centre of pressure is not directly determined but derived from the balance of all the reaction forces developed by the contact actuators. Its position is therefore correlated to the location of these actuators, the number of active contact point and the maximum force allowed.

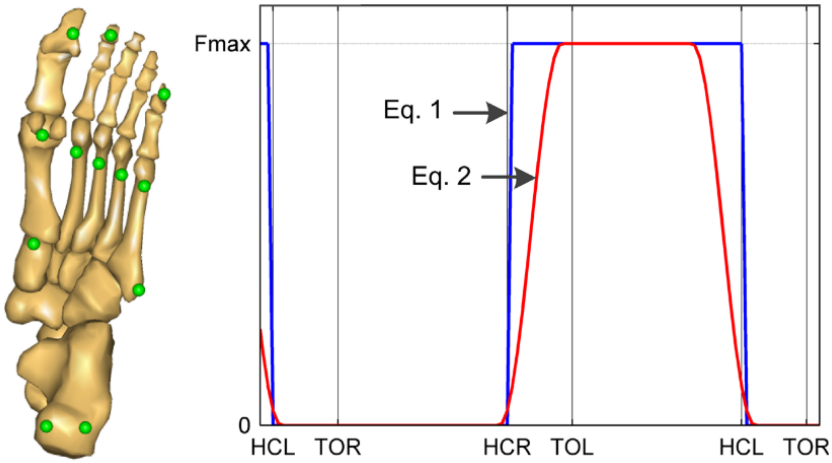

FIGURE 2.32: Left: Visualization of the 12 contact points for each foot. Points were defined at the medial and lateral side of the heel, at the base of the first and fifth metatarsal bone, at the head of each metatarsal bone and at the big, second and fifth toe. Right: Visualization of the characteristic strength function (Eq. (1)) and the smoothed strength function (Eq. (2)) for the right heel contact node during a gait cycle. Heel contact and toe-off of the right leg are abbreviated as HCR and TOR respectively and, analogously, for the left leg as HCL and TOL. (Fluit et al., 2014)

The model proposed by (García-Vallejo and Schiehlen, 2012) uses an evolving set of bilateral constraints in the equation of motion to impose the contact force on the system. This method was developed for direct dynamics simulation. This approach takes ideas from nonsmooth dynamics: no penetration

is allowed. The musculoskeletal model of the foot consists of a single rigid body and two contact points located on the heel and on the hallux. The predictive model is always in one of the 8 authorized contact configurations (see Figure 2.33). Depending on this configuration, bilateral constraints fix the translations of the contact points, leaving the rotations free. The Lagrange multipliers associated to these bilateral constraints represent the ground reaction forces. To change the configuration, the contact criterion of the following configuration must be verified: the vertical position of the contact points concerned by this new configuration must be zero. The centre of pressure is not defined by this model.

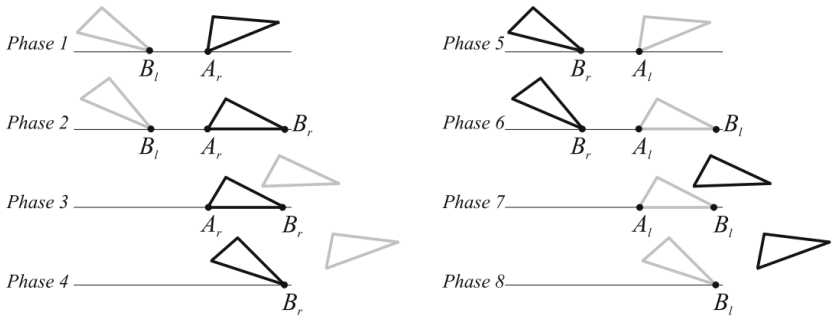

FIGURE 2.33: Sketch of the contact conditions (García-Vallejo and Schiehlen, 2012)

The last contact model presented in this chapter is the algorithm published by (Xiang et al., 2007). In this model developed for predictive studies in direct dynamics, the centre of pressure is first calculated from the zero moment point (ZMP). This point is defined as the point where all of the ground reaction forces acting on the body in motion do not generate a moment. When the body is in equilibrium and during the single support phase, the ZMP corresponds to the centre of pressure of the foot in contact with the ground. During the double support phase, the ZMP is located between the two feet. To find the two centres of pressure, a linear distribution of the load between the two supports is performed, like the model of (Koopman et al., 1995). Knowing the position of the centres of pressure over time, it is now possible to recheck the overall balance of forces at these points to find the ground reaction forces. This method, using ZMP, a concept also widely used in robotics, is perfectly suited for direct dynamics. In inverse dynamics, the precise location of the ZMP can be difficult: it depends significantly on the acceleration of the centres of gravity of each segment, a value obtained by time differentiation and smoothing.

Some recent models have also been implemented directly in the OpenSim software, as in (Di Pietro et al., 2025). This approach integrates calibrated foot–ground contact probes with an optimization framework based on computed muscle control to estimate the ground reaction forces and moments, as well as the centre of pressure.

In a recent work published after ours, (Gao et al., 2024) proposed a rigid foot–ground contact model to estimate GRFs and the COP during gait. As

this model is partly based on several of our proposed concepts, it will be discussed in Section 4.3.

Rigid contact models are more suitable for our approach. However, they exhibit certain limitations, particularly in the estimation of the centre of pressure, clarity in force estimation methods, and general applicability (such as the assumed contact sequence). Our objective is to develop a contact model capable of estimating ground reaction forces and moments, regardless of the support phase (zero, single, or double contact), while simultaneously determining the position of the centre of pressure, all while maintaining interpretable equations.

Critical analysis and remaining gaps

The literature shows that the problem of foot-ground contact modelling has been widely addressed, but never fully resolved in a unified and general framework. Existing approaches can broadly be classified into compliant and rigid contact models, each successfully addressing specific aspects of the problem while introducing their own limitations.

Compliant models provide a physically intuitive representation of the contact by explicitly modelling local deformations and allowing a continuous transition of forces. They are particularly well suited for direct dynamics and predictive simulations, where the deformation state is internally computed. However, their reliance on stiffness and damping parameters, often subject- and experiment-specific and difficult to measure, limits their applicability in inverse dynamics. Moreover, acquiring an accurate measurement of the foot sole deformation is beyond the capabilities of usual motion capture technologies. As a result, while compliant models can yield accurate GRFs, their use in experimental inverse-dynamics pipelines based on standard motion capture remains impractical.

Rigid contact models, on the other hand, are more compatible with inverse dynamics frameworks and experimental gait analysis. Early approaches based on global force balance and empirical load-sharing functions provide simple and robust estimations of vertical ground reaction forces, but they strongly depend on activity-specific assumptions, such as a predefined gait pattern or a linear transition during double support. More advanced rigid models introduce optimisation techniques, artificial neural networks, or muscle-like contact actuators to overcome these limitations. These methods improve accuracy and allow more flexibility in contact configurations, but at the cost of increased model complexity, reduced interpretability, and, in some cases, a strong dependence on training data or heuristic choices (number and location of contact points, maximum actuator forces).

Across both compliant and rigid approaches, several key challenges remain only partially addressed. First, the robust and direct estimation of the COP, independent of force redundancy, contact determination, or optimisation artefacts, remains an open issue. Second, many models are either

strongly task-dependent or require extensive calibration, limiting their generalisability. Third, there is often a trade-off between biomechanical interpretability and numerical performance: models that are simple and transparent tend to be less accurate, while more accurate models are harder to analyse and validate biomechanically.

These observations highlight a gap for a contact model that remains compatible with inverse dynamics and experimental data, provides interpretable equations, does not rely on local deformation parameters, and can be exploited to estimate ground reaction forces, moments, and the centre of pressure consistently across all support phases. The model proposed in this work aims to address these limitations by adopting a rigid-contact formulation with an explicit and continuous description of the centre of pressure evolution, while avoiding unnecessary numerical complexity.

2.6 Conclusion of the chapter

In this chapter, a summary of the literature and of the fundamental concepts of multibody system dynamics and biomechanics has been presented. The main concepts needed to establish and define a musculoskeletal system with contact elements have been defined.

A more detailed review of the existing contact models, with their qualities and their limitations, have also been described in this chapter.

This chapter will serve as a basic theoretical reference for the physical, mathematical and numerical developments mentioned in the following chapters.

Chapter 3

Experimental measurements

In this chapter, the experimental protocols used to acquire the experimental data required by the numerical models are described. These experimental protocols have been defined in order to obtain healthy gait data which will serve as a reference for our numerical model. These experimental data were also of interest to other studies within the Laboratory of Motion Analysis. During the 2015–2016 academic year, a Master's thesis in physiotherapy was conducted on the influence of subject-specific data on muscle force estimation (Gautier et al., 2016). The author of the present doctoral thesis supervised this work and was directly involved in the definition of the experimental protocols and data processing methodologies. The experimental data acquisition itself was carried out by the Master's student. This collaboration was specifically set up to ensure full control over the experimental design and data collection process.

3.1 Objective of the experimental tests

The main objective of this battery of tests is to provide a set of data which will serve as gold standard: the data measured by force platforms being extremely precise and the error made by the 3D cameras on the position of the markers being very low, it makes sense to rely on these data to establish our numerical model.

Several tests will be carried out by varying the walking parameters, such as the walking speed. From one subject to another we will be able to observe the importance of the speed variation on the kinematics as well as the ground reaction forces and the muscular activation.

The tests were performed in the Laboratory of Motion Analysis of the University of Liège.

3.2 Instrumentations and data acquisitions

3.2.1 Population

Five healthy adults male subjects participated to our first battery of gait tests. They were aged from 18 to 30 years old (23.8 ± 2.17), measuring 177.2 ± 6.5 cm, weighting 74.4 ± 7.47 kg, sedentary (less than two hours of physical activity per week) and with no traumatic history. In our second battery of tests,

Parameters	First battery	Second battery
Age	23.81 ± 2.17 years	27.23 ± 2.21 years
Height	1.77 ± 0.06 cm	1.68 ± 0.09 cm
Mass	74.40 ± 7.47 kg	72.12 ± 6.95 kg

TABLE 3.1: General parameters of the reference populations

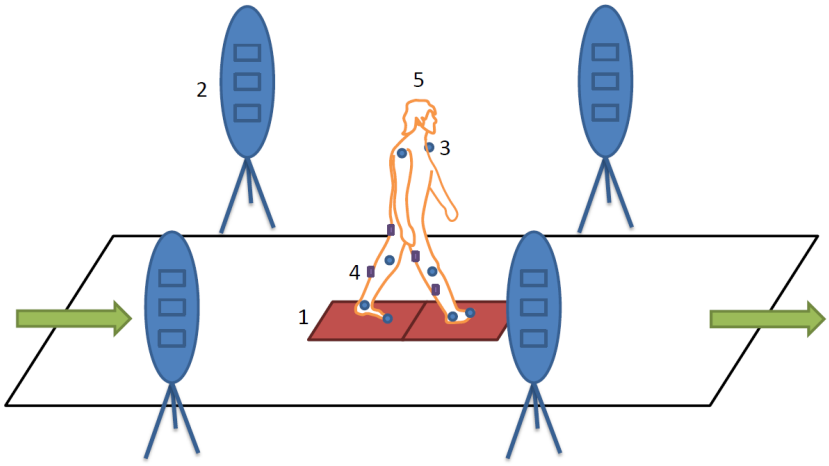

FIGURE 3.1: Instrumentation used during a gait test. 1: Force platforms, 2: 3D optoelectronic cameras, 3: 3D infrared markers, 4: electromyograph, 5: masses and inertia of the subject with anthropometric tables.

four healthy subject (one male, three female) took part. They were 27.3 ± 2.21 years old, and were measuring 168 ± 9 cm, and weighting 72.1 ± 6.95 kg.

They performed bare-foot gait tests (low, comfortable and high speed walking speed), jump tests (squat jumps, lateral jump and forward jump) and running tests.

3.2.2 Spatio-temporal data

3.2.3 Instrumentation

For our first battery of tests, a quantified gait analysis was performed, as can be seen in Figure 3.1. It includes a measurement of the kinematic of the limbs, of the ground reaction forces and of the muscular activity.

The kinematic measurement is performed by a system of four optoelectronic cameras CODAMOTION associated with active markers, at a frequency of 200 Hz. The ground reaction forces, moments and the centre of pressure measurements in 3D are based on two force platforms KISTLER integrated in a row at the ground level in the test track, and captured at a frequency of 1000 Hz. The muscular activity is captured by wireless surface electromyographic electrodes DELSYS TRIGNO, at a frequency of 1000 Hz. The three separate measurements were synchronized by the main computer.

EMG muscle	Letter in Figure 3.2
Vastus medialis	A
Vastus lateralis	B
Rectus femoris	C
Biceps femoris	D
Semitendinosus	E
Tibialis anterior	F
Gastrocnemius	G
Gluteus maximus	H

TABLE 3.2: Electromyographic electrodes

For the second battery of tests, the same instrumentation and frequencies of acquisition were used for the motion and ground reaction forces capture. The muscular activity was not measured for these tests.

3.2.4 Data acquisition

General data

Before equipping the subject, several data are collected concerning the age, the weight, the size and the reference hand. This information will be used when scaling our numerical model.

Electromyographic electrodes placement

The position of the sixteen surface electromyographic electrodes is shown in Figure 3.2 and in Table 3.2. The subject's skin is first shaved, then lightly abraded with a fine sandpaper to remove dead skin cells, and finally disinfected prior to electrode placement. This procedure reduces skin impedance and improves electrode adherence. This stage was only performed during the first battery of tests.

Maximum muscular activity estimations

After a ten-minute warm-up, the subject is positioned on a table and three maximum voluntary activation (MVA) tests are performed for each of the muscle groups monitored by the EMG. These three trials provide a signal envelope that defines the MVA level for each muscle group, which is subsequently used to normalize the EMG signals recorded during gait trials. This allows the estimation of the relative muscle activation, expressed as a percentage of each group's maximum activity, during dynamic movements.

The measured potential greatly depends on the exact position of the electrode. Therefore, if an electrode falls during a gait test, it is posed again and the maximum activity test is performed again.

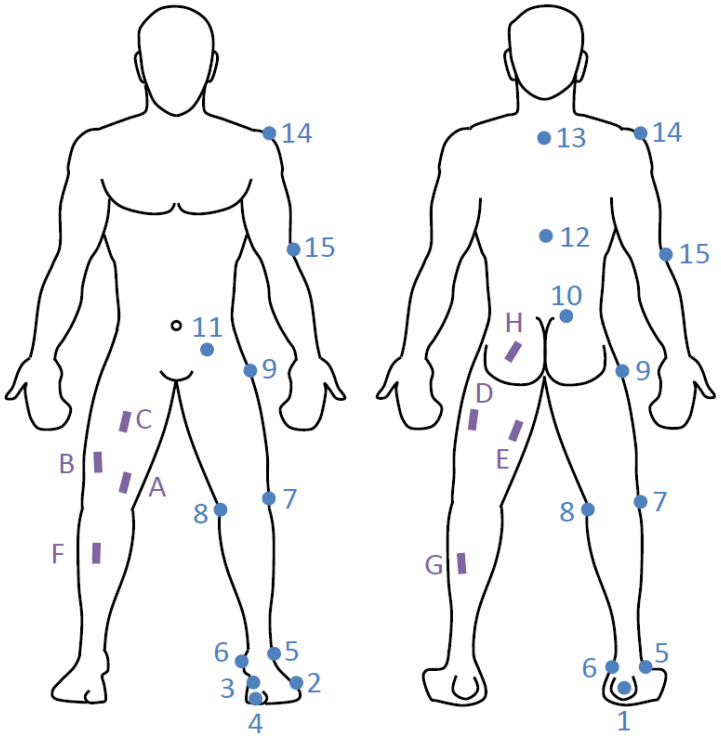

FIGURE 3.2: Position of the electromyographic electrodes, Table 3.2, and optoelectronic markers, Table 3.3

Optoelectronic markers placement

The position of the twenty-eight optoelectronic markers is shown in Figure 3.2 and in Table 3.3.

In this study, markers were placed only on anatomical points to track segment motion. While this approach simplifies the setup and allows for clear identification of joint centres, it is associated with known limitations. The placement of markers on the skin introduces potential errors due to soft tissue artifacts (STA), i.e., relative motion between the underlying bone and the overlying skin. Furthermore, relying solely on anatomical landmarks may reduce the spatial resolution of certain segment orientations, particularly for complex joints such as the hip or shoulder. Additional clusters of markers could improve the robustness of kinematic estimation, but at the cost of a more complex setup and increased preparation time. Therefore, the current choice represents a compromise between experimental feasibility and measurement accuracy.

Static test

To scale the numerical model to the subject, a first static test is performed. The subject stands straight on the force platforms with the forearm bending at 90°. This test also allows us to verify the proper functioning of the markers.

Marker position	Number on Figure 3.2
Heel (R-L)	1
5^{th} metatarsal (R-L)	2
1^{st} metatarsal (R-L)	3
Hallux (R-L)	4
External malleolus (R-L)	5
Internal malleolus (R-L)	6
External condyle (R-L)	7
Internal condyle (R-L)	8
Trochanter (R-L)	9
Posterior superior iliac spine (R-L)	10
Anterior superior iliac spine (R-L)	11
Dorsal vertebra D10	12
Cervical vertebra C7	13
Acromion (R-L)	14
Lateral epicondyle (R-L)	15

TABLE 3.3: Optoelectronic markers

Dynamic gait tests

Finally, the subject is fully equipped and dynamic tests are performed. For the first battery of tests, after several trials, two tests are completed. For the first one, the subject is asked to walk at a comfortable speed (CWS) in such a way that his right foot lands on the first platform and the left on the second one. If the subject missed this instruction, the test was rejected and performed again. The last test is performed at a higher walking speed (fast walking speed, FWS), with the same instructions about the landing feet. Both tests are completed three times each.

For the second battery of tests, four tests were performed. First, the subject is asked to walk at a comfortable speed, with his right foot landing first on the force platform. The second test is conducted at a lower speed (approximatively 30% slower, CWS-30), with the same instructions about the landing feet. The third test is conducted at a higher speed (CWS+30), with the same instruction about the landing foot. The fourth test is a squat jump test, where the subject is asked to stand still in equilibrium on one foot for at least two seconds (the counting starts only when equilibrium is reached), then jumps vertically and lands smoothly on the platform on the same foot. The test is conducted on each foot. The objective of this test is to assess an activity other than walking, still mostly restricted to the sagittal plane, and characterized by the presence of phases with no foot–ground contact.

Parameters	Comfortable gait	Fast gait
Walking speed	1.39 ± 0.19 m/s	2.00 ± 0.11 m/s
Stride length	1.38 ± 0.08 m	1.73 ± 0.06 m
Step length	0.69 ± 0.04 m	0.86 ± 0.03 m
Walking cadence	1.00 ± 0.11 s^{-1}	1.15 ± 0.08 s^{-1}
Stance phase	61.12 ± 6.61 %	57.28 ± 1.55 %
Swing phase	38.88 ± 6.61 %	42.72 ± 1.55 %

TABLE 3.4: Spatio-temporal parameters of the gait

3.3 Gait experimental results

As a reminder, Table 3.1 shows the general characteristics of the populations of reference, composed of five healthy and sedentary men for the first battery and of one healthy and sedentary man and three women for the second one.

3.3.1 Spatio-temporal data

Based on two consecutive gait cycles, the main general parameters of the gait cycle have been acquired and both groups are gathered in Table 3.4. The duration of the stance and swing phases are normalised with the cycle duration. The gait cycle begins with the heel strike of the right foot and ends with the same event.

3.3.2 Kinematic parameters

The results displayed in Figure 3.3 come from a representative gait test of one of the subjects involved in the study. The results for the comfortable and fast walking speed are compared and normalised with the cycle duration. To obtain the estimations of the different joint angles, we followed the procedure that will later be described in Section 4.1 and 5.1.2.

The flexion of the hip increases at the beginning and the end of the gait cycle with the walking speed. At mid-cycle, the flexion of the hip increases as well. This variation was expected given the increased stride length.

The amplitude of the knee flexion appears to increase during the double support reception phase. The maximum extension happens earlier in the cycle.

The d-flexion and p-flexion amplitudes of the ankle remain approximatively the same for the comfortable and fast gait tests. The maximum p-flexion happens also earlier in the cycle.

These results are comparable with similar results described in the literature (Uchida and Delp, 2021), see e.g. Figure 2.11 from (Winter, 1984).

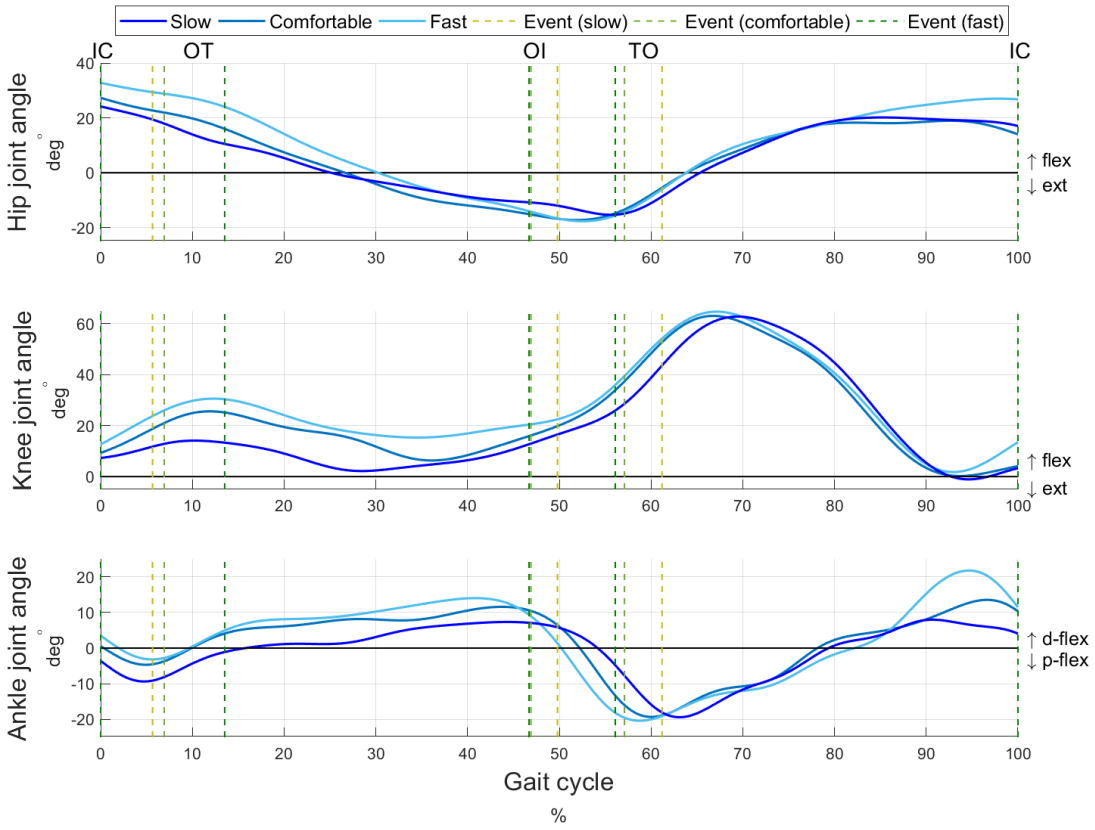

FIGURE 3.3: Comparison of the joint angle for a comfortable, a fast and a slow gait test. IC: initial contact; OT: opposite toe off; OI: opposite initial contact; TO: toe off.

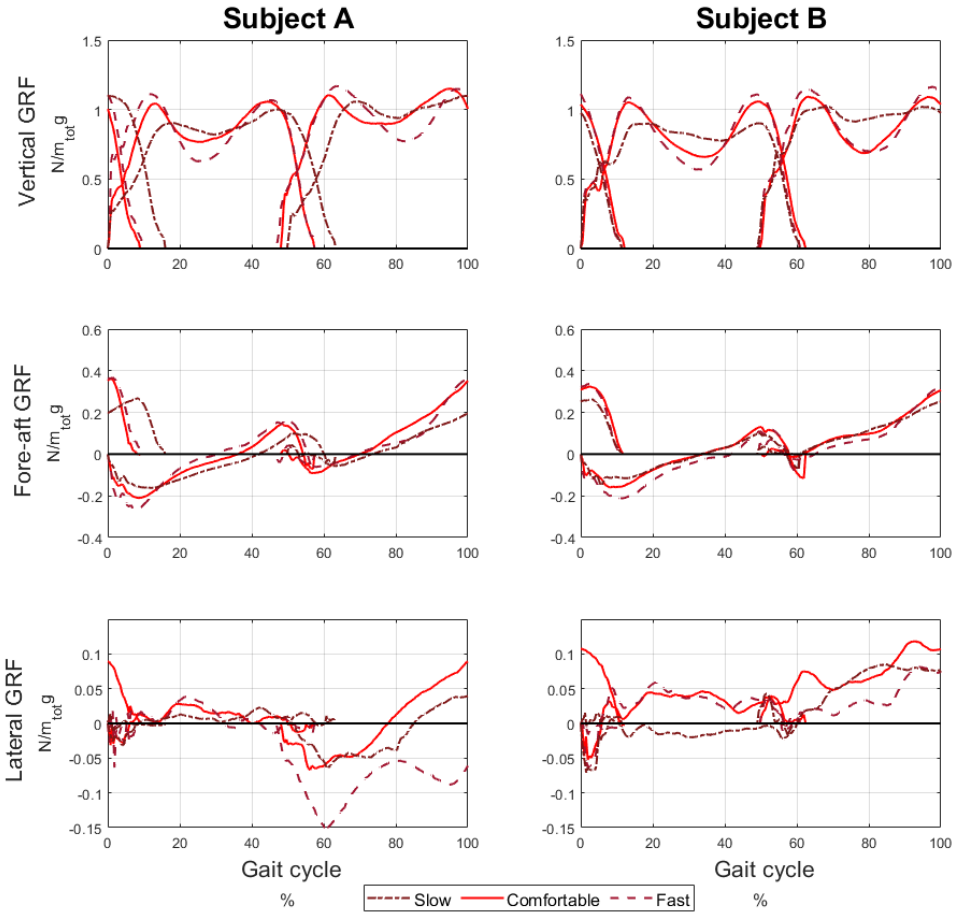

FIGURE 3.4: Comparison of the ground reaction forces for a comfortable, a fast and a slow gait test for two different subjects, where m_{tot} is the total mass of the subject.

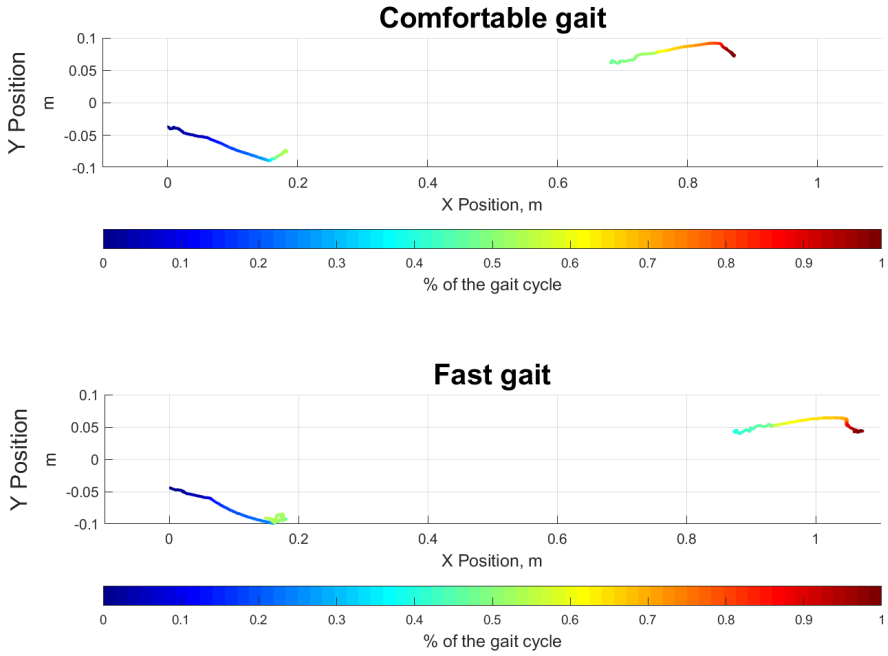

FIGURE 3.5: Comparison of the centre of pressure for a comfortable, a fast gait and a slow gait test. x and y represent the longitudinal and lateral coordinates.

3.3.3 Ground reaction forces and centre of pressure

The experimental force platforms results displayed in Figure 3.4 come from two different subject's gait tests. The results for the slow, comfortable, and fast walking speed are compared and normalised with the cycle duration and the total mass m_{tot} of the subject. It can be observed that these subjects exhibit slightly different curves in terms of peak magnitudes, plateau levels, loading rate,... These variations fall within the natural inter-subject variability and remain within the normal range of healthy gait patterns.

On the vertical axis, the reception peak increases with the walking speed. The propulsion peak conserves its amplitude but happens earlier. The double support phase duration is reduced.

On the horizontal axis, the amplitude increases with the walking speed. The heel rise (HR), representing the transition between the reception and propulsion phase, happens also earlier in the cycle.

On the lateral axis, the amplitude remains constant with respect to the gait events.

In Figure 3.5, the reference point to express the position of the centres of pressure of the right and left foot is located on the ground level in the frontal plane and with respect to the right heel strike. The results for the comfortable and fast walking speed are compared and normalised with the cycle duration.

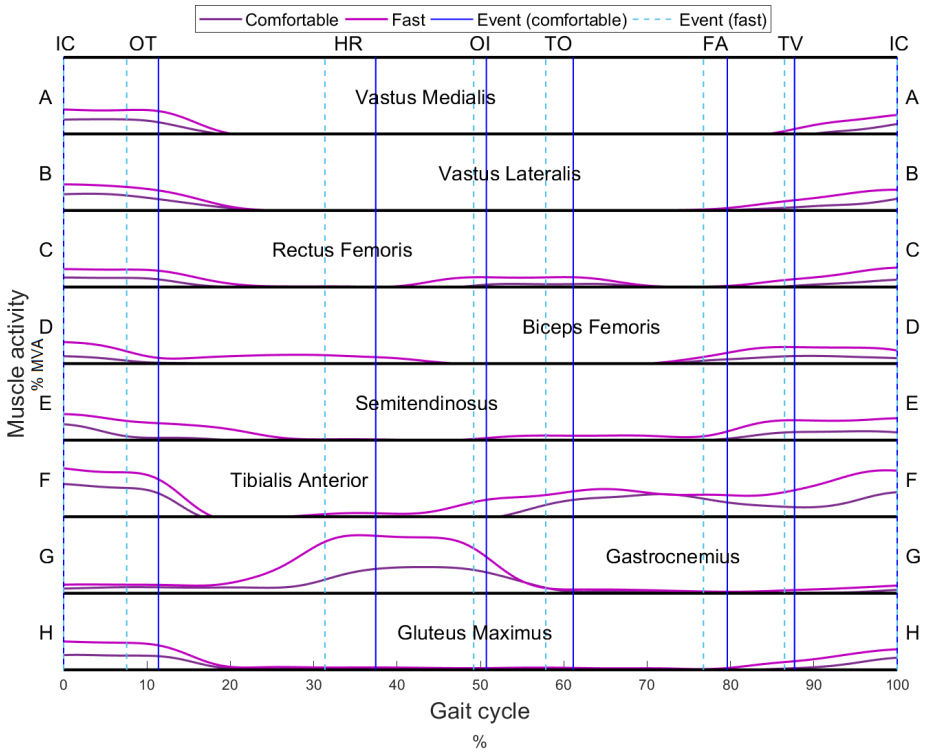

FIGURE 3.6: Comparison of the muscular activity for a comfortable and a fast gait test. IC: initial contact; OT: opposite toe off; HR: heel rise; OI: opposite initial contact; TO: toe off; FA: feet adjacent; TV: tibia vertical. Letters from Table 3.2 and Figure 3.2.

The stride length increases with respect to the walking speed. The position of the centre of pressure relatively to the foot moves also faster from heel to toe, the COP remaining for a longer period of time on the latter.

3.3.4 Muscle activity

The experimental EMG results displayed in Figure 3.6 come from the same representative gait test. The results for the comfortable and fast walking speed are compared and normalised with the cycle duration. The activity signals were scaled using the results of maximum voluntary activation (MVA) tests performed for each monitored muscle group. For each group, three MVA trials were recorded, and the envelopes of these signals were computed in order to define a representative maximal activation level. The peak value of this envelope was then used as a normalisation reference. Finally, the EMG envelopes obtained during the gait trials were scaled with respect to these MVA values, allowing the estimation of the relative activation level of each muscle group during the different gait tests.

The activity increases with respect to the walking velocity. For the biceps femoris, semitendinosus and tibialis anterior, the duration of the activity noticeably increases.

3.4 Discussion

The experimental data acquisitions were performed in the Laboratory of Motion Analysis (LAM). This choice was mainly motivated by the decision to acquire the experimental data in-house, in order to ensure full control and consistency over the entire experimental protocol, instead of relying on external data. In particular, this approach allowed precise control of key factors such as barefoot conditions, walking speed, reference foot definition, marker placement strategy and signal acquisition settings. The experimental data were therefore primarily intended to provide a reliable and coherent reference dataset for model development and validation.

Nevertheless, several sources of uncertainty can be identified. They include motion capture errors (marker placement, skin motion artefacts, occlusions and interpolation of missing trajectories), force platform accuracy, and EMG-related uncertainties such as electrode placement, skin impedance and signal normalization. These uncertainties are known to affect joint kinematics, kinetics and muscle activation estimates. These uncertainties associated with the experimental measurements were not explicitly quantified in terms of confidence intervals or formal error propagation. Rather than isolating each contribution, their combined effect was evaluated indirectly by comparing the obtained results with values reported in previous studies.

However, the representativeness of the experimental population constitutes an important limitation. The subjects were predominantly healthy young adults, mostly male, with no reported musculoskeletal pathology. As a result, the experimental data can not be considered representative of the general population. This limited diversity may influence the measured values and, consequently, some modelling choices or parameter values adopted in the following chapters. The proposed model should therefore be interpreted as validated for a healthy gait pattern, and caution should prevail when extrapolating the results to pathological populations, elderly subjects or high-performance athletic motions.

3.5 Conclusion of the chapter

In this chapter, the experimental protocols have been described. They were established to obtain a reliable set of healthy walking data in conjunction with a master's thesis from a physiotherapy student and the results obtained seem to correspond to the description of healthy walking in the literature.

These results will serve as a gold standard for numerical modelling and the study of the results of our contact models developed in Chapter 4 and 5.

Chapter 4

2D inverse dynamics skeletal model

In this chapter, the description of the skeletal model, including a rigid contact model between the foot and the ground, is given, as well as the numerical scheme used to determine the inverse dynamics solution. The purpose of the contact model is to provide an efficient method to account for the ground reaction forces when no measurement of these forces is available, see Chapter 3. As a rigid contact model is considered, the skeletal model is developed without requiring any data related to compliance of the foot. More precisely, every limb of the human body is considered rigid, and the indeterminacy in the force estimation (e.g., during double-support phase) is handled using an optimization approach in order to provide a numerical solution.

This chapter is divided into three main sections: the 2D model and its results, published in the Journal of Biomechanics (Van Hulle et al., 2020), and a discussion of results needed for the extension of our model to 3D.

The purpose of the skeletal model is to provide a general numerical approach to solve the inverse dynamics problem and determine the contact reaction forces and joint torques, while limiting the number of modelling parameters. The goal is to keep it as simple as possible in 2D, using a rigid body model of the foot and a skeletal model and eluding the muscle recruitment computation and avoiding compliance data. The contact between the foot and the ground is expressed using unilateral contact conditions at the centre of pressure (COP), and ground reaction forces (GRF) are modelled using Lagrange multipliers. The internal joint torques are represented by Lagrange multipliers associated with the driving constraints on the joint angles. The model assumes that the position of the centre of pressure is moving as a function of the segment rotation angle in agreement with experimental data. The whole set of joint torques and ground reaction forces are obtained by inversion of the equation of motion in a least square sense and a post-filtering method. The results obtained with this method are compared with experimental results obtained with force platforms considered here as the gold standard, and also with other rigid models found in the literature.

Segment	Segment weight/ Total body weight	Centre of mass/ Segment length (Proximal)
Foot	0.0145	0.5
Leg	0.0465	0.433
Thigh	0.1	0.433
Head, arms, trunk	0.678	0.626

TABLE 4.1: Anthropometric data (Winter, 2009)

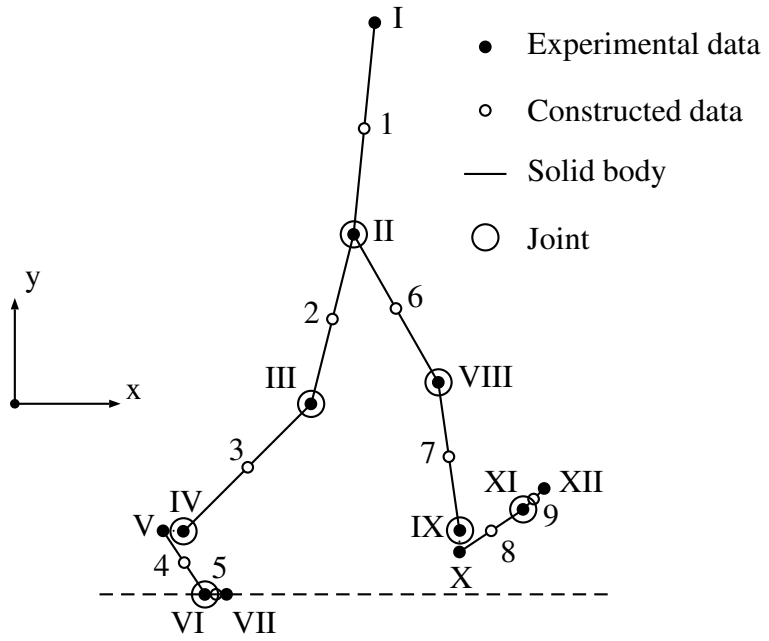

FIGURE 4.1: Muskuloskeletal model, constructed data based on Table 4.1

4.1 2D model

As shown in Figure 4.1, the human body is modelled with nine rigid bodies: torso, femur right-left, tibia right-left, foot right-left and toes right-left. These bodies evolve in the sagittal plane and are represented by three control points: the proximal and distal extremities and the centre of mass. The position of these centres of mass relatively to the extremities comes from the anthropometric Table 4.1 (Winter, 2009).

To describe the motion of a multibody system, relative or absolute coordinates can be chosen (Géradin and Cardona, 2001). For biomechanical problems, relative independent coordinates (e.g. joints angles and pelvis position and orientation) are usually used, and no bilateral constraint needs to be considered. In this model, absolute coordinates are chosen: compared to relative coordinate formulations, this approach leads to simpler equations of motion and a straightforward evaluation of the reactions forces in the bodies and joints, which are represented by the Lagrange multipliers. The following

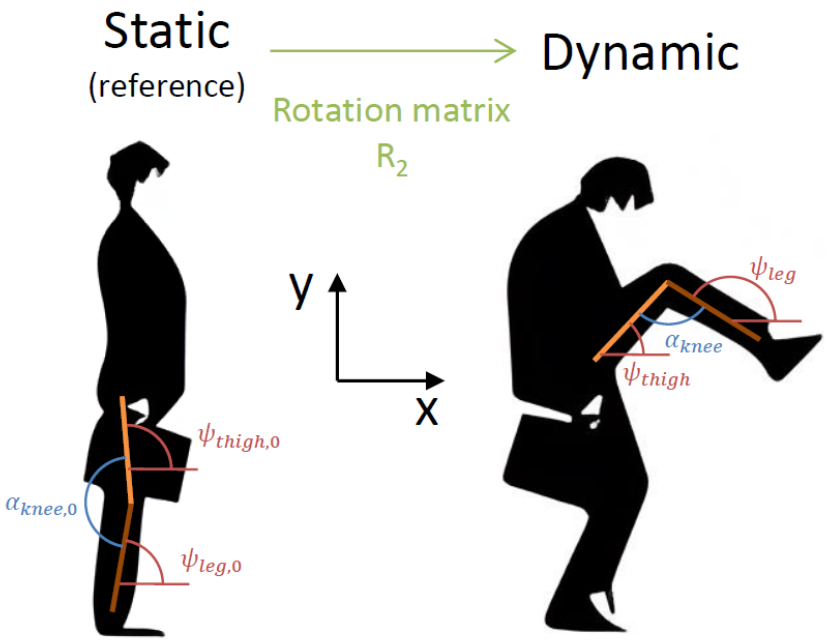

FIGURE 4.2: Segment orientation and joint angles. Illustration from "Monty Python's Ministry of silly walks"

generalized coordinates (g.c.) $\mathbf{q}(t)$ are chosen: the x and y coordinates of the extremities and of the centre of mass of each segment (42 g.c), the absolute orientation ψ (flexion/extension angle in the sagittal plane) of each segment (9 g.c) and the relative angle between two consecutive segments (8 g.c) are also taken into account.

To compute the orientation of a segment in 2D, a method similar to (Winter, 2009) is used. Figure 4.2 represents a schematic view of the relation between the orientation of the thigh and the leg, and the relative joint angle of the knee. The positions of the hip, knee and ankle are first measured during a static test, giving us a reference, and then during the dynamic tests. To find the orientation of the thigh at each time step for the dynamic test we solve the following equations:

$$\mathbf{x_{thigh,dynamic}} = \underbrace{\begin{bmatrix} \cos\psi_{thigh} & -\sin\psi_{thigh} \\ \sin\psi_{thigh} & \cos\psi_{thigh} \end{bmatrix}}_{\mathbf{R_2}} \mathbf{x_{thigh,0}} \tag{4.1}$$

Equation (4.1) is solved for the unknowns ψ for the nine segments of our skeletal model (the position of the extremities are measured experimentally and therefore known).

The eight relative joint angles are based on the orientation of the different limbs. For example, the relative angle of the knee is defined as

$$\alpha_{knee} = \psi_{thigh} - \psi_{leg} \tag{4.2}$$

For example, for the right thigh, the generalized coordinates are expressed as (see Figure 4.1):

$$\mathbf{q}_{thigh,r} = [x_{II}, y_{II}, x_2, y_2, x_{III}, y_{III}, \psi_{thigh,r}]^T \tag{4.3}$$

The complete vector $\mathbf{q}$ is constructed with the coordinates of every segments and the relative joint angles so that it contains 59 components. The displacements of segment extremities in the sagittal plane, labelled with I...XII in Figure 4.1 are either measured directly or follow virtual markers created based on experimental markers in post-processing, respecting the rigid body assumption. Hence, the fitting of these generalized coordinates on the measured and virtual marker trajectories is a trivial problem, which is an additional advantage of using an absolute coordinates model. The other coordinates are then calculated based on kinematic considerations to complete the vector. As the out-of-plane motion is ignored, the vector of generalized coordinates may slightly violate the rigidity constraints. In this study, this artefact leads to a variation of link lengths of maximum 1%, which can be neglected for the purpose of an inverse dynamics analysis. In case of larger out-of-plane motions, an optimization procedure could be used to ensure the consistency, as in (Alonso et al., 2010). This issue will be addressed in 3D in Chapter 5.

As the model has 11 degrees of freedom and 59 generalized coordinates, 48 scleronomic bilateral constraints are introduced and represent the rigid body conditions and the constraints defining the joint angles from the absolute coordinates. For example, the rigid body constraints between the hip and the centre of gravity of the right thigh are expressed as

$$\begin{cases} x_{II} - x_2 - L_{thigh,r}\cos(\psi_{thigh,r}) = 0 \\ y_{II} - y_2 - L_{thigh,r}\sin(\psi_{thigh,r}) = 0 \end{cases} \tag{4.4}$$

In the inverse dynamics analysis, the relative joint angles are piloted by the experimental data, leading to eight additional rheonomic driving constraints. For the right knee, the time-dependent driving constraint is

$$\alpha_{knee,r} - \alpha_{knee,r,exp}(t) = 0 \tag{4.5}$$

where the subscript exp refers to the experimental measurement of the motion.

The experimental acquisition of relative rotations is performed straightforwardly. The positions of the experimental markers (see Figure 4.1) are measured during a dynamic test. If a marker is not seen by any camera, its trajectory is missing. Interpolation was performed to estimate these missing marker trajectory segments when necessary. When the missing marker was redundant, meaning that the position and orientation of the corresponding segment could still be reliably reconstructed from the remaining markers, no interpolation was applied. When interpolation was required, the missing data were reconstructed by fitting a third-order polynomial, enforcing continuity of both the signal and its first derivative at the boundaries of the segment. Interpolation was only applied to short gaps ($<$ 100 ms), and longer gaps were excluded from the analysis. In 2D, the absolute orientation of each segment can be easily determined at each time step, as shown in Equation

(4.1). By knowing the absolute orientation of the segments, the relative angles between each consecutive segments over time are implicitly defined by solving Equation (4.2).

These obtained values then need to be imposed on the corresponding generalized coordinates using driving constraints, as in Equation (4.5). In the case of inverse dynamics, these constraints are self-satisfied since the motion is known, and do not provide new information. However, the constraint gradient and the Lagrange multipliers associated with these constraints help complete the dynamic equilibrium of forces, defined in the following sections and in Equation (4.15).

The set of 56 bilateral and driving constraints is expressed as:

$$\mathbf{g}^{\mathcal{B}}(\mathbf{q}, t) = \begin{bmatrix} \mathbf{g}^{bilateral} \\ \mathbf{g}^{driving} \end{bmatrix} = \mathbf{0} \tag{4.6}$$

As the joint angles are prescribed, three degrees of freedom remain: the vertical and lateral motion of the centre of gravity of the pelvis and its orientation. Although these data are given by the experimental measurement of the movement, no driving constraint is imposed here: these degrees of freedom are not directly controlled in our inverse dynamics formulation. If constraints were imposed here, that would imply the creation of Lagrange multipliers, and therefore of actuation forces on the centre of gravity of the pelvis in the equations of motion which would not be physical. On the other hand, a muscle torque is applied in the joints during motion, which justifies the introduction of driving constraints with Lagrange multipliers on the relative angles in the joints. In the end, we thus have 56 bilateral and driving constraints, 59 generalized coordinates and $59 - 56 = 3$ degrees-of-freedom.

The velocity vector $\dot{\mathbf{q}}(t)$ and the acceleration vector $\ddot{\mathbf{q}}(t)$ are computed to be consistent with respect to the bilateral constraints. To avoid a coupling between the computation of the velocities and accelerations and the algorithm for the activation of the contact constraints (Section 4.1.3), the contact constraints are disregarded at this level, following a similar strategy as in (Winter, 2009). The generalized coordinates are partitioned into two subsets: independent coordinates $\mathbf{q}^I$ (joints angles and pelvis position and orientation), and dependent coordinates $\mathbf{q}^D$ (the remaining positions and orientations):

$$\mathbf{q} = \begin{bmatrix} \mathbf{q}^I \\ \mathbf{q}^D \end{bmatrix} \tag{4.7}$$

First, the velocity and acceleration of the independent coordinates (joints angles and pelvis position and orientation) are obtained through numerical time differentiation, based on central difference scheme and filtered using a Butterworth fourth-order zero-shift low-pass filter, with a cut-off frequency of ω_{kin}, set to 6 Hz in accordance with the literature (Winter, 2009). The central difference formulae are:

$$\begin{cases} \dot{\mathbf{q}}^I(t^*) = \left(\mathbf{q}^I_{exp}(t^*+h) - \mathbf{q}^I_{exp}(t^*-h)\right)/2h \\ \ddot{\mathbf{q}}^I(t^*) = \left(\mathbf{q}^I_{exp}(t^*+h) - 2\mathbf{q}^I_{exp}(t^*) + \mathbf{q}^I_{exp}(t^*-h)\right)/h^2 \end{cases} \tag{4.8}$$

where h is the time step, linked to the sampling rate of the experimental acquisition.

The velocity and acceleration of the dependent coordinates are then reconstructed by solving the bilateral constraints at velocity and acceleration levels to be consistent with the rigid body assumption (Géradin and Cardona, 2001). Mathematically, we define the matrix:

$$\mathbf{S} = \begin{bmatrix} \mathbf{I} \\ -\left(\frac{\partial \mathbf{g}^{bilat}}{\partial \mathbf{q}^D}\right)^{-1} \frac{\partial \mathbf{g}^{bilat}}{\partial \mathbf{q}^I} \end{bmatrix} \tag{4.9}$$

And finally, the velocity and acceleration vector are evaluated as:

$$\begin{cases} \dot{\mathbf{q}} = \mathbf{S}\dot{\mathbf{q}}^I \\ \ddot{\mathbf{q}} = \mathbf{S}\ddot{\mathbf{q}}^I + \dot{\mathbf{S}}\dot{\mathbf{q}}^I \end{cases} \tag{4.10}$$

4.1.1 Model of the foot and contact constraints

As shown in Figure 4.3, the displacements of each foot are measured by four optoelectronic markers: on the heel, on the malleolus (representing the joint between the foot and the tibia), on the head of the first metatarsal bone (joint between the foot and the toes), and on the hallux. The developments are given for the left foot but the right foot is modelled in the same way. However, these markers never touch the ground, and moreover, depending on the orientation of the foot, the distance between the ground and those markers when contact occurs may change. To obtain a simple expression of the foot/ground distance, three new control points on the foot (A, B and C) are placed at the ground level and at the vertical of the experimental markers during a preliminary static test. These three points are assumed rigidly connected to the points V, VI and VII respectively, and follow the motion of the foot segments. As can be seen in Figure 4.3, the metatarsophalangeal joint was modelled at ground level in the present formulation. This choice was initially made to simplify the equations of motion of the first version of the model. From a kinematic standpoint, placing the joint at ground level introduces only a vertical offset and does not affect the relative angles of the segments obtained as explained above (the evaluation procedure does not involve the position of the joint axes). After solving the equations of motion, this modelling choice primarily impacts the metatarsophalangeal joint torque, whose contribution remains negligible compared to the overall joint loading during gait. Nevertheless, this simplification constitutes a limitation of the model, and positioning the joint at its anatomical location would be preferable in future refinements.

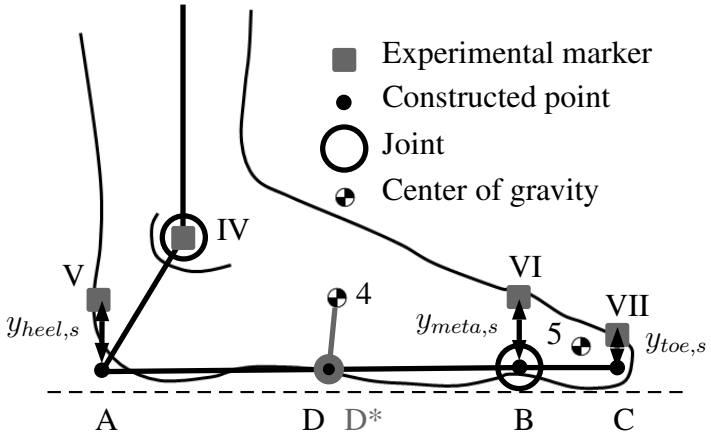

FIGURE 4.3: Model of the left foot

At this level, a first model of the foot is proposed by imposing a non penetration and a non-slipping condition at points A, B and C. At this point, the normal unilateral constraints for the left foot is written as follow:

$$\begin{cases} g^{A_n} = y_A \geq 0 \\ g^{B_n} = y_B \geq 0 \\ g^{C_n} = y_C \geq 0 \end{cases} \tag{4.11}$$

However, this approach leads to irregularities and jumps of the ground reaction moment (GRM) and of the position of the centre of pressure because of the coarse spatial localization of the centre of pressure (COP), as will be shown later in the results and in Figure 4.4.

To prevent these irregularities, a second model of the foot is proposed in this paper. Based on the three control points defined previously (A, B and C), one geometric point D moving from A to C and representing the COP is created. Experimentally, we observe that x_D is strongly correlated with the foot segment inclination ψ_4. Figure 4.4 shows the mean value of x_D as a function of ψ_4 obtained from the force platforms measurements for gait and squat jump tests. Based on the experimental data, the position of the COP x_D as a function of ψ_4 seems to be independent of the activity or subject. Hence, we assume that the position of the geometric point D is a function of y_A, y_B, y_C and ψ_4 as follows:

$$\begin{aligned} y_D &= \min(y_A, y_B, y_C) \\ x_D &= \mathcal{F}(\psi_4) \end{aligned} \tag{4.12}$$

where the function $\mathcal{F}$ is defined to fit mean experimental data. In this paper, we propose a function defined in three parts between major gait events: a first sinusoidal function between the heel strike ($\psi_4 = \delta_{HS}$) and the heel off ($\psi_4 = \delta_{HO}$), a second sinusoidal function between the heel off and the metatarsal off ($\psi_4 = \delta_{MO}$), and a linear function between the metatarsal off and the toe off ($\psi_4 = \delta_{TO}$). The function is thus fully determined by the four parameters δ_{HS}, δ_{HO}, δ_{MO} and δ_{TO}.

As the geometric point D is moving with respect to the foot, we then define the point D^* which instantaneously coincides with point D and is rigidly fixed to the foot. The four coordinates x_{D^*} and y_{D^*} of the two feet are thus added to the vector of generalized coordinates $\mathbf{q}(t)$, which contains now $n = 63$ components. Also, four new bilateral constraints are added to represent the rigid connexion between the D^* and the points 4 and 8 of the two feet.

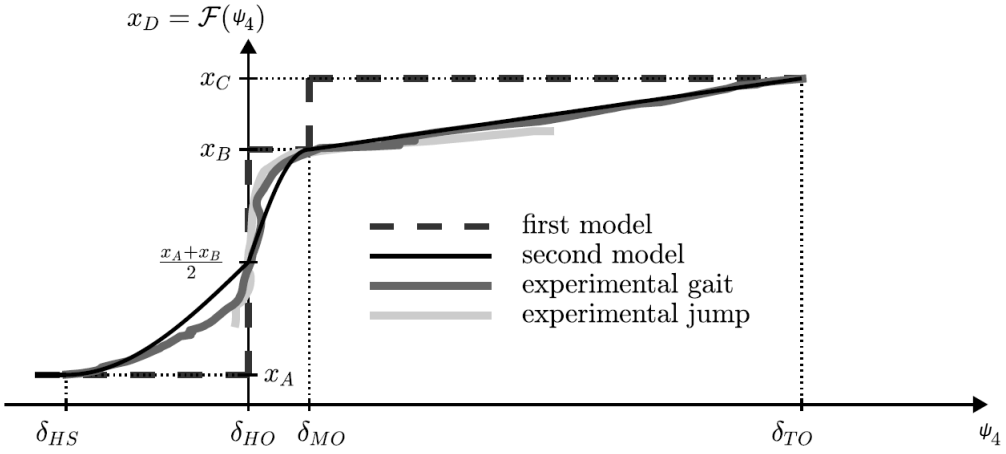

FIGURE 4.4: Evolution of the longitudinal position x of the COP in the sagittal plane

Finally, the GRF are computed by using a unilateral normal constraint and a tangential sticking constraint at the point D^*, see also the rolling without slipping tangential condition in (Caspers et al., 2017; Caspers, 2019). First, the normal non-penetration condition takes the form of a complementarity condition between the normal gap distance $\mathrm{g}^{D^*,n}$ and the normal force $\lambda^{D^*,n}$:

$$\mathrm{g}^{D^*,n}(\mathbf{q}) = y_D^* \geq 0, \quad \lambda^{D^*,n} \geq 0, \quad \mathrm{g}^{D^*,n}(\mathbf{q})\lambda^{D^*,n} = 0 \tag{4.13}$$

In the inverse dynamics analysis proposed in this thesis, these conditions are not explicitly imposed but they are exploited to build the algorithm for the generalized forces, as explained below.

In the tangent direction, the contact condition can be represented by a Coulomb friction model with a distinction between stick and slip situations. In this study, we assume that the foot does not slip on the ground so that all closed contact are in stick state (Pàmies-Vilà et al., 2018). This means that the tangent displacement $\mathrm{g}^{D^*,t}$ and the tangent reaction forces $\lambda^{D^*,t}$ satisfy:

$$\begin{aligned} &\text{if} \quad \mathrm{g}^{D^*,n}(\mathbf{q}) = 0 \quad \text{then} \quad \mathrm{g}^{D^*,t}(\mathbf{q}) = \Delta x_{D^*} = 0 \\ &\text{else} \quad \lambda^{D^*,t} = 0 \end{aligned} \tag{4.14}$$

The normal GRF (resp. tangent) is given by the Lagrange multipliers $\lambda^{D^*,n}$ and $\lambda^{D^*,t}$ of the normal (resp. tangent) constraints, for each foot. The centre of pressure (COP) of the foot is given by x_D.

The total set of bilateral constraints and contact constraints (such as Equations 4.13-4.14) are collected in the vector $\mathbf{g}(\mathbf{q}, t)$.

4.1.2 Dynamic equilibrium and least square evaluation of the forces

The dynamic equilibrium of the mechanical system is given by $n = 63$ equations, written in the following matrix form (Géradin and Cardona, 2001):

$$\mathbf{M}\ddot{\mathbf{q}} + \mathbf{g}_\mathbf{q}^\mathrm{T}(\mathbf{q}, t)\boldsymbol{\lambda} - \mathbf{f}^{ext} = \mathbf{0} \tag{4.15}$$

Notice that, as the system is planar and is represented using absolute coordinates, the dynamic equilibrium does not involve gyroscopic and centrifugal forces.

The $n \times n$ mass matrix $\mathbf{M}$ is constant and constructed thanks to anthropometric tables (Winter, 2009). The mass and inertia of each segment is attributed to the components x, y and orientation of the centre of mass only. The mass matrix is thus singular, square and diagonal. The construction of this matrix is based on the expression of the kinetic energy of each limb.

For the right thigh, based on Equation (4.3), the mass matrix is:

$$\mathbf{M}_{thigh,r} = diag[0, 0, m_{thigh,r}, m_{thigh,r}, 0, 0, I_{thigh,r}] \tag{4.16}$$

The complete mass matrix $\mathbf{M}$ is constructed by assembly of the mass matrices of the different segments.

In Equation (4.15), $\mathbf{g}_\mathbf{q}(\mathbf{q}, t) = \frac{\partial \mathbf{g}(\mathbf{q},t)}{\partial \mathbf{q}}$ is the matrix of bilateral, driving and unilateral constraints gradients, $\boldsymbol{\lambda}$ is the vector of bilateral, driving and unilateral Lagrange multipliers, and $\mathbf{f}^{ext}$ represent the gravity acting on the system. Equation (4.15) represents the balance between the inertial forces, the reaction forces resulting from the constraints $\mathbf{g}_\mathbf{q}^\mathrm{T}\boldsymbol{\lambda}$, composed of the joint reactions forces (enforcing the bilateral constraints), joint torques (enforcing the driving constraints) and ground reaction forces (enforcing the non-penetration and sticking constraints), and the external forces.

In the inverse dynamics problem, the accelerations $\ddot{\mathbf{q}}$ are given and the Lagrange multipliers constitute the sole unknowns. For a given $\ddot{\mathbf{q}}$, and in the case $m \leq n$, (García De Jalón and Gutiérrez-López, 2013) show that the global resultant of the forces $\mathbf{g}_\mathbf{q}^\mathrm{T}\boldsymbol{\lambda}$ is unique but that the vector of Lagrange multipliers $\boldsymbol{\lambda}$ remains indeterminate if the matrix $\mathbf{g}_\mathbf{q}^\mathrm{T}$ does not have maximum rank ($rank(\mathbf{g}_\mathbf{q}^\mathrm{T}) < m$), in other words, if the constraints are redundant. In our case, we also need to cover the case $m > n$ and it is important to distinguish bilateral constraints, active contact constraints and inactive contact constraints.

To obtain the unknowns $\boldsymbol{\lambda}$, we develop Equation (4.15), and use Equations (4.6) to (4.14) to define the set of active constraints. In Equation (4.15), it

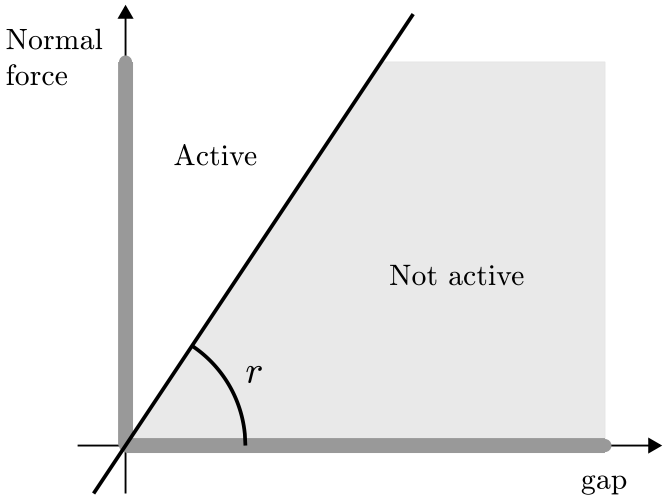

FIGURE 4.5: Complementarity condition (bold grey) and mixed constraint activation criterion, (Alart and Curnier, 1991)

is essential to separate the set of active constraints $\mathcal{A}$, whose Lagrange multipliers can differ from zero from inactive ones $\overline{\mathcal{A}}$, whose Lagrange multipliers are zero. The classification criterion will be detailed in Section 4.1.3. We obtain:

$$\mathbf{g}_{\mathbf{q}}^{\mathcal{A},\mathrm{T}}(\mathbf{q})\boldsymbol{\lambda}^{\mathcal{A}} = -\mathbf{M}\ddot{\mathbf{q}} + \mathbf{f}, \qquad \boldsymbol{\lambda}^{\overline{\mathcal{A}}} = \mathbf{0} \tag{4.17}$$

Depending on the number of active constraints $m^{\mathcal{A}}$ in the system and their degree of redundancy, the problem might be over- and/or underdetermined and the solution for the Lagrange multipliers $\boldsymbol{\lambda}$ might not be unique. However, at the global level, the resultant $\mathbf{g}_{\mathbf{q}}^{\mathcal{A},\mathrm{T}}(\mathbf{q})\boldsymbol{\lambda}^{\mathcal{A}}$ is unique and has a physical meaning. We postulate that usual overground motions tend to minimize the full set of reaction forces $\boldsymbol{\lambda}^{\mathcal{A}}$. Hence, the over/underdetermination is handled using the least square method and the pseudo-inverse as suggested by (García De Jalón and Gutiérrez-López, 2013; Blumentals et al., 2016) in other contexts:

$$\boldsymbol{\lambda}^{\mathcal{A}} = \left(\mathbf{g}_{\mathbf{q}}^{\mathcal{A},\mathrm{T}}(\mathbf{q})\right)^{+} \left(\mathbf{f} - \mathbf{M}\ddot{\mathbf{q}}\right), \qquad \boldsymbol{\lambda}^{\overline{\mathcal{A}}} = \mathbf{0} \tag{4.18}$$

To eliminate the possible indeterminacy, other optimisations could be performed. It would lead to another weighting of the constraints, or even to another equation to solve.

4.1.3 Contact activation criterion

The contact activation criterion is based on the complementarity condition, Equation (4.13), between the gap function $g^{j,n}$ (gap distance between the j^{th} contact point and the surface, along its normal axis) and the normal reaction

force $\lambda^{j,n}$. In our context, $g^{j,n}$ is evaluated from kinematic measurements and $\lambda^{j,n}$ is estimated by our inverse dynamics scheme. Hence, both variables are affected by some uncertainties, and a robust classification criterion is needed. Inspired by the work of (Alart and Curnier, 1991), a mixed criterion relying on both values of $g^{j,n}$ and $\lambda^{j,n}$ is proposed so that the set of active contacts $\mathcal{C}$ is defined as (Figure 4.5):

$$\mathcal{C} = \{j : \lambda^{j,n} - r g^{j,n} \geq 0\} \tag{4.19}$$

where $r \geq 0$ is a scalar parameter whose chosen value will be discussed in Section 4.3. We also define the set of inactive contacts:

$$\overline{\mathcal{C}} = \{j : \lambda^{j,n} - r g^{j,n} < 0\} \tag{4.20}$$

For every contact j in $\mathcal{C}$, the constraints $g^{j,n} = g^{j,t} = 0$, whereas for all contacts j in $\overline{\mathcal{C}}$, the Lagrange multipliers are fixed to zero $\lambda^{j,n} = \lambda^{j,t} = 0$. These conditions are thus fully equivalent to Equations (4.13) and (4.14). At every time, we thus impose:

$$\mathbf{g}^{\mathcal{A}} = \begin{bmatrix} \mathbf{g}^{\mathcal{B}} \\ \mathbf{g}^{\mathcal{C},n} \\ \mathbf{g}^{\mathcal{C},t} \end{bmatrix} = 0 \quad \text{and} \quad \boldsymbol{\lambda}^{\overline{\mathcal{A}}} = \begin{bmatrix} \boldsymbol{\lambda}^{\overline{\mathcal{C}},n} \\ \boldsymbol{\lambda}^{\overline{\mathcal{C}},t} \end{bmatrix} = 0 \tag{4.21}$$

where the sets $\mathcal{C}$, $\mathcal{A}$ and $\overline{\mathcal{A}}$ implicitly depend on $\mathbf{q}$ and $\boldsymbol{\lambda}$ (see Equations 4.19, 4.20 and 4.21).

Combining the activation criterion with Equation (4.17) leads to an implicit problem for $\boldsymbol{\lambda}$ which can be solved numerically. Here, an iterative Newton semi-smooth solver is selected (Figure 4.6). The process is initialized by considering that every contact constraint is active. Then, Equation (4.18) is used to evaluate a first guess of the Lagrange multipliers. The activation status is then reevaluated using these Lagrange multipliers and the activation criterion in Equations (4.19) and (4.20). A new distribution of the Lagrange multipliers is determined in the next iteration, and the set of active contact constraints is again updated, until the proper contact status of each constraint is found.

4.1.4 Final filtering

The least-square solution might exhibit sudden and abrupt changes from one sampling time to the next, especially when activating and deactivating contact constraints. To ensure the temporal continuity of the GRF, a post-process final filtering of the results is applied to the previous results, using a Butterworth fourth-order zero-shift low pass filter, with a cut-off frequency ω_{dyn}, whose chosen value will also be discussed in Section 4.3. After filtering, $\boldsymbol{\lambda}^{\overline{\mathcal{A}}}$ is reset to zero to ensure the consistency with the activation status.

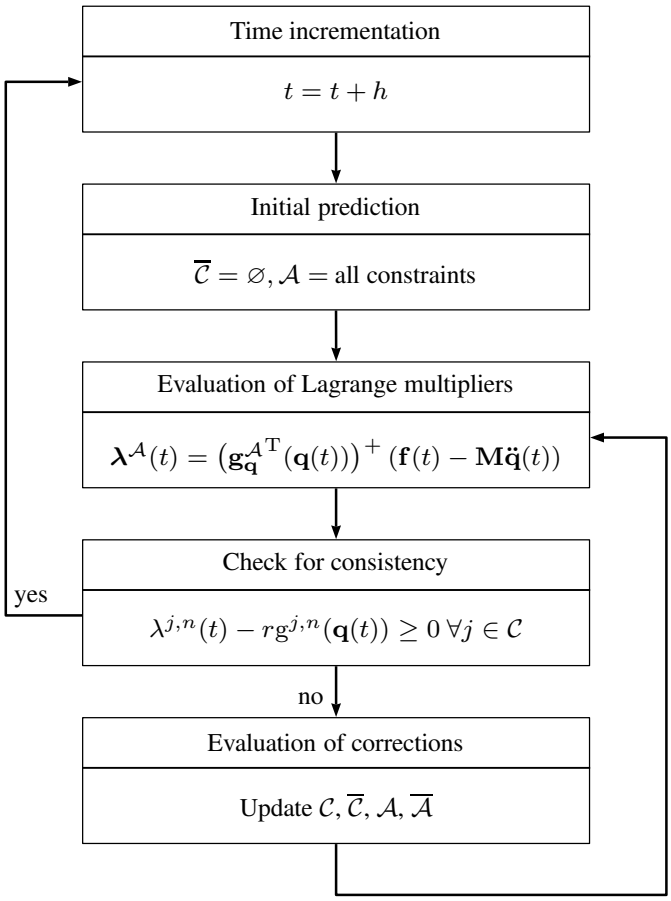

FIGURE 4.6: Evaluation of the force using a Newton semi-smooth solver

4.2 Results

The marker experimental data were first filtered to remove measurement noise using a zero-phase, low-pass Butterworth filter with a cut-off frequency of 6 Hz. Missing marker trajectories were extrapolated when necessary and when feasible, by enforcing continuity of both the signal and its time derivative. Once the vector of generalized coordinates was constructed, after estimating the COP position for each foot as a function of its orientation, the independent coordinates were temporally differentiated to obtain velocities and accelerations. The velocities and accelerations of the dependent coordinates were then reconstructed using the bilateral constraints. Finally, the algorithm described in Figure 4.6 was implemented to compute the Lagrange multipliers associated with the unilateral constraints, which represent the ground reaction forces.

The measurements on the force platforms are used as the reference results, and the errors in the numerically computed reaction forces are based on the Root Mean Square Error (RMSE), as defined in (Oh et al., 2013):

$$\text{RMSE} = \sqrt{\frac{1}{T}\int_0^T \left(u_{num}(t) - u_{exp}(t)\right)^2 dt} \tag{4.22}$$

where T is the duration of the test, limited to two steps, $u_{num}(t)$ and $u_{exp}(t)$ are respectively the numerical estimation and the experimental measurement of the GRF/GRM. The GRM are computed relatively to a point located between the force platforms.

Also, the relative Root Mean Square Error (rRMSE) is given by:

$$\text{rRMSE} = \frac{100 \quad \text{RMSE}}{\frac{1}{2}\left[max\left(u_{num}(t)\right) - min\left(u_{num}(t)\right) + max\left(u_{exp}(t)\right) - min\left(u_{exp}(t)\right)\right]} \tag{4.23}$$

Finally, in this study, the numerical value of the parameters are set to $\delta_{HS} = -0.3$ rad, $\delta_{HO} = 0$ rad, $\delta_{MO} = 0.15$ rad, $\delta_{TO} = 1$ rad, based on the mean value obtained experimentally for the 24 gait tests and consistent with the literature (Borghese et al., 1996), $r = 10^3$ N/m, $\omega_{kin} = 6$ Hz and $\omega_{dyn} = 12$ Hz.

4.2.1 Healthy gait tests

In Figure 4.7, the results are illustrated for one single gait test, with the two proposed foot models.

For the 24 tests, with the single point foot model, the rRMSE and standard deviation (SD) of the vertical GRF are 4.1%(1.1). The rRMSE and (SD) of the horizontal GRF are 11.2%(1.7). The rRMSE and (SD) of the GRM are only 5.3%(1.1), which is similar to the error on the vertical GRF.

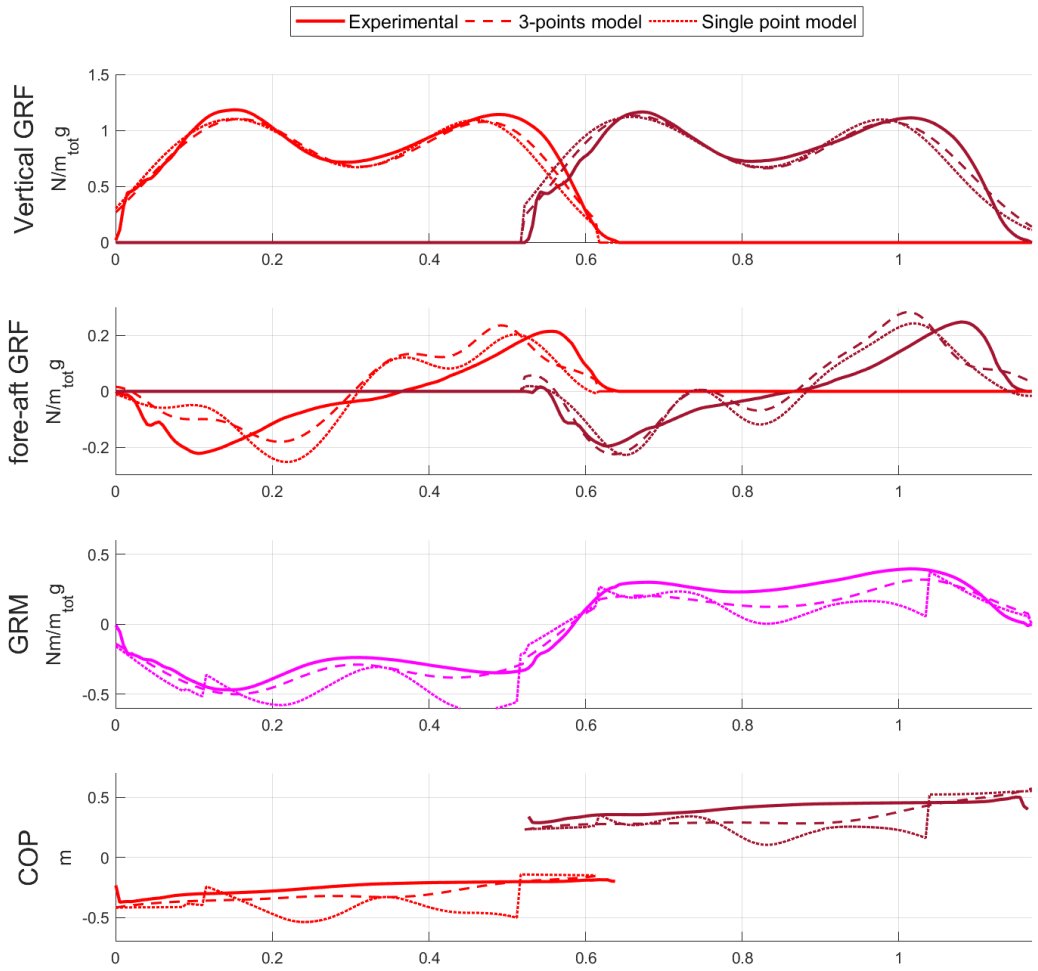

FIGURE 4.7: Comparison of the 3-points foot model and single point foot model with experimental measurements for one single gait test. Red: right foot; Brown: left foot; Magenta: right and left feet.

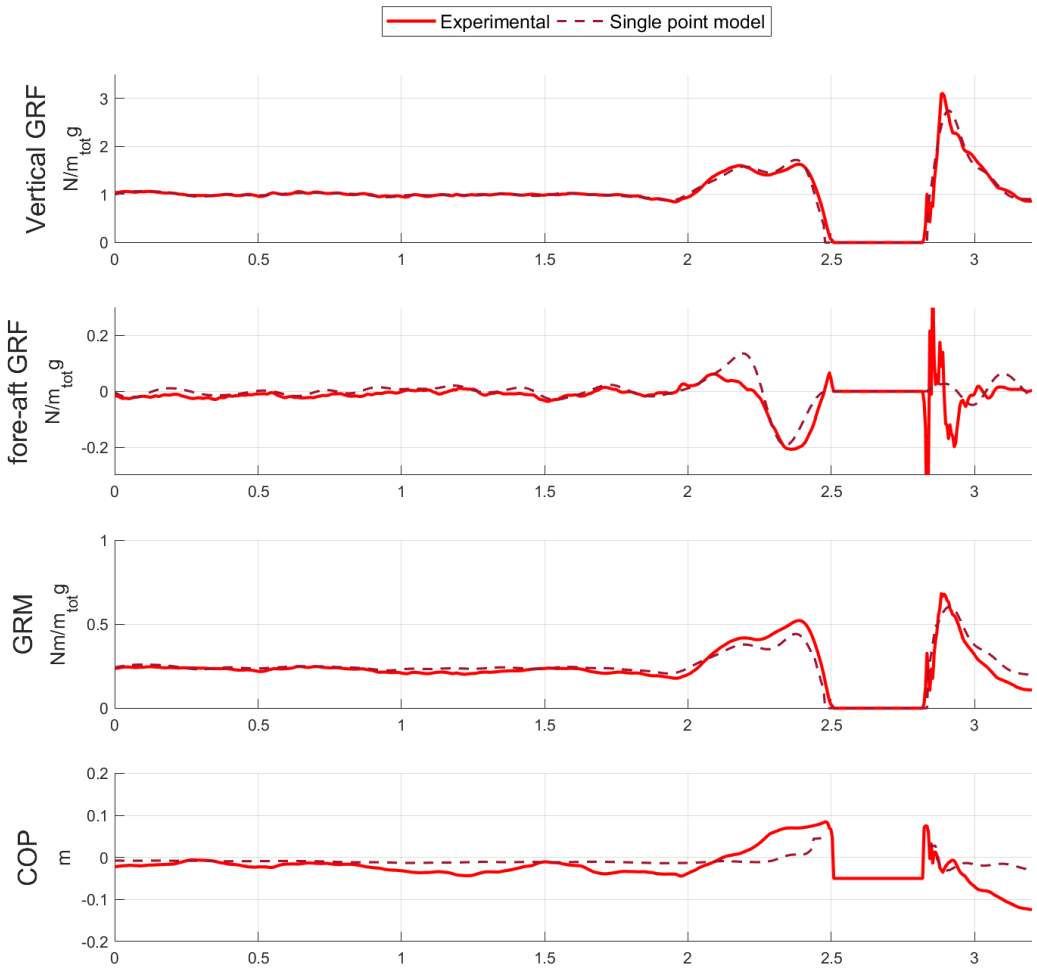

FIGURE 4.8: Comparison of the single point foot model numerical results with experimental measurement for one single squat jump test.

4.2.2 Jump tests

The method, coupled with the second foot model, is tested for a unilateral squat jump test and the results are shown in Figure 4.8. The rRMSE and (SD) are smaller for the vertical GRF, 2.4%(0.4), compared to the horizontal GRF, 5.6%(0.6). It comes from the fact that there is almost no movement on the horizontal direction, and mainly noise is measured. The rRMSE and (SD) of the GRM are 5%(0.4).

4.3 Discussion

A method is developed for the inverse dynamics analysis of the human motion, based on muskuloskeletal models using rigid segments and a unilaterally constrained foot-ground contact model. The proposed method provides results with limited errors. It relies on two main assumptions: the position

of the COP is assumed to be a function of the segment angle and the full set of reaction forces is evaluated in a least-square sense. The parameters are the activation parameter r, the cut-off frequencies ω_{kin} and ω_{dyn} of the filters, and the limit angles δ.

In the proposed model, the assumption that the COP evolves as a continuous function $\mathcal{F}$ of the foot segment angle is relevant for a variety of human movements (e.g. healthy gait, run, stance, jump,...). This assumption mostly affects the COP position (and thus the GRM), but a very limited influence on the value of the contact forces. It leads to a clear improvement of the GRM between the first and second model. In this work, the function $\mathcal{F}$ is defined by parts based on gait events (heel strike, heel off, metatarsal off and toe off) to fit properly the mean experimental data obtained during the gait and jump tests performed for this study. This assumption is clearly an approximation but our results confirm its relevance. The parameters δ of the function $\mathcal{F}$ have a clear biomechanical interpretation and have been measured and averaged for the 24 gait tests, leading to consistent values with the literature. Using a subject specific value of these parameters could further improve the results. However, in our experience, the results are quite robust with respect to these parameters and even to the choice of the function $\mathcal{F}$. Defining the function $\mathcal{F}$ on one population and validating it on an independent dataset would have been the preferred approach to formally assess generalizability. However, this was not feasible in the present study due to the limited number of available subjects, which did not allow for a meaningful separation between identification and validation populations. Alternative modelling strategies, such as data-driven or learning-based approaches, could also be considered. While such methods may improve generalization, they typically require larger datasets to be reliable and often lead to models that are less interpretable from a biomechanical standpoint. Given the available data, the choice to adopt a simple, physics-based formulation grounded in well-defined gait events, ensures robustness and ease of interpretation. Expanding the dataset or exploiting other public available datasets, e.g. (van der Zee et al., 2022), and exploring learning-based extensions remain natural perspectives for future work. In the case of high speed running or pathological gait, the motion of the COP can be more complex and a new COP function may thus be required (averaged or specific).

The model postulates a least-square distribution of the reaction forces, i.e., it assumes that during motion, the human body tends to minimize the value of those forces. This assumption is used to resolve the indeterminacy in the distribution of the horizontal GRF over the two feet which is particularly critical during the double support phase. It seems reasonable for many day-to-day activities and is confirmed by our results for gait and squat jump tests. The assumption that the human body tends to minimize the magnitude of internal and reaction forces during motion is generally accepted for basic locomotor tasks such as level walking in healthy subjects (Ackermann and van den Bogert, 2010). In this context, gait is often interpreted as an energetically efficient and mechanically economical movement. However, this assumption may no longer hold in pathological conditions, where pain

avoidance, muscle weakness, or joint degeneration alter motor strategies, or in high-performance sports, where force production and power output are deliberately maximized rather than minimized. Therefore, the proposed hypothesis should be regarded as task- and context-dependent. While it is appropriate for the study of fundamental activities of daily living such as walking, it would require reformulation or extension for pathological gait or performance-oriented movements. Incorporating alternative or additional cost functions reflecting injury avoidance, stability, or performance objectives constitutes an important perspective for future work, see e.g. (Ackermann and van den Bogert, 2010; Razavian and McPhee, 2015; Falisse et al., 2019; Haralabidis et al., 2021).

The activation parameter r can be selected to obtain robust results with respect to the measurement of the error on the displacement of the foot. With a small r, the activation criterion is more sensitive to the errors on the force estimation. Conversely, with a large r, the criterion is more sensitive to the errors in the gap measurement. If $r = 0$, it only relies on the repulsive computed forces and if $r = +\infty$, it is only influenced by the kinematics. As the errors on the kinematic measurements are usually quite small, a large value of r is recommended: in our experience with standard gait and jump tests, the criterion is robust and leads to equivalent results for any $r > 10$ N/m. Lower values, $r < 10$ N/m, lead to over-activation of the constraints. To test the robustness of this criterion with respect to uncertainties in the gap distance measurement, the ground level is virtually shifted up or down by 1 cm, which may represent an error in the calibration of the motion capture devices or irregularities in the ground plane. The value of r had to be chosen in the smaller interval $[10^2, 10^4]$ N/m to obtain acceptable results. In particular, values lower than 10^2 N/m create the same issues than in the undisturbed case, and values higher than 10^4 N/m lead to an over/under-activation of the constraints.

The kinematic data (velocities and accelerations) are computed using a Butterworth 4^{th} order low-pass filter with a cut-off frequency ω_{kin} set to 6 Hz, as usually recommended (Winter, 2009). The cut-off frequency ω_{dyn} of the post-filtering process is used to ensure the temporal continuity of the GRF, especially during the activation and deactivation of the contact constraints (e.g. the transition between single and double support). With a low cut-off frequency, the loss of information might become significant and the value of the GRF non-physical. With a high value, discontinuities appear in the GRFs, leading to larger errors. In this study, it was selected as twice the value of ω_{kin}, hence $\omega_{dyn} = 12$ Hz.

In Table 4.2, the proposed method is compared with the methods of (Ren et al., 2007), of (Oh et al., 2013), of (Fluit et al., 2014) and of (Gao et al., 2024) for the healthy gait test. One observes that the proposed method provides comparable results for the vertical GRF and the GRM. The main advantage of the proposed method is in the simplicity of the foot/ground contact model which only involves a limited number of parameters which do not necessarily need to be adapted to the specific subject or task under study. Several assumptions have been made: the planar motion, no slipping conditions, ideal

Method	Smooth transition assumption method (Ren et al., 2008)	Hybrid kinematics-neural method (Oh et al., 2013)	Muscle-like actuators method (Fluit et al., 2014))	**Proposed 2D non-smooth method (Van Hulle et al., 2020)**	COP-PTCM (Gao et al., 2024)
Participants	$N = 5$	$N = 48$	$N = 9$	$N = 4$	$N = 10$
Axes/Planes	rRMSE (SD)	rRMSE (SD)	rRMSE (SD)	**rRMSE (SD)**	rRMSE (SD)
Vertical	5.6 (1.5)	5.8 (1.0)	6.6 (1.1)	**4.1 (1.1)**	4.7 (1.4)
Anterior	10.9 (0.8)	7.3 (0.8)	9.3 (2.0)	**11.2 (1.7)**	10.9 (2.1)
Sagittal	12.2 (4.8)	9.9 (1.9)	12.4 (3.5)	**5.3 (1.1)**	-

TABLE 4.2: Gait test: results comparison

distribution of masses and inertia (according to anthropometric tables), absence of friction in the simplified articular joints, unilateral contact between the foot and the ground, and simple function of the COP evolution. Despite these assumptions, the robustness of the model and the activation criterion make it possible to obtain valuable results. The model developed by (Gao et al., 2024), published after and citing our own work, builds upon several concepts similar to those proposed in this thesis, including the rigid-body assumption, energy minimization principles, and a COP evolution governed by a function of foot orientation. The main difference lies in the strategy used to distribute the load between the feet during the double-support phase. The convergence of these approaches supports the relevance of the proposed methodology.

4.4 Conclusion of the chapter

A method is proposed to compute the GRF and GRM for healthy gait tests and jumps based on a least square estimation of the Lagrange multipliers of a unilaterally constrained foot model. A mixed criterion is used for a robust and consistent activation of the contact constraints and a simple model of the foot serves to evaluate the position of the center of pressure.

This method produces reliable results. Easy to implement, it could be used to estimate the GRF and GRM in many cases: healthy and pathological gait, jumping, running, treadmill, etc. In the next chapter, the model will be generalized in order to obtain exploitable results for the GRF along the lateral axis as well as the GRM in the transverse and frontal planes.

Chapter 5

3D inverse dynamics skeletal model

The 2D model developed in Chapter 4 was extended and adapted to 3D in this chapter. The goal is to obtain results that can be used to compute the joints torques and muscular activity and forces.

The main hypothesis remains: each limb is considered as a rigid body and the indeterminacy of the double-support phase is handled using a least-square approach, and the assumption on that the COP evolves as a function of the foot orientation in the sagittal plane.

The model was used for comfortable gait, fast gait, and jump tests, and gave exploitable results. These results will be used in Chapter 6 to estimate the joint torques and muscular activity and forces.

5.1 3D model

In 3D, the human body is modelled with nine rigid bodies as in the 2D model: the pelvis-trunk, femur right-left, tibia right-left, foot right-left and toes right-left. A schematic view can be seen on Figure 5.1.

The nine bodies evolve in space and are still represented by three points: proximal and distal extremities and centre of gravity.

To build the vector of generalized coordinates $\mathbf{q}(t)$, as for the 2D model, absolute coordinates are chosen : the position x, y and z of the extremities and centre of gravity of each segment, the absolute orientation ψ (flexion/extension), ϕ (adduction/abduction) and θ (internal/external rotation) and finally the relative rotation between each segments.

5.1.1 Modelling the joints

In 2D, the modelling of the joints was trivial: the skeletal model being projected in the sagittal plane, only one degree of freedom was authorized for the rotations, and each joint was modelled as a revolute joint.

In 3D, three degrees of freedom are defined for the rotations. The choice of the type of joint model thus deserves more attention.

The hip joint effectively allows three degrees of relative rotational freedom between the pelvis and femur. This joint allows flexion/extension, adduction/abduction and internal/external rotation. The spherical joint was

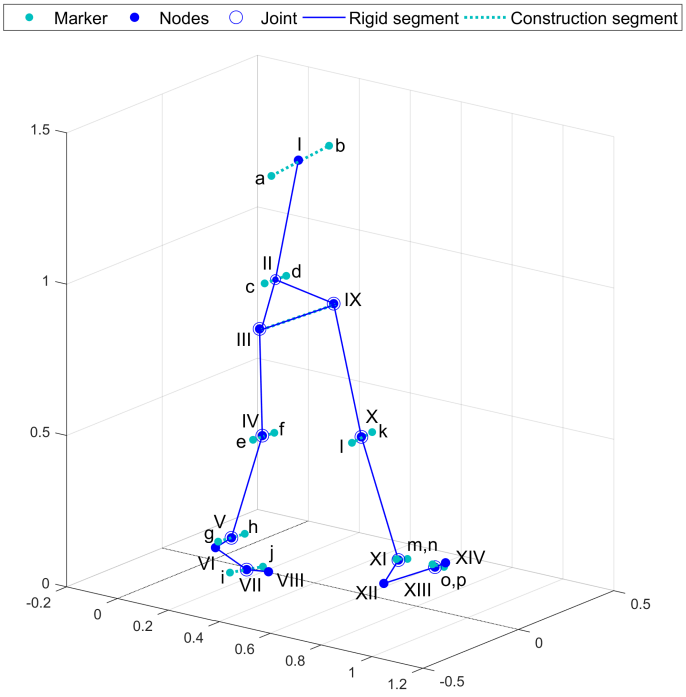

FIGURE 5.1: 3D skeletal model, nodes and segments

selected to model this articulation, as frequently done in the literature (Anderson and Pandy, 2001; Taylor et al., 2004).

The knee joint is a more complex joint, mainly allowing only flexion-extension. Sometimes, it is modelled numerically based on an equivalent 4-bars mechanism as in (Singh et al., 2018; Xie et al., 2014). In our case, as in (Arnold et al., 2010), a spherical joint model is used. This choice is mainly motivated by the desire not to transmit the eventual measurement errors of the knee position markers in the rest of the kinematics. Two markers are used to measure the position of the knee: one inside the knee, the other outside. If the external marker is permanently visible, this is not the case for the internal marker, which can become invisible for the optoelectronic cameras when it is close to the other knee. This short disappearance induces a lack of information on the orientation of the segment, corrected by assumptions of continuity with the other segments and by kinematic constraints of the knee model. However, if a brief occlusion happens at the same time at the inner ankle marker, an error can occur on the absolute and relative orientation between all the different leg segments. By choosing a spherical joint, the number of kinematic constraints of the knee model is reduced and fewer errors are transmitted. Allowing additional rotational degrees of freedom of the joints prevents inaccuracies in skeletal motion reconstruction, due to marker placement errors, soft tissue artefacts or sensor noise, from being artificially transferred to adjacent joints or segments. The driving constraints on the relative rotation over time will impose an almost perfect flexion/extension, and the Lagrange multipliers associated with the adduction/abduction and the internal/external rotation will give the reaction forces maintaining the knee

in its configuration.

The ankle joint, in 3D, allows the flexion/extension, adduction/abduction and internal/external rotation as the hip joint, and is also modelled as a spherical joint, as in (Koopman et al., 1995).

The metarsophalangial joint could be described as a simple hinge joint. The occlusion issue with disappearance of position markers occurs less often in this case and would not generate important issues. However, for the sake of consistency, we decided to model it as a spherical joint also, as in (Koopman et al., 1995). Rheonomic bilateral constraints on the abduction/adduction and internal/external rotation and their associated Lagrange multipliers will provide the internal forces in this joint.

In summary, all joints are modelled as spherical joints and the relative rotations shall be driven by the experimental data using rheonomic bilateral constraints.

5.1.2 Vector of generalized coordinates

As mentioned previously, the model comprises 9 segments. As the 2D model (see Section 4.1), absolute coordinates are preferred to relative coordinates. Therefore, the position of each segment is defined by the x, y and z coordinates of the centre of gravity, proximal and distal extremities, leading to 81 generalized coordinates.

The extremities of the segment being measured experimentally, it is possible to define the position of the centres of gravity using anthropometric tables:

$$\mathbf{x}_{CG} = \mathbf{x}_{dist} + \beta_{CG}(\mathbf{x}_{dist} - \mathbf{x}_{prox}) \tag{5.1}$$

where β_{CG} represents the anthropometric coefficient making it possible to calculate the position of the centre of gravity from the positions of the distal and proximal extremities of a segment.

The orientation of each segment is defined as the three absolute angles of flexion/extension, adduction/abduction and internal rotation of the centre of gravity, leading to an additional 27 generalized coordinates. Between successive segments, three relative angles are also defined, thus adding 24 generalized coordinates. To find the values of the absolute and relative angles of each segment, the positions of at least three non-aligned experimental markers per segment are used together with Equation (2.15) and Equation (2.16). The extraction of the angles from the rotation matrix can be solved either analytically or using a Newton-based numerical solver. In our code, the angles are found numerically. A Bryant angle-like parametrization was adopted to define absolute segment orientations and relative joint angles. Given that gait is predominantly a sagittal plane activity, and with an appropriate choice of reference configuration, this parametrization does not lead to singularities (gimbal lock) in the present study. However, if a broader generalization of the model were sought to study a wider range of movements involving large 3D rotations, an alternative representation of rotations would be preferable.

In particular, quaternions inherently avoid gimbal lock and would therefore constitute a suitable choice for such applications.

It is possible to reduce the number of generalized coordinates. Indeed, the segments being joined at their extremities, some positions coordinates are redundant and the vector of the active generalized coordinates can be reduced to 69 positions (x, y and z for each of the 23 extremities and centres of gravity), 27 angular positions and 24 relative angles, that is to say 120 active generalized coordinates.

The active generalized coordinate vector in 3D is comparable to that in 2D. The main difference comes from the out-of-plane degrees of freedom added to the model, increasing the number of coordinates in position and orientation (absolute and relative).

5.1.3 Bilateral constraints

Defined as above, the model has 30 degrees of freedom: the 24 relative rotations angles, the x, y and z positions and the θ, ϕ, ψ absolute orientation angles of the pelvis, for example.

As the model has 120 generalized coordinates, 90 scleronomic bilateral constraints must be introduced. Of these 90 constraints, 66 ensure that the rigid body assumption is respected. For example:

$$\mathbf{x}_{dist} - \mathbf{x}_{prox} + \mathbf{R}_{abs,3} \begin{bmatrix} 0 \\ 0 \\ L \end{bmatrix} = \mathbf{0} \tag{5.2}$$

defines a set of 3 bilateral constraints, where $\mathbf{x}_{dist}$ and $\mathbf{x}_{prox}$ are the distal and proximal coordinates of a segment, $\mathbf{R}_{abs,3}$ is the 3D absolute rotation matrix defined in (2.15) based on the orientation of the centre of gravity of the segment, and L is the length of the segment, oriented vertically by definition.

The remaining 24 bilateral constraints are used to verify the assembly and to ensure the relation between the absolute and the relative orientation of two joined segments. The constraints $\mathbf{g}$ derive from a relation between the absolute orientation of the proximal and distal segment and their relative orientation. Equation (2.16) can be rewritten as:

$$\mathbf{R}_{rel}^{\mathrm{T}} \mathbf{R}_{abs,proximal}^{\mathrm{T}} \mathbf{R}_{abs,distal} - \mathbf{I} = \mathbf{0} \tag{5.3}$$

where, for two neighbour segments, $\mathbf{R}_{abs,proximal}$ is the absolute rotation matrix of the proximal segment, $\mathbf{R}_{abs,distal}$ is the absolute rotation matrix of the distal segment and $\mathbf{R}_{rel}$ is the relative rotation matrix between the two segments. $\mathbf{I}$ is the identity matrix. To obtain three independent constraints per joint, we enforce the value of the non-diagonal elements of the matrix $\mathbf{R}_{rel}^{\mathrm{T}} \mathbf{R}_{abs,proximal}^{\mathrm{T}} \mathbf{R}_{abs,distal}$:

$$\begin{bmatrix} [\mathbf{R}_{rel}^{\mathrm{T}}\mathbf{R}_{abs,proximal}^{\mathrm{T}}\mathbf{R}_{abs,distal}]_{2,3} \\ [\mathbf{R}_{rel}^{\mathrm{T}}\mathbf{R}_{abs,proximal}^{\mathrm{T}}\mathbf{R}_{abs,distal}]_{1,3} \\ [\mathbf{R}_{rel}^{\mathrm{T}}\mathbf{R}_{abs,proximal}^{\mathrm{T}}\mathbf{R}_{abs,distal}]_{1,2} \end{bmatrix} = \mathbf{0} \tag{5.4}$$

Since the 24 relative angles are controlled over time, the model also includes 24 rheonomic driving constraints. For example:

$$\psi - \psi_{exp}(t) = 0 \tag{5.5}$$
$$\phi - \phi_{exp}(t) = 0 \tag{5.6}$$
$$\theta - \theta_{exp}(t) = 0 \tag{5.7}$$

where ψ, ϕ and θ are the relative angles between segments, and ψ_{exp}, ϕ_{exp} and θ_{exp} are their corresponding experimental value.

As in 2D, the experimental acquisition of relative rotations in 3D is performed directly using the position of experimental markers (see Figure 5.1). In 3D, the absolute orientation of each segment is defined for each time step using at least three non-aligned experimental markers and Equation (2.15). Once the absolute orientation of each segment is known, the relative rotation matrix is computed using Equation (2.16), and the relative angles are obtained numerically from $\mathbf{R}_{rel}$.

These obtained values are applied to the corresponding generalized coordinates via driving constraints. In the case of inverse dynamics, these constraints are self-satisfied; the gradient of the constraints and the associated Lagrange multipliers complete the dynamic force equilibrium in Equation (5.8).

Only six degrees of freedom remain: the position and orientation, in 3D, of the centre of mass of the whole body. These degrees of freedom will be determined using the foot/ground contact model and the equations of motion.

The vector of bilateral constraints in 3D is comparable to that in 2D. The main difference comes from the degrees of freedom added to the model, going from 3 (2 positions and 1 orientation of the pelvis in 2D) to 6 (3 positions and 3 orientations of the pelvis in 3D), as well as the increased number of active generalized coordinates. The process for generating these constraints, however, remains identical between the 2D and 3D models.

5.1.4 Model of the foot and contact constraints

The foot is modelled as two segments, foot and toes, linked by a spherical joint.

The contact with the ground is modelled as a mobile contact point rigidly connected to the centre of gravity of the foot. Following the same methodology used in the 2D COP estimation model, the position of the COP is first measured experimentally in order to estimate a law linking the orientation of the foot in its sagittal plane and the centre of pressure. The evolution of the

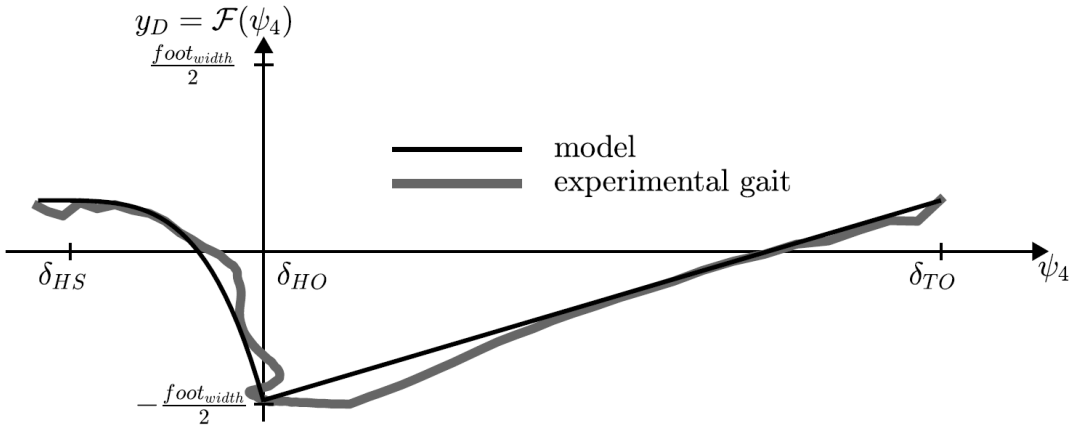

FIGURE 5.2: Evolution of the position of the COP of the right foot in the lateral direction as a function of the angle ψ_4 representing the foot inclination in the sagittal plane

COP in the longitudinal direction is the same as in the 2D model, and shown in Figure 4.4. In the lateral direction, two new laws are defined for each foot, as shown for the right foot in Figure 5.2.

Note that x_D and y_D are now expressed in the local coordinate system of the foot. In the 2D model, the foot segment was projected onto the global sagittal plane, assuming minimal deviation from that plane during walking. In 3D, however, this simplification is no longer valid, as foot orientation varies from subject to subject and from step to step. Therefore, modelling the evolution of the COP in the local foot frame, in both the x and y directions, is more appropriate. This local position will subsequently be transformed into the global coordinate system, taking into account the sign change due to the symmetry in COP evolution between the left and right feet. These two laws were established in two parts. The first, between the 'heel strike' (δ_{HS}) and the 'heel off' (δ_{HO}), follows a quadratic behaviour. The second, from 'heel off' to 'toe off'(δ_{TO}), is linear. The lateral distance is calibrated based on the width of the foot, which we estimate as the distance between the two experimental metatarsal markers (i and j for the right foot in Figure 5.1). We also assume that the sagittal plane of the foot passes through the numerical markers of the heel and metatarsal joint (VI and VII in Figure 5.1).

Based on this information, it is possible to estimate the x and y coordinates of the COP according to the orientation of the foot in its sagittal plane.

5.1.5 Dynamic equilibrium and least-square evaluation of the contact forces

In 3D, the dynamic equilibrium of the system is given by $n = 126$ equations written in the same matrix form as in 2D (Géradin and Cardona, 2001):

$$\mathbf{M}\ddot{\mathbf{q}} + \mathbf{g}_{\mathbf{q}}^{\mathrm{T}}(\mathbf{q}, t)\boldsymbol{\lambda} - \mathbf{f}^{ext} = \mathbf{0} \tag{5.8}$$

All the terms in Equation (5.8) have the same physical meaning as in the 2D model in Equation (4.15). In general 3D problems, gyroscopic and centrifugal forces should be included in the dynamic equilibrium. However, the problems treated in this thesis are almost 2D problems and the angular velocities remain moderate. In this case, considering that the equations are expressed in absolute coordinates, we assume that the gyroscopic and centrifugal contributions can be neglected.

As in the 2D model (see Equations (4.7) to (4.10)), the vector of generalized coordinates $\mathbf{q}$ is separated into two sets of dependent and independent coordinates. The independent coordinates are derived twice to obtain the vector of independent acceleration $\ddot{\mathbf{q}}^I$, and thanks to the bilateral constraints it is possible to compute the complete vector of acceleration $\ddot{\mathbf{q}}$ to be consistent with the rigid body assumption (Géradin and Cardona, 2001)

As in 2D, Equation (5.8) is solved for the Lagrange multipliers. At first, it is possible to find a unique solution and a physical meaning for the term $\mathbf{g}_{\mathbf{q}}^{\mathcal{A},\mathrm{T}}(\mathbf{q})\boldsymbol{\lambda}^{\mathcal{A}}$ representing the reaction forces, namely the bilateral reaction forces, the unilateral reaction forces (resulting from the contact constraints) and the actuation torques (resulting from the driving constraints).

$$\mathbf{g}_{\mathbf{q}}^{\mathcal{A},\mathrm{T}}(\mathbf{q})\boldsymbol{\lambda}^{\mathcal{A}} = -\mathbf{M}\ddot{\mathbf{q}} + \mathbf{f}, \qquad \boldsymbol{\lambda}^{\overline{\mathcal{A}}} = \mathbf{0} \tag{5.9}$$

Using the Moore-Penrose pseudo inverse, it is possible to solve this last equation for $\boldsymbol{\lambda}^{\mathcal{A}}$ in a least-square sense, meaning that this solution represents the minimal reaction forces needed to execute the given motion.

$$\boldsymbol{\lambda}^{\mathcal{A}} = \left(\mathbf{g}_{\mathbf{q}}^{\mathcal{A},\mathrm{T}}(\mathbf{q})\right)^{+}\left(\mathbf{f} - \mathbf{M}\ddot{\mathbf{q}}\right), \qquad \boldsymbol{\lambda}^{\overline{\mathcal{A}}} = \mathbf{0} \tag{5.10}$$

Finally, it remains to define the "activated" or nonactivated" status of the unilateral constraints, using a contact activation criterion.

5.1.6 Contact activation criterion

The contact activation criterion is the same as in 2D, based on a complementarity condition between the gap function $g^{j,n}$ and the normal reaction force $\lambda^{j,n}$. Based on the work of (Alart and Curnier, 1991), it is mathematically written as:

$$\mathcal{C} = \{j : \lambda^{j,n} - r g^{j,n} \geq 0\} \tag{5.11}$$

and represented graphically in Figure 4.5.

The contact status is first supposed "active" for each unilateral constraint. If the criterion is not satisfied for a given constraint and time-step, the unilateral constraint is deactivated. The new vector of Lagrange multipliers is reevaluated until the system reaches convergence. The process can be assimilated to an iterative Newton semi-smooth solver.

Once convergence is reached, a final filtering is applied to the result to smooth the eventual jumps that may occur during the transition from single- to double-support phase.

5.2 Results

In Figure 5.3, the results of a single gait test are illustrated, and a comparison is made with the 2D model of Chapter 4. In Table 5.1 the relative Root Mean Square Error, as proposed by (Oh et al., 2013), is compared for the 3D and 2D model. As a reminder, the RMSE and rRMSE were given in Equation (4.22) and (4.23).

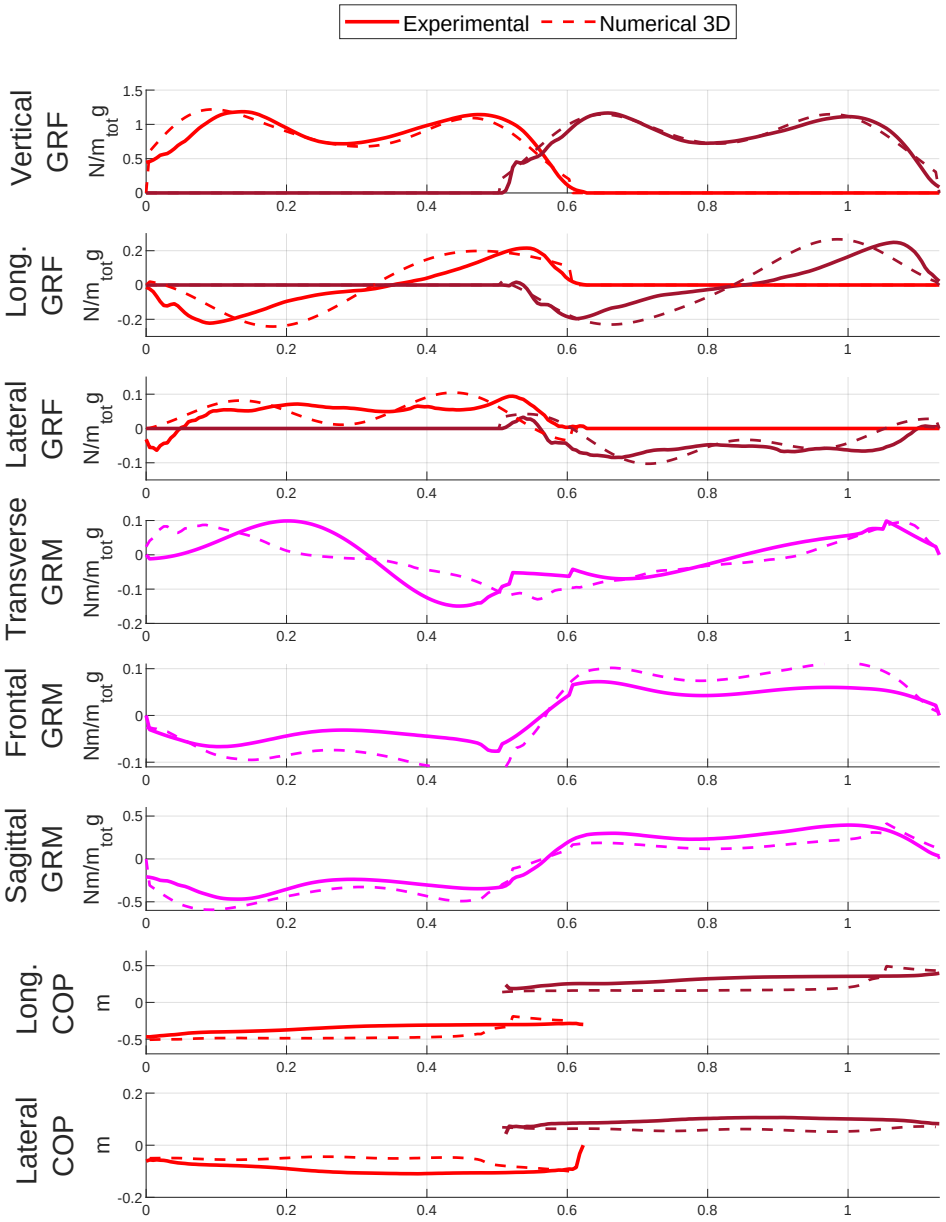

FIGURE 5.3: Comparison of the 3D foot/ground model with experimental measurements. Red: right foot; Brown: left foot; Magenta: right and left feet.

Method	3D model	2D model
Participants	$N = 4$	$N = 4$
Axes/Planes	rRMSE (SD) %	rRMSE (SD) %
Vertical	4.9 (1.3)	4.1 (1.1)
Anterior	10.7 (1.5)	11.2 (1.7)
Lateral	10.3 (1.4)	-
Sagittal	6.3 (1.3)	5.3 (1.1)
Frontal	12.3 (1.7)	-
Transverse	12.1 (1.6)	-

TABLE 5.1: Relative RMS error comparison between 2D and 3D models

5.3 Discussion

The method, previously developed in 2D, has been extended to 3D. For an essentially two-dimensional movement, such as walking, the results on the two main axes (vertical and longitudinal) based on the 2D and 3D models are closely correlated, demonstrating that the addition of the third dimension does not disturb the results along the two main axes. However, it's worth noting that while the extension to 3D does not degrade the previous results, it also does not enhance them, mainly due to the fact that walking primarily occurs in the sagittal plane.

This 3D model depends on the same parameters as the 2D model, namely: the activation parameter r, the cut-off frequencies ω_{kin} and ω_{dyn} of the filters, and the limit angles δ.

This 3D model assumes that the position of centre of pressure (COP) on the foot sole evolves as a 2D function of the foot orientation $\mathcal{F}(\psi_{foot})$. This assumption is fundamental for the determination of the position of the COP but has little influence on the evaluation of the forces. The piecewise definition of the function $[x_{COP}, y_{COP}] = \mathcal{F}(\psi_{foot})$ was chosen to best match the mean experimental COP trajectories observed across the studied subjects. The limit angles δ_{HS}, δ_{HO} and δ_{TO}, which govern the transitions between the different phases of the function, are directly related to identifiable gait events and therefore have a clear biomechanical interpretation. Although a more rigorous validation procedure, such as defining the function on a modelling dataset and validating it on an independent test population, would be desirable, this was not feasible due to the limited number of available subjects. More general approaches, including learning-based methods, could also be envisaged to improve generalization. However, such methods typically require larger datasets and often lead to reduced model interpretability. In the present work, considering the available dataset, the chosen formulation represents a first-order approximation that prioritizes physical interpretability and consistency with experimental observations, and proved sufficient for a

preliminary estimation of COP evolution in the context of gait.

The least-square distribution of the reaction forces is used to resolve the over/underdetermination of the model during the single or double support phase. Since the Cartesian generalized coordinates and external forces are clearly expressed along the three main axis, the least-square distribution does not mix up the data and the distribution of the forces along the vertical, longitudinal and lateral axis is performed independently. Moreover, this independent distribution of forces along each axis opens up the possibility of refining parameters individually for each axis. This refinement could further enhance the correlation with experimental results.

For lateral forces, while the magnitude and general trend are generally respected, the errors remain significant. However, these errors have a limited impact on the final result as lateral forces are less significant than vertical and longitudinal forces in the case of gait, which primarily occurs in the sagittal plane. The impact of these errors on the joint torques and muscle forces will be estimated in Chapter 6. The more significant errors probably stem from the evaluation of lateral acceleration and thus from kinematic filtering. The equations, assumptions, and contact model for the lateral axis are equivalent to those for the longitudinal axis, so that is is reasonable to assume that the results and errors along these two axes would be of similar magnitude if the kinematics were as accurate as in the frontal plane.

The activation criterion r is chosen to address the eventual measurement errors. By choosing $r = +\infty$, the model relies only on the kinematic measurements, and with $r = 0$, the results are based solely on the numerical estimation of the contact forces. The high quality of the measurement of optoelectronic cameras motivates us to choose a high value for the parameter r, namely between $[10^2, 10^4]$ N/m.

In Table 5.2, the results obtained with the proposed 3D model are compared with representative methods from the literature for healthy gait analysis. Overall, the proposed approach yields ground reaction forces and moments that remain within the range reported by existing models, particularly for the vertical component, which is the dominant contributor during walking, and the obtained results are consistent with those reported in previous studies.

The 3D model is inherently more complex than our 2D model but does not significantly improve the results. However, its implementation is nonetheless valuable for utilization in a comprehensive gait analysis scheme: starting from kinematics, the calculation of the reaction and internal efforts, is a necessary step before the evaluation of muscle activation and efforts. To achieve this, we shall integrate this model with the OpenSim software, which is a 3D biomechanical analysis tool, in the next chapter of the thesis.

Method	Smooth transition assumption method (Ren et al., 2008)	Hybrid kinematics-neural method (Oh et al., 2013)	Muscle-like actuators method (Fluit et al., 2014))	COP-PTCM (Gao et al., 2024)	**Proposed 3D non-smooth method**
Participants	$N = 5$	$N = 48$	$N = 9$	$N = 10$	$N = 9$
Axes/Planes	rRMSE (SD)	rRMSE (SD)	rRMSE (SD)	rRMSE (SD)	**rRMSE (SD)**
Vertical	5.6 (1.5)	5.8 (1.0)	6.6 (1.1)	4.7 (1.4)	**4.9 (1.3)**
Anterior	10.9 (0.8)	7.3 (0.8)	9.3 (2.0)	10.9 (2.1)	**10.7 (1.5)**
Lateral	20.0 (2.7)	10.9 (1.8)	14.9 (3.4)	15.2 (1.7)	**10.3 (1.4)**
Sagittal	12.2 (4.8)	9.9 (1.9)	12.4 (3.5)	-	**6.3 (1.3)**
Frontal	32.5 (4.3)	22.8 (4.9)	22.9 (5.9)	-	**12.3 (1.7)**
Transverse	26.2 (9.4)	25.5 (4.5)	40.6(11.3)	-	**12.1 (1.6)**

TABLE 5.2: Gait test: results comparison

5.4 Conclusion of the chapter

The method developed in 2D in the previous chapter has been extended to 3D. It produces results for the reaction forces that can be exploited with other tools to pursue a more in-depth analysis of the biomechanical behaviour. In the next Chapter, the 3D model will be combined to OpenSim, to carry out comprehensive biomechanical inverse dynamics studies.

Chapter 6

Evaluation of muscle forces

In the last chapter of this thesis, we will evaluate not only joint torques but also muscle forces and muscle activation by inverse dynamics computation to demonstrate the complete workflow with our contact model. For this, the 3D method developed in Chapter 5 will be exploited to evaluate the contact force between the foot and the ground which is needed by OpenSim.

The first part of this chapter presents the flowcharts used by OpenSim, using experimental acquisitions of contact forces. By directly using kinematic and force platform data acquired during our experimental gait measurements, the results provided by OpenSim can be considered as our gold standard. Alternatively, joint torques and muscle forces will be evaluated again in OpenSim, this time using the ground reaction forces and position of the center of pressure estimated by our contact model, while keeping the same kinematic data.

The second part of this chapter studies and compares the results obtained for the joint torques and for the muscle activation.

6.1 OpenSim software

OpenSim is a software developed by Stanford University and specifically designed for modelling and simulating the human movement and the biomechanical behaviour (Delp et al., 2007; Seth et al., 2018; Dembia et al., 2020). OpenSim is primarily used in the field of biomechanics and biomechanical engineering to create musculoskeletal models of the human body and simulate various movements and activities. These models can be used to study human gait, analyse the mechanics of joints and muscles, understand movement disorders, and evaluate the effectiveness of medical treatments or assistive devices.

The software allows users to customize and configure musculoskeletal models, simulate muscle forces, analyse joint kinetics and kinematics, and visualize the results.

6.2 OpenSim muskuloskeletal model

The "Gait2354" model, used in this thesis, was developed by D. Thelen (Thelen et al., 2003) based on several works (Delp et al., 1990; Yamaguchi and

Zajac, 1989; Anderson and Pandy, 1999; Anderson and Pandy, 2001; Carhart, 2000).

This musculoskeletal model is three-dimensional with 23 degrees of freedom and 54 musculotendon actuators. The lower limbs are modelled by fifteen rigid body segments: pelvis, thighs (femur), legs (tibia and fibula), talus, feet and toes.

The hip joint is modelled as a spherical "ball-and-socket" joint, the knee joint is a single-degree-of-freedom joint developed by (Yamaguchi and Zajac, 1989), and ankle ant metatarsophalangeal joints are represented by frictionless revolute joints.

Finally, as the proposed model of the Chapters 4 and 5, the inertial parameters and anthropometric table are based on (Anderson and Pandy, 1999).

6.3 Inverse dynamics analysis workflows

Figure 6.1 represents the workflow available in OpenSim. The method comprises four successive stages: scaling, inverse kinematics, inverse dynamics to obtain the joint torques and muscle dynamics for the muscle forces and activations.

6.3.1 Numerical procedure with contact forces acquisitions

The procedure in Figure 6.1 using experimental measurement of the contact forces represents the "gold standard", and the usual utilisation of OpenSim.

The first stage is the scaling. Based on a static acquisition, the general "Gait2354" model is scaled to represent more accurately the subject. Each segment of the musculoskeletal model receives a mass, an inertia and dimensions.

The second stage is the inverse kinematics. Based on the motion of a restricted set of nodes recorded during a dynamic acquisition, the independent generalized coordinates of the scaled model are computed.

The third stage is the inverse dynamics where the external forces, i.e. foot/ground contact forces measured by force platforms and the estimated gravity, are applied to the scaled model under motion. This allows OpenSim to resolve the equations of motion and to compute velocities, acceleration and joint efforts of the system.

Finally, based on the computed joint efforts, it is possible to use a muscle dynamics model to estimate the muscle activations and the muscle forces. Two methods are implemented in OpenSim for this problem: Static Optimization and Computed Muscle Control.

Static Optimization is a static model where the results are established independently for each time step, and the unknowns are the muscles forces and activation levels. We thus have to solve one static optimization problem per time step. This method is therefore fast and numerically stable. However, the solution does not take into account some physiological aspects linked to the muscle activation dynamics.

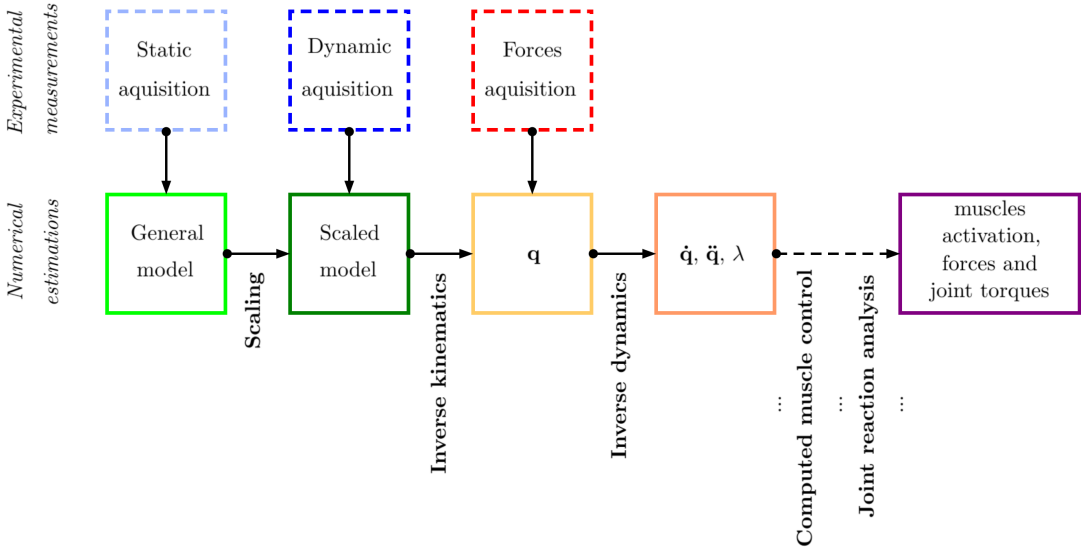

FIGURE 6.1: Flowchart of OpenSim software

Computed Muscle Control is a combination of proportional-derivative control and static optimization, involving the global time history of the simulation (Neptune et al., 2001), and takes into account the muscle activation dynamics. The muscle forces are obtained from the time history of the activations. This solver aims to better represent several physiological aspects. However, it allows the modification of the kinematics imposed on the musculoskeletal model in order to calculate muscle activation, and it is less stable than the static optimization.

Anderson and Pandy (Anderson and Pandy, 2001) have shown that the static optimization approach gives comparable results to the CMC approach. For our workflow, in order to compare results coming from identical kinematics, we opted for the static optimization approach.

6.3.2 Numerical procedure with contact forces estimation

Now, we discuss the adaptation of the OpenSim workflow when the contact forces are not obtained from force platforms acquisition but from our inverse dynamics procedure.

The first two stages, scaling and inverse dynamics, remain unchanged. Instead of using the acquisition file for the contact forces measured experimentally, a new file generated using the numerical estimation computed by our 3D inverse dynamics code.

6.4 Results: joint torques

The results displayed in Figure 6.2 correspond to a representative individual trial, selected a posteriori as being consistent with the overall trends observed across the dataset, and show the hip, knee, and ankle joint torques of the left leg evaluated using both experimental force platform data and

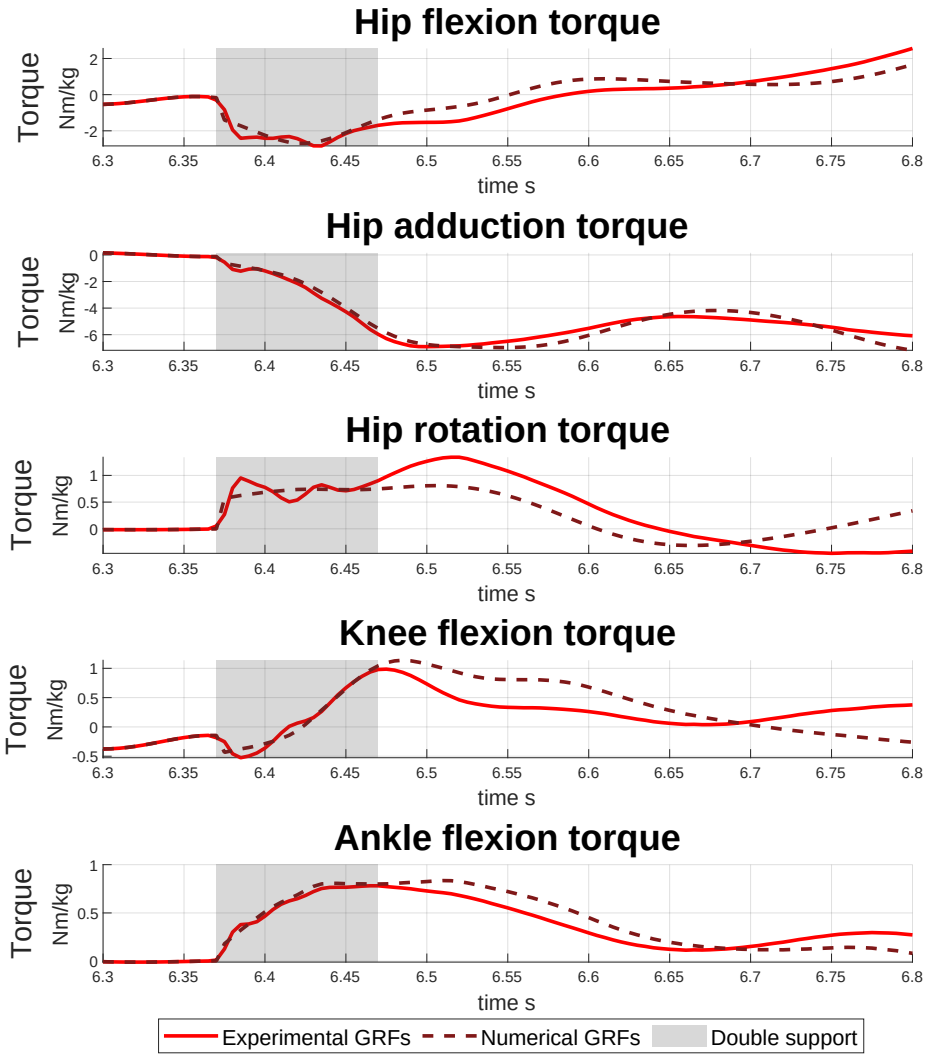

FIGURE 6.2: Comparison of left hip (flexion, adduction, rotation), knee flexion and ankle flexion torques evaluated in OpenSim

Axes	Hip rRMSE	Knee rRMSE	Ankle rRMSE
Flexion	10.74	19.94	12.68
Adduction	5.74	-	-
Rotation	23.77	-	-

TABLE 6.1: Differences in joint torques evaluated in OpenSim using experimental and numerical GRFs

the proposed numerical foot–ground contact model. This comparison allows joint and muscle efforts obtained from directly measured ground reaction forces to be contrasted with those estimated using the numerical model, in order to assess the impact of modelling assumptions and estimation errors in a more global musculoskeletal analysis framework. Three phases are presented : balancing, double support (in grey shaded area) and single support. The signal covers a little less than a complete stride in order to have an almost complete and physical representation of the force and muscular results. In our experimental protocol, the right foot is the first to come into contact with a force platform. The experimental results at the moment of the right heel strike do not yet have any physical meaning, since the reaction force of the left foot (during the initial double support phase) is not measured. The results are therefore displayed from the second phase of double support, after the left heel strike.

The root mean square error is defined as in previous chapters, see Equation 4.23. The Table 6.1 represents the relative Root Mean Square Error of the different joint torques evaluated, averaged for 24 tests.

The matching between joint torques results from experimental and numerical GRFs appears uneven, depending on the selected joint and axis of rotation. Indeed, for the hip adduction the numerical and experimental results are closely correlated. Although the error is slightly larger, the same can be said for hip and ankle flexion. On the other hand, notable errors are present for knee flexion and hip rotation. In addition to the rRMSE which is of the order of 20%, the results are sometimes of the same amplitude but of opposite sign. The following section aims to analyse the origin of these errors.

6.4.1 Origin and causes of the error on the knee flexion and hip rotation torques

Pelvis residual forces

The OpenSim solver works in a recursive manner, that is to say that the reaction forces are applied to the first body (the foot in contact), then depending on the imposed kinematics, to the joint and to the next body (the leg), etc. All the forces are thus distributed step by step from the foot to the pelvis. This

recursive approach is applicable for systems with an open loop topology but the treatment of closed kinematics loops requires cumbersome adaptations.

If the model would perfectly define the human body and there would be no error in the measured reaction forces, the model would be in equilibrium and the residual forces would be zero at the level of the pelvis. In OpenSim, the residual forces on the pelvis are often used as a measure of the quality of the inverse dynamics results. Figure 6.3 represents the residual forces along the three axes, using experimental and numerical data.

In Figure 6.3 , the residual forces are maximum in or close to the double support zone, both in the experimental and numerical case. This variation may come from OpenSim's recursive method, and its difficulty to deal with the closed loop topology which appears in the double support phase (both feet are in contact with the ground).

Also, we immediately notice that it is along the longitudinal axis that the residual forces are the most important, whatever the data used. This probably indicates a larger defect in the kinematics along this axis, which could come from the filtering of the measurement or the weight allocated to this axis when solving the equations of motion.

The main difference between the experimental and numerical curves is found in the double support phase along the vertical axis, where the numerical data provide lower residual forces on this component. It seems that the least squares distribution at the core of our numerical procedure for the evaluation of the ground reaction forces ensures a better balance of forces, leading to residual forces closer to zero.

Component-wise study of the reaction forces

The analysis of the pelvis residual forces revealed that the quality of the modelling is not uniform along the different axes.

Three new simulations were implemented in order to isolate the contribution of each GRF component to the overall error. Each of them uses the experimental COP position and the experimental forces, except on one axis for which the numerical estimation is used. Figure 6.4, similar to Figure 6.2, shows the results thus obtained. Table 6.2 summarizes these results and shows the average rRMSE for 24 tests. The "Vert." column represents the case where only the vertical force is estimated numerically, "Long." only numerical longitudinal forces and "Lat." only numerical lateral forces.

As can be seen in Figure 6.4 and Table 6.2, the main component of the error comes from the contribution of the longitudinal reaction force. In Figure 5.3, we can also note that the peaks in this component are not correlated with the experimental measurements, which corroborates the anticipated observations of the residual forces (Figure 6.3).

We conclude that the forces and movements (position, speed and acceleration) along the longitudinal axis contain modelling errors. These errors can come from the chosen cut-off frequencies of the low-pass filters used to establish the kinematics, or from an under-evaluation of the importance of this component during the resolution by the least-squares method. Currently,

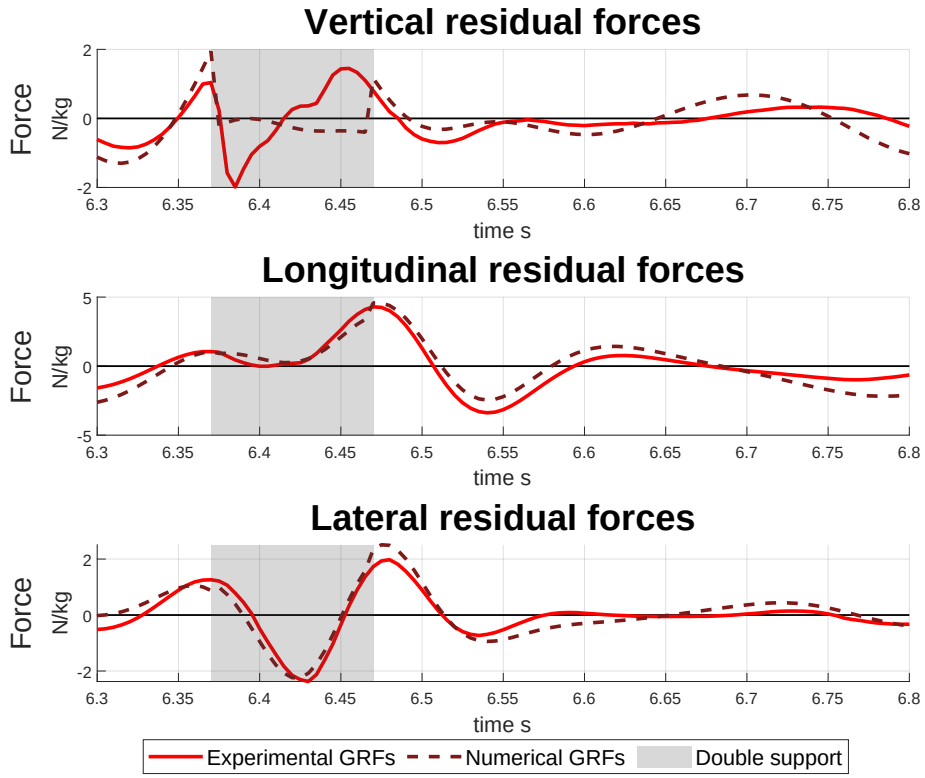

FIGURE 6.3: Residual pelvis forces

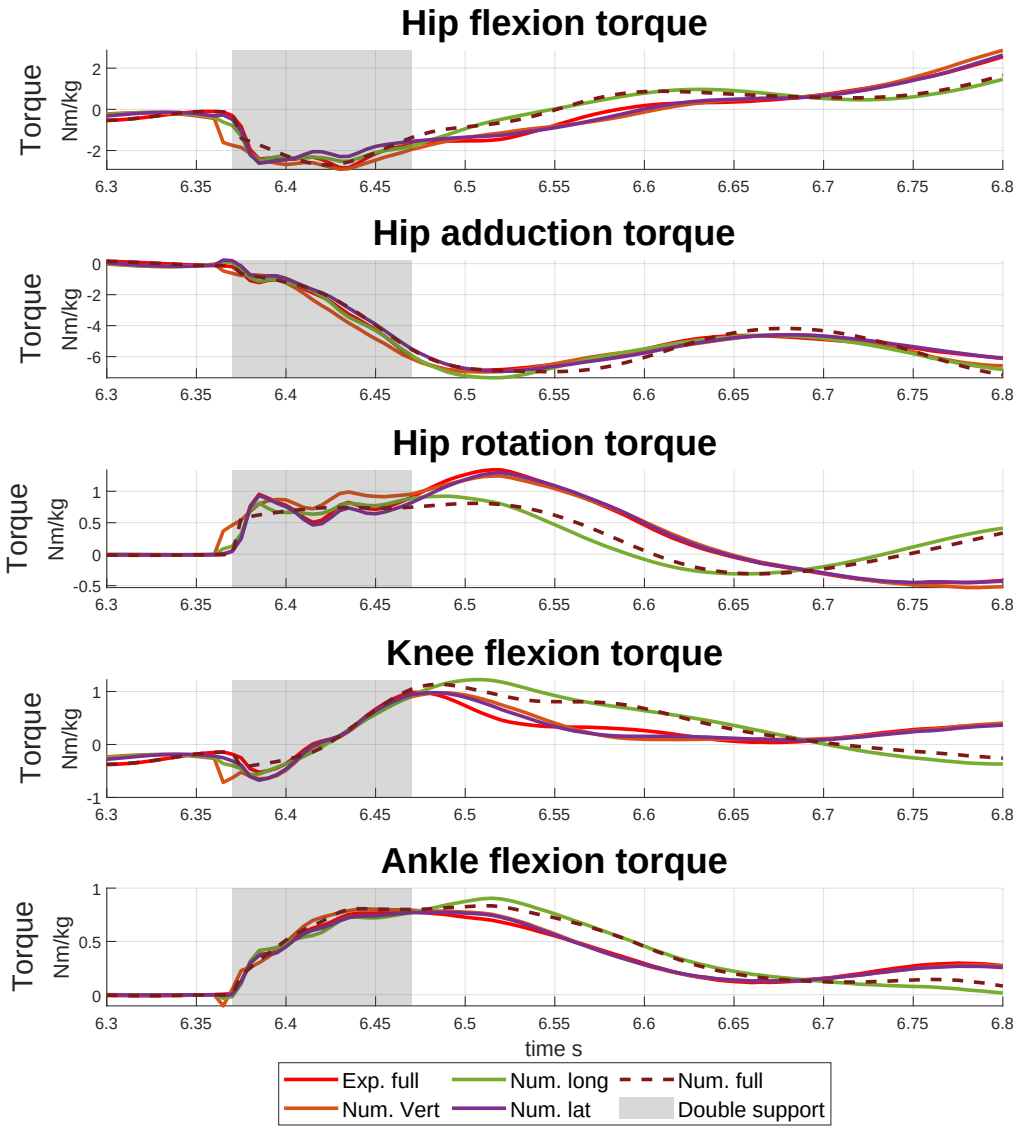

FIGURE 6.4: In-depth comparison of hip (flexion, adduction, rotation), knee flexion and ankle flexion torque

	Hip rRMSE %			Knee rRMSE %			Ankle rRMSE %		
Axes	Vert.	Long.	Lat.	Vert.	Long.	Lat.	Vert.	Long.	Lat.
Flexion	5.55	12.12	3.53	8.32	23.02	5.37	3.69	15.37	2.45
Adduction	3.97	3.61	3.19	-	-	-	-	-	-
Rotation	5.67	26.26	2.19	-	-	-	-	-	-

TABLE 6.2: Differences in joint torques evaluated in OpenSim using experimental and numerical GRFs

each constraint was treated with the same weight. A model with a different weighting, or even a dynamic weighting of the constraints could lead to better results. Likewise, the cut-off frequencies were chosen at 6 and 12 Hz regardless of the axes.

Finally, the influence of the arms was neglected for this study. According to (Angelini et al., 2016), the spatio-temporal parameters of walking are not affected by arm kinematics. However, they also note a slight influence on ground reaction forces (from 1 to 3% of the body weight on the longitudinal axis). The experimental data obviously take into account the movement of the arms, but the numerical data neglect them. The model could therefore be augmented to take into account the movement of the arms.

Since these errors are present when evaluating joint torques, it is likely that they will also affect the estimation of muscle activations.

6.5 Results: muscle activations and forces

The muscle activations are calculated using OpenSim's "Static Optimization" solver, and depend on a number of pre-implemented modelling parameters. In particular, each muscle group has its own maximum activation, strength, speed, and power.

As for the joint reaction forces, a new set of simulations has been performed where only the vertical, longitudinal or lateral numerical estimation of the ground reaction forces are used together with the experimental measurements. The experimental and numerical results can be seen in Figure 6.5.

In contrast to joint torques, we observe the emergence of some oscillations and peaks in the muscle activation curves. This can be attributed to the presence of multiple muscle groups contributing to the same joint torque component. The optimization algorithm, which distributes activation levels time step by time step, does not ensure a perfect continuity in the curves.

Errors observed in joint torques are logically reflected in the muscle activations. Certain muscle groups, such as the "Rectus Femoris" and "Biceps Femoris", directly linked to the knee joint and its flexion, present different behaviours, while the curves of the "Vastus medialis", "Vastus Lateralis" and

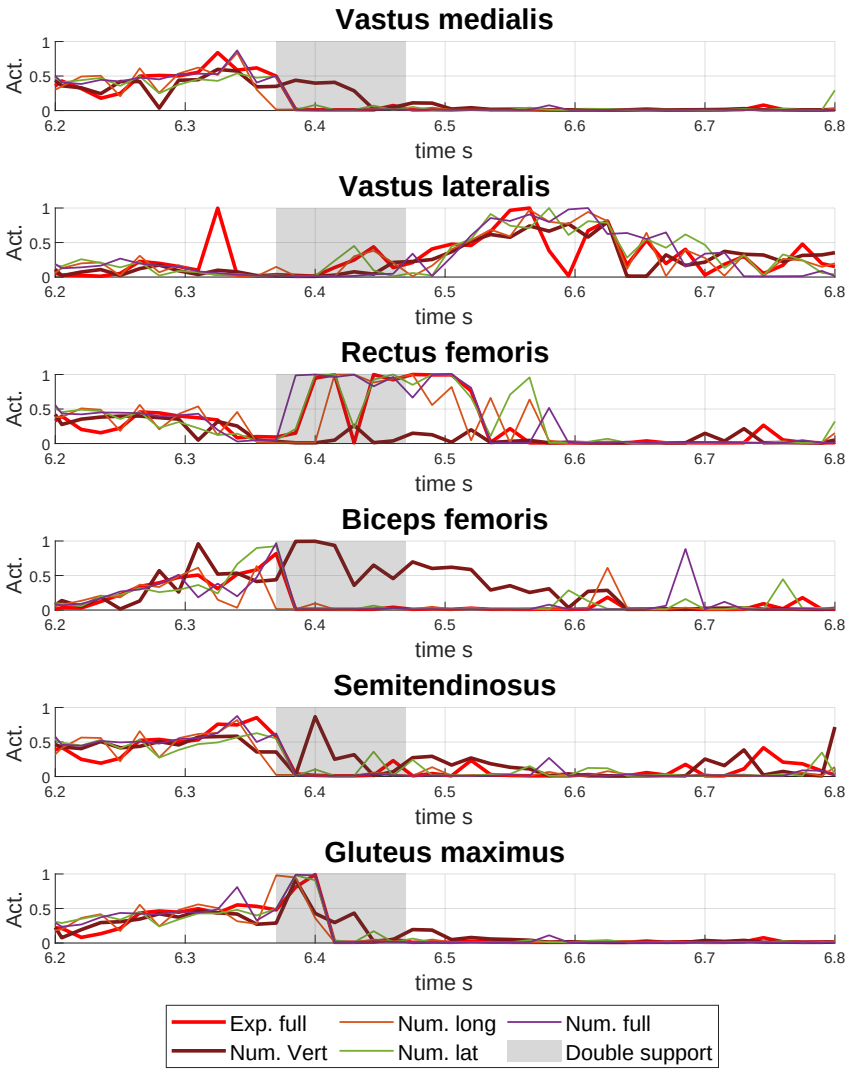

FIGURE 6.5: Muscle activations

"Gluteus Maximus" are well correlated. However, the error on the longitudinal component observed for the joint torques seems to have a smaller impact on the numerical error. The errors observed in muscle activations likely stem from the accumulation of various small errors throughout the modelling process rather than being solely attributed to the longitudinal GRF component: isolating the error of a single force component, such as the longitudinal component, becomes less clear-cut. Instead, it is the collective effect of inaccuracies that manifests in the discrepancies observed in the results.

The muscle forces estimation curves are presented in Figure 6.6. Given the static nature of the solver and the inherent correspondence between muscle activation and forces, the observed curves exhibit uniform behaviour, with a consistent manifestation of oscillations and error patterns across the data.

The substantial variability in results and errors renders the establishment of result tables for relative Root Mean Square Error (rRMSE) unnecessary and irrelevant.

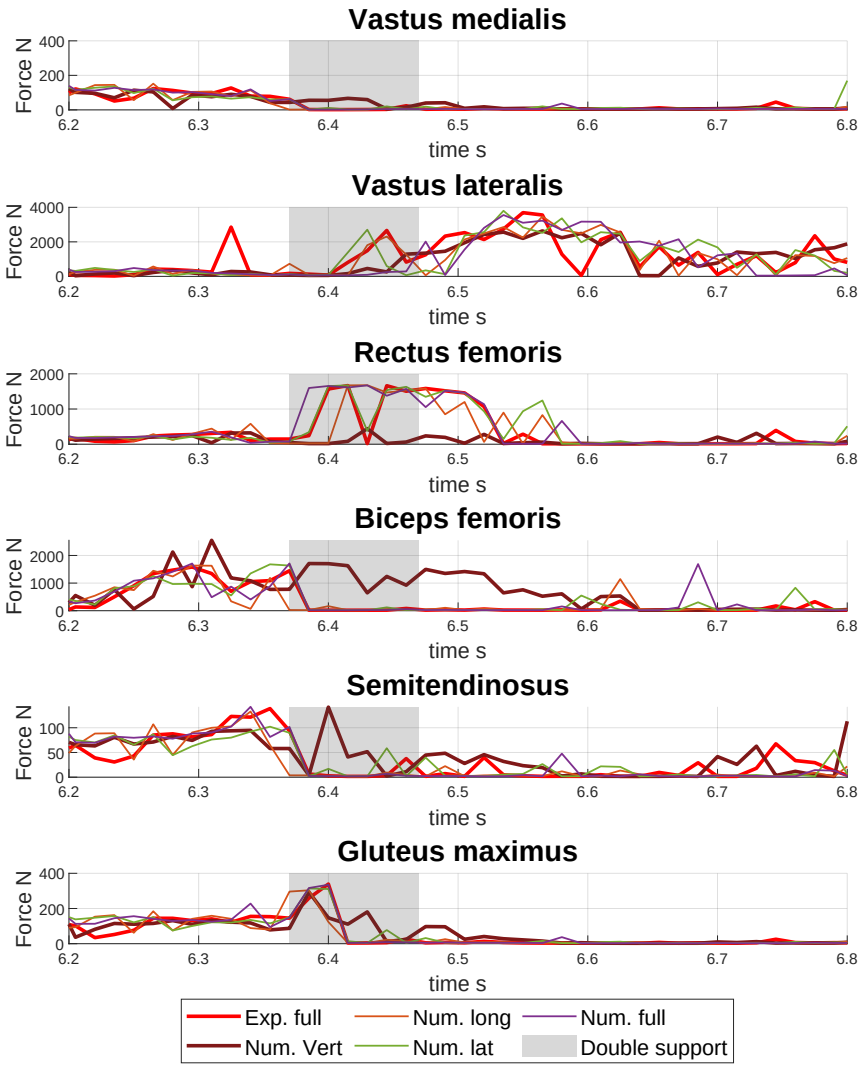

FIGURE 6.6: Muscle forces

6.6 Discussion

In this final chapter, joint torques, muscle activations, and forces are evaluated using OpenSim, software designed for modelling and simulating biomechanical behaviour. The chapter is divided into two parts: one on joint torques, the other on muscle activation and forces.

First, OpenSim and the musculoskeletal model "Gait2354" are introduced. This 3D model, with 23 degrees of freedom and 54 musculotendon actuators, provides a detailed representation of the lower limbs. OpenSim's workflow includes four steps: scaling, inverse kinematics, inverse dynamics, and muscle activation dynamics. Two muscle activation methods, Static Optimization and Computed Muscle Control, are available. Static Optimization, used here for its efficiency, offers fast and stable results. The degrees of freedom of the OpenSim model do not match those of the model used to estimate the ground reaction forces. The OpenSim model includes a lower number of degrees of freedom, while providing sufficient kinematic richness to estimate joint torques and muscle forces. This difference, however, does not fundamentally compromise the analysis. The objective of this comparison was not to establish a one-to-one correspondence between the two models, but rather to assess whether the ground reaction forces estimated by the proposed approach can be meaningfully exploited within a standard musculoskeletal analysis workflow.

It is important to notice that OpenSim was used here as a musculoskeletal solver, and that the objective was not to assess its intrinsic ability to predict muscle activations in an absolute sense. As is well-established in the literature, muscle activation estimation strongly depends on the underlying musculoskeletal model, the chosen cost function (static versus dynamic optimisation), and the treatment of muscle redundancy, all of which are known to influence inter-subject variability (Mathieu et al., 2023). In this work, the comparison was performed using the same OpenSim model, identical kinematic data, and identical optimisation settings, while only replacing the experimentally measured ground reaction forces with the numerically estimated ones provided by the proposed contact model. This strategy was chosen to isolate the impact of force estimation errors on joint torques and muscle-related outputs.

It is likely that a simpler and more generic musculoskeletal model, with fewer degrees of freedom and muscle actuators, would reduce sensitivity to modelling assumptions and improve consistency across subjects. Several approaches exist to address the inherently ill-posed nature of muscle activation estimation; in this study, a static optimisation framework was selected for its robustness and numerical stability. More advanced dynamic approaches implemented in OpenSim allow for kinematic adjustments during optimisation, but were intentionally avoided here in order to ensure a fair comparison under identical motion conditions. Regarding the prediction of pathological or protective muscle actions, a similar optimisation framework could potentially capture such behaviour (Mathieu et al., 2023), but this would require a dedicated modelling strategy and cost function tailored to pathological or

protective movement patterns, which lies beyond the scope of this work.

A comparison between the joint torque results obtained from experimental measurements and numerical estimations of the ground reaction forces has been presented for joint torques, particularly focusing on the hip, knee, and ankle. The root mean square error (rRMSE) is calculated and tabulated, revealing varying degrees of accuracy for different joints and axes of rotation. Notable errors, especially in knee flexion and hip rotation, prompt an investigation into the origin of these discrepancies.

Pelvis residual forces are analysed, revealing discrepancies, particularly in the double support phase along the vertical axis. The contribution of each GRF component to the overall error is assessed through additional simulations, pinpointing the longitudinal reaction force as a major source of error. These modelling errors can come from the chosen cut-off frequencies of the low-pass filter used to evaluate the kinematics, and/or from the least-square approach while solving the equation of motion for the Lagrange multipliers. A refined model could be implemented using different cut-off frequencies and using different weight on the constraints, in order to place greater emphasis on the longitudinal component of the ground reaction forces.

The chapter concludes with an exploration of the impact of errors in joint torques on muscle activation. The results highlight the challenges of studying muscle activations and forces through inverse dynamics. When using the OpenSim framework with our standard experimental data, muscle activation evaluations are irregular, with noticeable peaks, even though the joint torque curves appear smooth. Replacing these input values with our numerical estimates, which already contain known errors, does not improve the "noisy" behaviour of the final responses. Nonetheless, some muscle groups show converging trends in activations and forces, while others exhibit clear inconsistencies.

Given the difficulty in achieving smooth results with experimental data in a standard study framework, one possible solution could be to use a simpler model in OpenSim. It is likely that the current chosen OpenSim's model, which includes 54 musculotendon actuators, may not resolve the muscle activation optimization properly for our given gait tests. A model with fewer muscle groups and degrees of freedom might potentially improve the final results.

Overall, the chapter provides a detailed and critical evaluation of the proposed contact model and its exploitation for joint torques and muscle activations estimation, shedding light on potential sources of error and avenues for further refinements in future biomechanical studies.

6.7 Conclusion of the chapter

In conclusion, this chapter assessed the joint torque and muscle activation evaluation process in OpenSim, exploiting the proposed 3D foot/ground contact model. Discrepancies between results from experimental and numerical GRFs were scrutinized, highlighting specific challenges in knee flexion and hip rotation. The study also explored the impact of errors in joint

torques on muscle activations and muscle forces estimation, revealing correlation in certain muscle groups, and inconsistencies in other, although the experimental results for muscle activations and forces exhibit peaks and noise, further demonstrating the complexity of evaluating muscle efforts in inverse dynamics. The findings underscore the need for refinement in modelling parameters and methodologies to enhance the accuracy of such biomechanical simulations in OpenSim.

Chapter 7

Conclusion and perspective

7.1 Summary and main contributions

Compared to classical approaches such as isokinetic testing, which provide valuable but localized joint torques measurements under controlled conditions, inverse dynamics models combined with 3D motion capture offer a broader and more functional view of human movement. Rather than isolating a single joint or muscle group, it allows the estimation of net joint torques and forces during natural, unconstrained activities such as walking, running, etc. While motion capture systems can accurately measure the position and velocity of body segments, they cannot directly reveal the underlying muscular and joint efforts. This is where inverse dynamics becomes indispensable. By using kinematic data, external forces, and mechanical principles, it allows us to estimate driving forces like joint torques and muscle activations and forces, helping us understand how movements are generated and controlled, for a variety of activities. This enables the analysis of neuromuscular coordination in real-life conditions, accounting for multi-joint interactions and the influence of gravity and inertia. Although inverse dynamics relies on model-based assumptions, it complements direct measurements by extending their interpretability and by making it possible to estimate internal variables that cannot be directly accessed in vivo. In this way, it provides clinicians and researchers with a more global and integrative understanding of movement, which is essential for diagnosis, treatment planning, or sport evaluation. However, the accuracy of inverse dynamics is highly dependent on the availability and quality of experimental data.

To obtain muscle efforts and activation levels during 3D motions, the kinematics of the human body must be measured, usually along with the contact forces between the feet and the ground. Over the years, kinematic measurement of various body parts has significantly improved, allowing data acquisition in diverse environments. Kinematic studies can now readily extend beyond laboratory settings and be conducted in-situ wherever deemed relevant. However, the direct measurement of ground contact forces remains challenging. Force platforms are not easily transportable and are prohibitively expensive. Consequently, they are confined to motion analysis laboratories, limiting external studies primarily to kinematic analysis only.

The primary objective of this thesis was to develop a new foot-ground contact model for inverse dynamics procedures, based solely on kinematic

measurements. To achieve this, a state-of-the-art review was conducted on kinematic and dynamic analysis of multibody movements with and without contacts, direct and inverse dynamics, human movement description, and existing foot-ground contact models and their limitations. Experimental gait data were acquired with the assistance of physiotherapists to establish a gold standard.

Ground reaction forces (GRFs) play indeed a critical role in the inverse dynamics analysis, as they provide essential reaction force data necessary for accurately estimating joint torques, muscle forces, and activations. Without precise GRF information, the force distribution and the resulting moments acting on the joints cannot be reliably computed, leading to inaccuracies in the biomechanical model. GRFs act as the interface between the body and the ground: this interaction, especially in activities like walking or running, with single- and double-support phase, generates complex forces patterns that contribute significantly to the total body dynamics. Therefore, obtaining accurate GRFs is vital for ensuring the reliability of inverse dynamics calculations, as even minor errors in force estimation can propagate throughout the model, impacting joint torque and muscle force predictions. In cases where direct GRF measurements are not feasible, developing robust numerical models to estimate GRFs becomes crucial for the success of biomechanical simulations.

A first two-dimensional model was developed based on a limited number of assumptions, primarily that the feet and ground do not penetrate each other and their deformations can be ignored (utilizing unilateral constraints), that reaction efforts to various constraints acting on a moving human body distribute optimally (Lagrange multipliers are solved using a least squares method) and that the trajectory of the centre of pressure (COP) is a function of the foot inclination. The 2D model presented in this thesis was designed as a simplified and preliminary approach to investigate inverse dynamics without relying on force plate data. It was tested and validated by comparing the numerically estimated GRFs with experimental measurements from force platforms. Four participants were involved in the study, each completing six walking trials (24 in total) and two jumping trials (8 in total). While certain limitations and modelling inaccuracies were observed (as expected in a simplified framework) the results proved encouraging. The estimated GRFs showed reasonable agreement with the experimental data, supporting the relevance of the modelling approach. These findings, complemented by comparisons with similar methods from the literature, provided a strong foundation and motivation to extend the approach toward a more complete and robust 3D model.

Although walking primarily occurs in the sagittal plane and could be reasonably approximated using a 2D model, extending the formulation to three dimensions was a necessary step to evaluate our approach within a complete musculoskeletal simulation framework. This extension enabled integration into a full OpenSim workflow, which included subject-specific scaling, computation of joint kinematics from motion capture, and muscle force estimation using Static Optimization. To assess the validity and usefulness of the

approach, two parallel simulations were performed in OpenSim: one using fully experimental data, including measured GRFs, and another replacing the experimental GRFs with those estimated numerically using our inverse dynamics model. This dual comparison was especially relevant, as muscle activations and forces are internal quantities that can hardly be directly measured. Evaluating both workflows allowed for a critical comparison of standard practice against our alternative estimation method.

The joint torques computed from our estimated GRFs showed encouraging consistency with those obtained using experimental force plate data. However, discrepancies were observed for certain degrees of freedom, most notably in knee extension and hip internal rotation, highlighting areas where the sensitivity of the model or limitations in the estimation process still affect performance. Nonetheless, the general trends remained coherent, and many joint torques were well correlated between both workflows. Muscle activations and forces, by contrast, proved to be more challenging to interpret. These quantities are known to be highly sensitive to errors in input data, including even small discrepancies in joint kinematics or joint torques. In both simulations, whether using experimental or estimated GRFs, the resulting muscle activations showed some irregularities, including noise and implausible peaks, especially for certain muscle groups. Despite this, convergent activation patterns were still observed in several major muscle groups.

Overall, the contributions of this thesis are significant in several respects. We revisited and re-established the entire inverse dynamics mathematical framework, redefining the meaning and role of bilateral, unilateral, and driving constraints and their associated Lagrange multipliers. This allowed us to define a complete set of constraints in the mechanical model that eliminates the need for direct GRFs measurements while allowing us to solve the equations of motion. The proposed model was evaluated by comparing its outputs, specifically joint torques and muscle activations, to those obtained using a more conventional inverse dynamics approach based on experimentally measured GRFs. While the results sometimes deviate from the reference value, the model shows good agreement in joint torques for most degrees of freedom, and provides reasonable trends in muscle activation for several key muscle groups. These internal quantities, which are typically unmeasurable, thus become accessible without force platforms.

This work offers a lighter alternative framework for estimating joint and muscular efforts in three-dimensional motion, with the potential for applications beyond laboratory environments. By identifying the model's strengths and current limitations, the contribution of this thesis establishes a basis for future improvements and more accessible biomechanical analysis studies.

7.2 Limitations

The previous chapters have demonstrated that the proposed modelling approach provides coherent and physically interpretable results when compared with experimental measurements and established modelling frameworks. While these results support the relevance of the methodology, assessing the credibility and generalisability of a model requires a more structured evaluation framework.

The VVUQ (Verification, Validation and Uncertainty Quantification) framework provides a rigorous methodology to assess the credibility and generalisability of computational models. A full VVUQ analysis was not performed in this work, as it would have required a substantially larger experimental dataset, systematic uncertainty propagation and sensitivity analyses, which were beyond the scope of this thesis. Nevertheless, the proposed approach can be positioned with respect to the main VVUQ principles.

Model verification was addressed at a numerical and methodological level by ensuring consistency of the inverse dynamics formulation and by comparing two independent computational workflows, namely a classical approach relying on experimentally measured ground reaction forces and the proposed method using a numerical foot–ground contact model. The observed agreement in trends and orders of magnitude suggests a correct implementation of the governing equations and treatment of input data.

Validation was performed qualitatively by confronting the estimated joint torques, ground reaction forces and muscle activations with experimental measurements and reference data from the literature. The objective was not to achieve subject-specific prediction accuracy, but to assess whether the proposed method could reproduce biomechanically meaningful patterns under controlled conditions of healthy gait.

Uncertainty quantification was not explicitly carried out. Several sources of uncertainty are known to affect the results, including anthropometric parameter estimation, marker placement, soft tissue artefacts, kinematic differentiation, sensor noise and assumptions related to the foot–ground contact model. The influence of these uncertainties was indirectly assessed through robustness analyses and comparative studies, but no formal uncertainty propagation or sensitivity analysis was conducted. Such analysis would be a relevant topic for future investigations.

Regarding credibility and generalisability, the proposed method is intended for applications involving basic human movements, such as healthy walking, where simplifying assumptions (planar motion for the 2D model, no slipping, simplified contact evolution) remain acceptable. The approach is not expected to be directly applicable to pathological gait or high-performance sports without revisiting the underlying assumptions and cost functions.

7.3 Perspective

Future work could explicitly integrate VVUQ principles by performing sensitivity analyses on key model parameters, propagating experimental uncertainties through the inverse dynamics pipeline, validating the method on independent populations, and combining the proposed physics-based model with data-driven approaches when sufficient experimental data are available, e.g. by using open-source wider datasets when they are available.

Various perspectives have been proposed to improve the model in the future, such as revisiting the weighting applied to each constraint during the resolution of motion equations, a better and possibly subject-specific model for determining the centre of pressure between the foot and the ground, further signal processing enhancements with alternative filters and cut-off frequencies or studying a larger diversity of tasks and subjects.

From a clinical perspective, one of the main outlooks of this work lies in the progressive translation of inverse dynamics methodologies beyond highly instrumented laboratory environments. By reducing the reliance on force platforms and simplifying the foot–ground contact modelling, the proposed approach contributes to the development of biomechanical assessment tools that are more flexible and potentially deployable in non-laboratory settings.

The next steps toward such translation involve improving the generality and robustness of the model, particularly with respect to inter-subject variability, pathological gait patterns and sport-specific movements. This includes refining the contact model, extending validation to larger and more diverse populations, and integrating alternative measurement technologies (e.g., wearable sensors). Ultimately, this line of research aims to support clinicians and practitioners by providing access to estimations of joint and muscle efforts in contexts where traditional force measurement is impractical or unavailable, thereby opening new perspectives for clinical assessment, rehabilitation monitoring and field-based performance analysis.

Appendix A

Scientific resume and list of publications

A.1 List of publications related to the thesis

A.1.1 Journal publications

Van Hulle, R., C. Schwartz, V. Denoël, J.-L. Croisier, B. Forthomme and O. Brüls (2020), "**A foot/ground contact model for biomechanical inverse dynamics analysis**". In: *Journal of Biomechanics* 100, pp. 109412. DOI: https://doi.org/10.1016/j.jbiomech

A.1.2 Conference presentation

Van Hulle, R., C. Schwartz and O. Brüls (2019), "**Evaluation of ground reaction forces using a rigid foot/ground contact model**". In: *ECCOMAS Thematic Conference on Multibody Dynamics* (Duisburg, Germany). URL: https://orbi.uliege.be/handle/2268/241562

A.1.3 Conference posters

Van Hulle, R., C. Schwartz, J.-L. Croisier, V. Denoël, B. Forthomme and O. Brüls (2015), "**Towards a predictive modelling of the normal and pathological gait**". In: *Biomedica 2015, The European Life Sciences Summit* (Genk, Belgium). URL: https://orbi.uliege.be/handle/2268/183673

Van Hulle, R., C. Schwartz, V. Denoël, J.-L. Croisier, B. Forthomme and O. Brüls (2016), "**Evaluation of the contact force between two rigid bodies using kinematic data only**". In: *22th Congress of the European Society of Biomechanics* (Lyon, France). URL: https://orbi.uliege.be/handle/2268/200931

Van Hulle, R., C. Schwartz and O. Brüls (2017), "**Evaluation of ground reaction forces based on kinematic data**". In: *National Day on Biomedical Enggineering & IEEE EMBS Benelux chapter* (Bruxelles, Belgium). URL: https://orbi.uliege.be/handle/2268/216653

Van Hulle, R., C. Schwartz, V. Denoël, J.-L. Croisier, B. Forthomme and

O. Brüls (2018), "**Rigid foot/ground contact model for inverse dynamic analysis solely based on kinematic data**". In: *8th World Congress of Biomechanics* (Dublin, Ireland). URL: https://orbi.uliege.be/handle/2268/227971

Van Hulle, R., C. Schwartz, V. Denoël, J.-L. Croisier, B. Forthomme and O. Brüls (2018), "**P054 - Evaluation of ground reaction forces by inverse dynamics analysis**". In: *Gait and Posture* 65, pp. 72-73. DOI: https://doi.org/10.1016/j.gaitpost.2018.06.207

A.2 List of publications unrelated to the thesis

A.2.1 Journal publications

Denoël, V., O. Bruyère, G. Louppe, V. D'Orio, S. Fontaine, L. Gillet, M. Guillaume, E. Haubruge, A.-C. Lange, F. Michel, **R. Van Hulle**, M. Arnst, A.F. Donneau and C. Seagerman (2022), "**Decision-based interactive model to determine re-opening conditions of a large university campus in Belgium during the first COVID-19 wave**". In: *Archives of Public Health* 80. DOI: https://doi.org/10.1186/s13690-022-00801-w

Arnst, M., G. Louppe, **R. Van Hulle**, L. Gillet, F. Bureau and V. Denoël (2022), "**A hybrid stochastic model and its Bayesian identification for infectious disease screening in a university campus with application to massive COVID-19 screening at the University of Liège.**". In: *Mathematical Biosciences* 347, pp. 108805. DOI: https://doi.org/10.1016/j.mbs.2022.108805

Messina, A., M. Schyns, B.-O. Dozo, V. Denoël, **R. Van Hulle**, A.-M. Etienne, S. Delroisse, O. Bruyère, V. D'Orio, S. Fontaine, M. Guillaume, A.C. Lange, G. Louppe, F. Michel, A.-S. Nyssen, F. Bureau, E. Haubruge, A.-F. Donneau, L. Gillet and C. Saegerman (2023), "**Developing a video game as an awareness and research tool based on SARS-CoV-2 epidemiological dynamics and motivational perspectives**". In: *Transboundary and Emerging Diseases*. DOI: https://doi.org/10.1155/2023/8205408

Bibliography

Ackermann, M. and A. J. van den Bogert (2010). "Optimality principles for model-based prediction of human gait". In: *Journal of Biomechanics* 43.6, pp. 1055–1060. DOI: 10.1016/j.jbiomech.2009.12.012.

Alart, P. and A. Curnier (1991). "A mixed formulation for frictional contact problems prone to Newton like solution methods". In: *Computer Methods in Applied Mechanics and Engineering* 92.3, pp. 353–375. DOI: 10.1016/0045-7825(91)90022-X.

Allard, P., A. Cappozzo, A. Lundberg, and C. Vaughan (1998). *Three-Dimensional Analysis of Human Locomotion*. New York, US: John Wiley & Sons, Inc.

Alonso, F. J., J. Cuadrado, U. Lugrís, and P. Pintado (2010). "A compact smoothing-differentiation and projection approach for the kinematic data consistency of biomechanical systems". In: *Multibody System Dynamics* 24.1, pp. 67–80. DOI: 10.1007/s11044-010-9191-1.

Anderson, A. E. (2007). "Computational modeling of hip joint mechanics". PhD thesis. University of Utah.

Anderson, F. C. and M. G. Pandy (2001). "Dynamic optimization of human walking". In: *Journal of Biomechanical Engineering* 123.5, pp. 381–390. DOI: 10.1115/1.1392310.

Anderson, F. C. (1999). "A Dynamic Optimization Solution for a Complete Cycle of Normal Gait". PhD thesis. The University of Texas at Austin.

Anderson, F. C. and M. G. Pandy (1999). "A Dynamic Optimization Solution for Vertical Jumping in Three Dimensions". In: *Computer Methods in Biomechanics and Biomedical Engineering* 2.3. PMID: 11264828, pp. 201–231. DOI: 10.1080/10255849908907988.

Angeles, J. and A. Kecskeméthy (1995). *Kinematics and Dynamics of Multi-Body Systems*. Ed. by J. Angeles and A. Kecskeméthy. Vol. 360. CISM International Centre for Mechanical Sciences. Vienna: Springer Vienna. DOI: 10.1007/978-3-7091-4362-9.

Angelini, L., F. Di Puccio, T. Zander, and H. Schmidt (Nov. 2016). "Influence of Arm Motion on Spatio-temporal Gait Parameters and on Force Data". In: *Journal of Sports and Physical Education* 3, pp. 12–16. DOI: 10.9790/6737.

Aratow, M., R. Ballard, A. Crenshaw, J Styf, D. Watenpaugh, N. Kahan, and A. R. Hargens (1993). "Intramuscular pressure and electromyography as indexes of force during isokinetic exercise". In: *Journal of applied physiology* 74.6, pp. 2634–2640. DOI: 10.1152/jappl.1993.74.6.2634.

Arnold, E. M., S. R. Ward, R. L. Lieber, and S. L. Delp (2010). "A Model of the Lower Limb for Analysis of Human Movement". In: *Annals of Biomedical Engineering* 38.2, pp. 269–279. DOI: 10.1007/s10439-009-9852-5.

Baker, R. and J. Robb (2006). "Foot models for clinical gait analysis". In: *Gait and Posture* 23.4, pp. 399–400. DOI: 10.1016/j.gaitpost.2006.03.005.

Blumentals, A., B. Brogliato, and F. Bertails-Descoubes (2016). "The contact problem in Lagrangian systems subject to bilateral and unilateral constraints, with or without sliding Coulomb's friction: a tutorial". In: *Multibody System Dynamics* 38.1, pp. 43–76. DOI: 10.1007/s11044-016-9527-6.

Borghese, N. A., L Bianchi, F Lacquaniti, I. Scientifico, and S. L. I. Nb (1996). "Kinematic determinants of human locomotion". In: *The Journal of physiology, 494 (Pt 3)*, pp. 863–879. DOI: 113/jphysiol.1996.sp021539.

Buchanan, T. S., D. G. Lloyd, K. Manal, and T. F. Besier (2004). "Neuromusculoskeletal Modeling: Estimation of Muscle Forces and Joint Moments and Movements from Measurements of Neural Command". In: *Journal of Applied Biomechanics* 20.4, pp. 367–395. DOI: 10.1123/jab.20.4.367.

Byrne, D. P., K. J. Mulhall, and J. F. Baker (2010). "Anatomy & Biomechanics of the Hip". In: *The Open Sports Medicine Journal* 4.1, pp. 51–57. DOI: 10.2174/1874387001004010051.

Calais-Germain, B. (2004). *Anatomy of Movement*. Eastland Press.

Cappozzo, A., U. Della Croce, A. Leardini, and L. Chiari (2005). "Human movement analysis using stereophotogrammetry". In: *Gait & Posture* 21.2, pp. 186–196. DOI: 10.1016/j.gaitpost.2004.01.010.

Carbone, V., R. Fluit, P. Pellikaan, M. van der Krogt, D. Janssen, M. Damsgaard, L. Vigneron, T. Feilkas, H. Koopman, and N. Verdonschot (2015). "TLEM 2.0 – A comprehensive musculoskeletal geometry dataset for subject-specific modeling of lower extremity". In: *Journal of Biomechanics* 48.5, pp. 734–741. DOI: 10.1016/j.jbiomech.2014.12.034.

Carhart, M. R. (2000). *Biomechanical analysis of compensatory stepping: implications for paraplegics standing via FNS*. Ed. by A. S. University.

Caspers, L. (2019). "Die Modellierung des Abrollverhaltens beim Fuß-Boden-Kontakt in der Sagittalebene während des menschlichen Gangs". PhD thesis. Universität Duisburg-Essen.

Caspers, L., M. Siebler, H. Hefter, U. Lugrís, and A. Kecskeméthy (2017). "Using Kinematic Rolling Surfaces for Fast Foot-Ground Modeling in the Forward Dynamics of Human Gait—A Sagittal Plane Analysis". In: *ECCOMAS Thematic Conference on Multibody Dynamics, Prague, Czech Republic*, pp. 7–8.

Chen, Q.-z., V. Acary, G. Virlez, and O. Brüls (2013). "A nonsmooth generalized- α scheme for flexible multibody systems with unilateral constraints". In: *International Journal for Numerical Methods in Engineering* 96.8, pp. 487–511. DOI: 10.1002/nme.4563.

De Wit, B., D. De Clercq, and P. Aerts (2000). "Biomechanical analysis of the stance phase during barefoot and shod running". In: *Journal of Biomechanics* 33.3, pp. 269–278. DOI: 10.1016/S0021-9290(99)00192-X.

Delp, S. L., F. C. Anderson, A. S. Arnold, P. Loan, A. Habib, C. T. John, E. Guendelman, and D. G. Thelen (2007). "OpenSim: Open-Source Software to Create and Analyze Dynamic Simulations of Movement". In: *IEEE Transactions on Biomedical Engineering* 54.11, pp. 1940–1950. DOI: 10.1109/TBME.2007.901024.

Delp, S., J. Loan, M. Hoy, F. Zajac, E. Topp, and J. Rosen (1990). "An interactive graphics-based model of the lower extremity to study orthopaedic surgical procedures". In: *IEEE Transactions on Biomedical Engineering* 37.8, pp. 757–767. DOI: 10.1109/10.102791.

Dembia, C. L., N. A. Bianco, A. Falisse, J. L. Hicks, and S. L. Delp (2020). "OpenSim Moco: Musculoskeletal optimal control". In: *PLOS Computational Biology* 16.12. Ed. by K. S. Campbell, e1008493. DOI: 10.1371/journal.pcbi.1008493.

Di Pietro, A., F. Di Puccio, and L. Modenese (2025). "OpenGRF: Predicting Ground Reaction Forces and Moments During Daily Living Activities in OpenSim". In: *bioRxiv*. DOI: 10.1101/2025.09.27.678739.

Dickens, W. E. and M. F. Smith (2006). "Validation of a visual gait assessment scale for children with hemiplegic cerebral palsy". In: *Gait & Posture* 23.1, pp. 78–82. DOI: 10.1016/j.gaitpost.2004.12.002.

Doorenbosch, C. A. and J. Harlaar (2004). "Accuracy of a practicable EMG to force model for knee muscles". In: *Neuroscience letters* 368.1, pp. 78–81. DOI: 10.1016/j.neulet.2004.06.055.

Ebashi, S., M. Endo, and I. Ohtsuki (1969). "Control of muscle contraction". In: *Quarterly Reviews of Biophysics* 2.4, pp. 351–384. DOI: 10.1017/S0033583500001190.

Falisse, A., G. Serrancolí, C. L. Dembia, J. Gillis, I. Jonkers, and F. De Groote (Aug. 2019). "Rapid predictive simulations with complex musculoskeletal models suggest that diverse healthy and pathological human gaits can emerge from similar control strategies". In: *Journal of The Royal Society Interface* 16.157, p. 20190402. DOI: 10.1098/rsif.2019.0402.

Farley, C. T. and O. González (1996). "Leg stiffness and stride frequency in human running". In: *Journal of Biomechanics* 29.2, pp. 181–186. DOI: 10.1016/0021-9290(95)00029-1.

Fluit, R., M. S. Andersen, S. Kolk, N. Verdonschot, and H. F. Koopman (2014). "Prediction of ground reaction forces and moments during various activities of daily living". In: *Journal of Biomechanics* 47.10, pp. 2321–2329. DOI: 10.1016/j.jbiomech.2014.04.030.

Forner-Cordero, A., H. J. Koopman, and F. C. Van Der Helm (2006). "Inverse dynamics calculations during gait with restricted ground reaction force information from pressure insoles". In: *Gait and Posture* 23.2, pp. 189–199. DOI: 10.1016/j.gaitpost.2005.02.002.

Gao, X., L. Wang, L. Jiang, X. Chen, Z. Wang, S. Zhao, Q. Sun, and B. Huo (2024). "A novel rigid Foot-Ground contact model for Predicting ground reaction forces and center of pressure during normal gait". In: *Journal of Biomechanics* 176, p. 112383. DOI: 10.1016/j.jbiomech.2024.112383.

García De Jalón, J. and M. D. Gutiérrez-López (2013). "Multibody dynamics with redundant constraints and singular mass matrix: Existence, uniqueness, and determination of solutions for accelerations and constraint forces". In: *Multibody System Dynamics* 30.3, pp. 311–341. DOI: 10.1007/s11044-013-9358-7.

García-Vallejo, D. and W. Schiehlen (2012). "3D-Simulation of human walking by parameter optimization". In: *Archive of Applied Mechanics* 82.4, pp. 533–556. DOI: 10.1007/s00419-011-0571-7.

Gautier, N., C. Schwartz, and R. Van Hulle (2016). "Modélisation musculosquelettique de la marche saine : influence de la prise en compte de données patient-spécifique de la force musculaire". MA thesis. University of Liège.

Géradin, M. and A. Cardona (2001). *Flexible Multibody Dynamics: A Finite Element Approach*. Chichester, England: John Wiley & Sons Ltd.

Gilchrist, L. and D. Winter (1996). "A two-part, viscoelastic foot model for use in gait simulations". In: *Journal of Biomechanics* 29.6, pp. 795–798. DOI: 10.1016/0021-9290(95)00141-7.

Gupta, S. and A. Kumar (2017). "A brief review of dynamics and control of underactuated biped robots". In: *Advanced Robotics* 31.12, pp. 607–623. DOI: 10.1080/01691864.2017.1308270.

Haralabidis, N., G. Serrancolí, S. Colyer, I. Bezodis, A. Salo, and D. Cazzola (2021). "Three-dimensional data-tracking simulations of sprinting using a direct collocation optimal control approach". In: *PeerJ* 9. DOI: 10.7717/peerj.10975.

Hatze, H. (1975). "A New Method for the Simultaneous Measurement of the Moment of Inertia , the Damping Coefficient and the Location of the Centre of Mass of a Body Segment in situ". In: *European Journal of Applied Physiology and Occupational Physiology* 34, pp. 217–226. DOI: 10.1007/BF00999935.

Hill, A. (1938). "The Heat of Shortening and the Dynamic Constants of Muscle". In: *Proceedings of the Royal Society of London* 126.843, pp. 136–195. DOI: 10.1098/rspb.1938.0050.

Keller, T., A. Weisberger, J. Ray, S. Hasan, R. Shiavi, and D. Spengler (1996). "Relationship between vertical ground reaction force and speed during walking, slow jogging, and running". In: *Clinical Biomechanics* 11.5, pp. 253–259. DOI: 10.1016/0268-0033(95)00068-2.

Kitaoka, H. B., X. M. Crevoisier, D. Hansen, B. Katajarvi, K. Harbst, and K. R. Kaufman (2006). "Foot and Ankle Kinematics and Ground Reaction Forces During Ambulation". In: *Foot & Ankle International* 27.10, pp. 808–813. DOI: 10.1177/107110070602701010.

Knorz, S., F. Kluge, K. Gelse, S. Schulz-Drost, T. Hotfiel, M. Lochmann, B. Eskofier, and S. Krinner (2017). "Three-Dimensional Biomechanical Analysis of Rearfoot and Forefoot Running". In: *Orthopaedic Journal of Sports Medicine* 5.7, p. 232596711771906. DOI: 10.1177/2325967117719065.

Koman, L. A., J. F. Mooney, B. P. Smith, A. Goodman, and T. Mulvaney (1994). "Management of Spasticity in Cerebral Palsy with Botulinum-A Toxin: Report of a Preliminary, Randomized, Double-Blind Trial". In: *Journal of Pediatric Orthopaedics* 14.3, pp. 299–303. DOI: 10.1097/01241398-199405000-00005.

Koopman, B., H. J. Grootenboer, and H. J. de Jongh (1995). "An inverse dynamics model for the analysis, reconstruction and prediction of bipedal

walking". In: *Journal of Biomechanics* 28.11, pp. 1369–1376. DOI: 10.1016/0021-9290(94)00185-7.

Krebs, D. E., J. E. Edelstein, and S. Fishman (1985). "Reliability of Observational Kinematic Gait Analysis". In: *Physical Therapy* 65.7, pp. 1027–1033. DOI: 10.1093/ptj/65.7.1027.

Lankarani, H. M. and P. E. Nikravesh (1994). "Continuous contact force models for impact analysis in multibody systems". In: *Nonlinear Dynamics* 5.2, pp. 193–207. DOI: 10.1007/BF00045676.

Leardini, A., J. O'Connor, F. Catani, and S. Giannini (1999). "A geometric model of the human ankle joint". In: *Journal of Biomechanics* 32.6, pp. 585–591. DOI: 10.1016/S0021-9290(99)00022-6.

Lin, Y.-C., J. P. Walter, and M. G. Pandy (2018). "Predictive Simulations of Neuromuscular Coordination and Joint-Contact Loading in Human Gait". In: *Annals of Biomedical Engineering* 46.8, pp. 1216–1227. DOI: 10.1007/s10439-018-2026-6.

Maathuis, K. G. B., C. P. van der Schans, A. van Iperen, H. S. Rietman, and J. H. B. Geertzen (2005). "Gait in Children With Cerebral Palsy". In: *Journal of Pediatric Orthopaedics* 25.3, pp. 268–272. DOI: 10.1097/01.bpo.0000151061.92850.74.

Marasovič, T., M. Cecič, and V. Zanchi (2009). "Analysis and interpretation of ground reaction forces in normal gait". In: *WSEAS Transactions on Systems* 8.9, pp. 1105–1114. DOI: 10.5555/1718216.1718223.

Martin, A. E. and J. P. Schmiedeler (2014). "Predicting human walking gaits with a simple planar model". In: *Journal of Biomechanics* 47.6, pp. 1416–1421. DOI: 10.1016/j.jbiomech.2014.01.035.

Mathieu, E., S. Crémoux, D. Duvivier, D. Amarantini, and P. Pudlo (2023). "Biomechanical modeling for the estimation of muscle forces: toward a common language in biomechanics, medical engineering, and neurosciences". In: *Journal of NeuroEngineering and Rehabilitation* 20.1, p. 130. DOI: 10.1186/s12984-023-01253-1.

McMahon, T. A. and G. C. Cheng (1990). "The mechanics of running: How does stiffness couple with speed?" In: *Journal of Biomechanics* 23, pp. 65–78. DOI: 10.1016/0021-9290(90)90042-2.

Mok, K.-M., D. T.-P. Fong, T. Krosshaug, A. S.-L. Hung, P. S.-H. Yung, and K.-M. Chan (2011). "An ankle joint model-based image-matching motion analysis technique". In: *Gait & Posture* 34.1, pp. 71–75. DOI: 10.1016/j.gaitpost.2011.03.014.

Moreira, P., M. Silva, and P. Flores (2009). "Ground foot interaction in human gait: modelling and simulation". In: *7th EUROMECH Solid Mechanics Conference*. Lisbon.

Nasr, A. and J. McPhee (2025). "Scalable musculoskeletal model for dynamic simulations of lower body movement". In: *Computer methods in biomechanics and biomedical engineering* 28.8, pp. 1196–1222. DOI: 10.1080/10255842.2024.2316240.

Neptune, R. R., S. A. Kautz, and F. E. Zajac (2001). "Contributions of the individual ankle plantar flexors to support, forward progression and swing

initiation during walking". In: *Journal of Biomechanics* 34.11, pp. 1387–1398. DOI: 10.1016/S0021-9290(01)00105-1.

Nilsson, J. and A. Thorstensson (1989). "Ground reaction forces at different speeds of human walking and running". In: *Acta Physiologica Scandinavica* 136.2, pp. 217–227. DOI: 10.1111/j.1748-1716.1989.tb08655.x.

Novacheck, T. F. (1998). "The biomechanics of running". In: *Gait & Posture* 7.1, pp. 77–95. DOI: 10.1016/S0966-6362(97)00038-6.

Oberg, T., A. Karsznia, and K. Oberg (1993). "Basic gait parameters: Reference data for normal subjects, 10-79 years of age". In: *Journal of Rehabilitation Research and Development* 30.2, pp. 210–223.

Oh, S. E., A. Choi, and J. H. Mun (2013). "Prediction of ground reaction forces during gait based on kinematics and a neural network model". In: *Journal of Biomechanics* 46.14, pp. 2372–2380. DOI: 10.1016/j.jbiomech.2013.07.036.

Ong, A., S. Hillman, and J. Robb (2008). "Reliability and validity of the Edinburgh Visual Gait Score for cerebral palsy when used by inexperienced observers". In: *Gait & Posture* 28.2, pp. 323–326. DOI: 10.1016/j.gaitpost.2008.01.008.

Pàmies-Vilà, R., F. González, J. Kövecses, and J. M. Font-Llagunes (2018). "Use of performance indicators in the analysis of running gait impacts". In: *Multibody System Dynamics* 43.2, pp. 131–151. DOI: 10.1007/s11044-017-9580-9.

Phillips, A., P. Pankaj, C. Howie, A. Usmani, and A. Simpson (2007). "Finite element modelling of the pelvis: Inclusion of muscular and ligamentous boundary conditions". In: *Medical Engineering & Physics* 29.7, pp. 739–748. DOI: 10.1016/j.medengphy.2006.08.010.

Raison, M. (2009). "On the quantification of joint and muscle efforts in the human body during motion". PhD thesis. Université catholique de Louvain.

Ralston, H. J. (1976). "Energetics of Human Walking". In: pp. 77–98. DOI: 10.1007/978-1-4757-0964-3_5.

Razavian, R. S. and J. McPhee (2015). "Minimization of muscle fatigue as the criterion to solve muscle forces-sharing problem". In: *Proceedings of the ASME 2015 Dynamic Systems and Control Conference, DSCC*. DOI: 10.1115/DSCC2015-9678.

Ren, L., R. K. Jones, and D. Howard (2005). "Dynamic analysis of load carriage biomechanics during level walking". In: *Journal of Biomechanics* 38.4, pp. 853–863. DOI: 10.1016/j.jbiomech.2004.04.030.

Ren, L., R. K. Jones, and D. Howard (2007). "Predictive modelling of human walking over a complete gait cycle". In: *Journal of Biomechanics* 40.7, pp. 1567–1574. DOI: 10.1016/j.jbiomech.2006.07.017.

Ren, L., R. K. Jones, and D. Howard (2008). "Whole body inverse dynamics over a complete gait cycle based only on measured kinematics". In: *Journal of Biomechanics* 41.12, pp. 2750–2759. DOI: 10.1016/j.jbiomech.2008.06.001.

Richard, V., G. Lamberto, T.-W. Lu, A. Cappozzo, and R. Dumas (2016). "Knee kinematics estimation using multi-body optimisation embedding a knee

joint stiffness matrix: a feasibility study". In: *PloS one* 11.6. DOI: 10.1371/journal.pone.0157010.

Saraiva, L., M. Rodrigues da Silva, F. Marques, M. Tavares da Silva, and P. Flores (2022). "A review on foot-ground contact modeling strategies for human motion analysis". In: *Mechanism and Machine Theory*, p. 105046. DOI: 10.1016/j.mechmachtheory.2022.105046.

Schwartz, C., B. Forthomme, O. Bruls, V. Denoël, S. Cescotto, and J.-L. Croisier (2010). "Using 3D to understand human motion". In: *3D Stereo Media*.

Scott, S. H. and D. A. Winter (1993). "Biomechanical model of the human foot: Kinematics and kinetics during the stance phase of walking". In: *Journal of Biomechanics* 26.9, pp. 1091–1104. DOI: 10.1016/S0021-9290(05)80008-9.

Seth, A., J. L. Hicks, T. K. Uchida, A. Habib, C. L. Dembia, J. J. Dunne, C. F. Ong, M. S. DeMers, A. Rajagopal, M. Millard, S. R. Hamner, E. M. Arnold, J. R. Yong, S. K. Lakshmikanth, M. A. Sherman, J. P. Ku, and S. L. Delp (2018). "OpenSim: Simulating musculoskeletal dynamics and neuromuscular control to study human and animal movement". In: *PLOS Computational Biology* 14.7. Ed. by D. Schneidman, e1006223. DOI: 10.1371/journal.pcbi.1006223.

Singh, R., H. Chaudhary, and A. K. Singh (2018). "A novel gait-based synthesis procedure for the design of 4-bar exoskeleton with natural trajectories". In: *Journal of Orthopaedic Translation* 12, pp. 6–15. DOI: 10.1016/j.jot.2017.09.001.

Skals, S., M. K. Jung, M. Damsgaard, and M. S. Andersen (2017). "Prediction of ground reaction forces and moments during sports-related movements". In: *Multibody System Dynamics* 39.3, pp. 175–195. DOI: 10.1007/s11044-016-9537-4.

Spägele, T., A. Kistner, and A. Gollhofer (1999). "Modelling, simulation and optimisation of a human vertical jump". In: *Journal of Biomechanics* 32.5, pp. 521–530. DOI: 10.1016/S0021-9290(98)00145-6.

Stoquart, G., C. Detrembleur, and T. Lejeune (2008). "Effect of speed on kinematic, kinetic, electromyographic and energetic reference values during treadmill walking". In: *Neurophysiologie Clinique/Clinical Neurophysiology* 38.2, pp. 105–116. DOI: 10.1016/j.neucli.2008.02.002.

Sutherland, D. (2005). "The evolution of clinical gait analysis part III – kinetics and energy assessment". In: *Gait & Posture* 21.4, pp. 447–461. DOI: 10.1016/j.gaitpost.2004.07.008.

Swanson, S. C. and G. E. Caldwell (2000). "An integrated biomechanical analysis of high speed incline and level treadmill running". In: *Medicine & Science in Sports & Exercise* 32.6, pp. 1146–1155. DOI: 10.1097/00005768-200006000-00018.

Taylor, W. R., M. O. Heller, G. Bergmann, and G. N. Duda (2004). "Tibiofemoral loading during human gait and stair climbing". In: *Journal of Orthopaedic Research* 22.3, pp. 625–632. DOI: 10.1016/j.orthres.2003.09.003.

Thelen, D. G., F. C. Anderson, and S. L. Delp (2003). "Generating dynamic simulations of movement using computed muscle control". In: *Journal of Biomechanics* 36.3, pp. 321–328. DOI: 10.1016/S0021-9290(02)00432-3.

Todorov, E. and M. I. Jordan (2002). "Optimal feedback control as a theory of motor coordination". In: *Nature Neuroscience* 5.11, pp. 1226–1235. DOI: 10.1038/nn963.

Uchida, T. K. and S. L. Delp (2021). *Biomechanics of movement: the science of sports, robotics, and rehabilitation*. Mit Press.

van der Zee, T. J., E. M. Mundinger, and A. D. Kuo (2022). "A biomechanics dataset of healthy human walking at various speeds, step lengths and step widths". In: *Sci Data* 9, p. 704. DOI: 10.1038/s41597-022-01817-1.

Van Hulle, R., C. Schwartz, V. Denoël, J. L. Croisier, B. Forthomme, and O. Brüls (2020). "A foot/ground contact model for biomechanical inverse dynamics analysis". In: *Journal of Biomechanics* 100, p. 109412. DOI: 10.1016/j.jbiomech.2019.109412.

Whittle, M. W. (2007). *Gait Analysis*. Elsevier. DOI: 10.1016/B978-0-7506-8883-3.X5001-6.

Winter, D. A. (1984). "Kinematic and kinetic patterns in human gait: Variability and compensating effects". In: *Human Movement Science* 3.1-2, pp. 51–76. DOI: 10.1016/0167-9457(84)90005-8.

— (2009). *Biomechanics and Motor Control of Human Movement*. Hoboken, NJ, USA: John Wiley & Sons, Inc. DOI: 10.1002/9780470549148.

Wismans, J., F. Veldpaus, J. Janssen, A. Huson, and P. Struben (1980). "A three-dimensional mathematical model of the knee-joint". In: *Journal of Biomechanics* 13.8, pp. 677–685. DOI: 10.1016/0021-9290(80)90354-1.

Xiang, Y., H. Chung, A. Mathai, S. Rahmatalla, J. Kim, T. Marler, S. Beck, J. Yang, J. Arora, K. Abdel-Malek, and J. Obusek (2007). "Optimization-based Dynamic Human Walking Prediction". In: *SAE Technical Papers*. DOI: 10.4271/2007-01-2489.

Xiang, Y., J. S. Arora, and K. Abdel-Malek (2011). "Optimization-based prediction of asymmetric human gait". In: *Journal of Biomechanics* 44.4, pp. 683–693. DOI: 10.1016/j.jbiomech.2010.10.045.

Xie, H., S. Wang, and F. Li (2014). "Knee joint optimization design of intelligent bionic leg based on genetic algorithm". In: *International Journal Bioautomation* 18.3, pp. 195–206.

Yamaguchi, G. T. and F. E. Zajac (1989). "A planar model of the knee joint to characterize the knee extensor mechanism". In: *Journal of Biomechanics* 22.1, pp. 1–10. DOI: 10.1016/0021-9290(89)90179-6.